Quenching and tempering effects on Rheo-cast F357 aluminium alloy during Nd:YAG laser welding

by

Maritha Theron

A dissertation submitted to the faculty of Engineering and the Built Environment of the University of Cape Town in fulfilment of the requirements for the degree of MSc (Engineering) in Materials Engineering

Centre for Materials Engineering
Department of Mechanical Engineering
University of Cape Town
February 2010

CSIR

UNIVERSITY OF CAPE TOWN

DECLARATIONS

(i) I hereby grant the University of Cape Town free licence to reproduce for the purpose of research, either the whole or any portion of the contents in any manner whatsoever of the above dissertation. I am presenting this dissertation in complete fulfilment of the requirements for my MSc(Eng) degree.

(ii) I know the meaning of plagiarism and declare that all of the work in this document, apart from that which is properly acknowledged, is my own.

Signature:... Signed by candidate

Date:.....04/02/2010.....

ACKNOWLEDGEMENTS

All the glory and honour goes to God who gave me the opportunity to stretch my boundaries and to enjoy my work!

My gratitude also goes to God for giving me the most wonderful husband and children, who support me, believe in me and never complain when I have to give priority to work. I love you with all my heart and everything in me, and I praise God for the privilege of having you in my life and Him in the centre of it all! Thanks to God also for my parents who always carry me through their prayers!

Then I have to thank my friend and mentor, Dr. Lilian Ivanchev, without whom I could not have done this work. Thank you for the encouragement, guidance and help to solve problems. Thank you also for walking the extra mile with me for the project!

A sincere "thank you" to my friends and colleagues, Herman Burger and Corney van Rooyen who are always available for discussions, who are never too busy to help and without whom I could not have done the execution of this work. Thank you for the encouragement, proof reading of my reports and for allowing me the time to sit in front of my computer to write-up my dissertation. It is a privilege working with you! Thank you also, Herman, for all the help with set-ups and sample preparation, it is really appreciated!

My gratitude also goes to my supervisor, Prof. Robert Knutsen, for all the discussions and encouragement and for challenging me and keeping me focused. Thank you very much!

Appreciation and acknowledgement also goes to:

- The personnel of the Laser Materials Processing group at the CSIR National Laser Centre, especially Chris Kruger and Herman Rossouw, for their support and willingness to help and to 'make a plan'.
- The Materials Science and Manufacturing unit for supplying all the F357 cast material, for the cast and tensile sample preparation and tensile testing. Special thanks to Danie Wilkens, André Grobler and Chris McDuling.
- Dr. Ganka Zlateva from the Institute of Metal Science at the Bulgarian Academy of Sciences, Sofia, who voluntarily poured her knowledge and effort into the project by doing the TEM analyses of the samples and explaining the findings.
- CSIR National Laser Centre for funding the project.

GLOSSARY

ASM	American Society for Metals
BM	Base metal
BOP	Bead-on-plate
CO_2	Carbon dioxide
CW	Continuous wave
DOF	Depth of focus
FZ	Fusion zone
GP zones	Guinier-Preston
HAZ	Heat affected zone
HPDC	High pressure die casting
LBW	Laser beam welding
Nd:YAG	Neodymium-doped yttrium aluminium garnet laser (1064 nm wave length)
PFZ	Precipitate-free zone
PID	Power intensity distribution
PMZ	Partly melted zone
PW	Pulsed wave
PWHT	Post weld heat treatment
QFA	Quench Factor Analysis
RDC	Rheo-diecast
SSD	Spot separation distance
SSM	Semi-solid-metal
TEM	Transmission electron microscopy
TIG welding	Tungsten-arc inert gas welding
TTP curve	Time-Temperature-Property curve
TTT curve	Time-Temperature-Transformation curve
WM	Weld metal

DEFINITIONS

Laser beam welding (LBW): A welding technique used to join multiple pieces of metal through the use of a laser. The beam provides a concentrated heat source (monochromatic, coherent and directional light), allowing for narrow, deep welds and high welding rates.

Autogenous laser welding: Laser welding without the use of filler material.

Fusion line: The cut-off area between the weld metal and base metal.

Weld face: The top side of the weld.

Weld root: The bottom side of the weld.

Weld toe: The top and bottom part of the fusion line, visible on the surface.

Heat affected zone (HAZ): The area adjacent to the weld, which did not melt, but was affected by the heat of the weld. It is a region of altered hardness (less than 90% of that of the base metal) and variable microstructure.

Keyhole: This is the formation of a vapour pocket surrounded by liquid metal, which is necessary for deep penetration welding.

Deep penetration welding: Non-conductive welding which requires extremely high power densities to produce a deep, narrow weld with the depth up to ten times greater than the weld width.

Interface: Discontinuity between two solid layers, e.g. in this study it represents the discontinuity between the two Al plates to be welded together.

Solution heat treatment: A process in which an alloy or metal is heated to a suitable temperature, is held at that temperature long enough to allow a certain constituent to enter into solid solution, and is then cooled rapidly to hold that constituent in solution.

Heat Treatment Conditions:

F: As fabricated. In this project it is equivalent to "as-cast";

T4: Solid solution heated to 540 ℃ for 6 hours, quenched in water at ambient temperature and followed by natural aging at ambient temperature for minimum of 5 days;

T4+: Solid solution heated to 540 ℃ for 6 hours, quenched in water at ambient temperature, followed by natural aging at ambient temperature for minimum of 5 days and artificial aging at 170°C for 6 hrs after welding;

T6: Solid solution heated to 540 ℃ for 6 hours, quenched in water at ambient temperature, naturally aged for 20 hrs at ambient temperature and then artificially aged at 170℃ for 6 hrs.

ABSTRACT

Al-Si-Mg casting alloys are being used in automotive applications, aerospace applications and other applications requiring heat-treatable permanent mould castings that combine good weldability with high strength and toughness (ASM) (1). These casting alloys are also known for their excellent castability, corrosion resistance and, in particular, a range of mechanical properties in the heat-treated condition. A357 aluminum alloy has been extensively used for semi-solid processing for more than three decades, and a large amount of components like fuel rails, engine mounts, engine brackets and suspension parts have been produced (2). This alloy is also included in the Statement for Work between the Council for Scientific and Industrial Research (CSIR) and Boeing Co, USA (3, 4).

F357, a hypo-eutectic aluminium alloy, Al-7%Si-0.6%Mg without beryllium, was processed with CSIR-Rheo technology to the Semi-Solid Metal (SSM) state and cast in plates with a 50 Ton High Pressure Die Casting machine. The castings were either left in the as-cast (F) condition or subjected to T4, T4+ or T6 heat treatments prior to laser welding.

Welding of aluminium alloys poses many problems like porosity, loss of alloying elements, poor bead geometry and softening of the heat affected zone. Laser welding is however widely used in industrial production owing to the advantages such as low heat input, high welding speed and high production rate. Due to these unique advantages, the potential of autogenous Nd:YAG laser welding as manufacturing process for this cast aluminium alloy was evaluated. A welding operating window was established and the optimum parameters were found to be a laser power of 3.8 kW at the workpiece and a welding speed of 4 m/min with a twin spot laser light configuration. These laser welding parameters were applied for the welding of the heat treated plates and resulted in very low weld joint porosity and almost no loss of alloying elements.

The mechanical properties of age-hardenable Al-Si-Mg alloys are dependent on the rate at which the alloy is cooled after the solution heat treatment. Because of the high cooling rate during laser welding, the possibility of producing weld seams through deep penetration laser welding, with mechanical properties matching those of the T6 temper condition, but without a post-weld solid solution heat treatment, was investigated. The quench rate after laser welding was measured and compared well with that measured after solution treatment. The resulting mechanical properties of

F357 aluminium welded in the T4 condition and only artificially aged after welding (T4+ condition), compares very well with the T6 base material properties. The strengthening mechanisms obtained during laser welding and the different heat treatments were studied by means of transmission electron microscopy (TEM) and are consistent with the expected precipitation hardening processes in Al-Si-Mg alloys. The quench sensitivity of SSM F357 aluminium alloy is thus sufficiently low to obtain such an increase in strength values during laser welding, that no post-weld solution heat treatment is necessary to achieve mechanical properties to the T6 performance specification.

TABLE OF CONTENTS

CHAPTER ONE
Introduction

1.1 Background

Al-Si-Mg casting alloys are being used in the applications involved with weight reduction and improved fuel economy as well as other applications requiring heat-treatable permanent mould castings that combine good weldability with high strength and toughness together with a range of mechanical properties in the heat-treated condition.

A semi-solid metal (SSM) casting process, capable of producing aluminium components of high integrity and improved performance, has been developed at the Council for Scientific and Industrial Research (CSIR). This process is based on the concept of decreasing, or even eliminating porosity. A357 aluminum alloy has been extensively used for semi-solid processing for more than three decades and has been chosen as base material to be investigated in this study.

Good weldability is a pre-requisite for using Al-Mg-Si alloys. However, welding of aluminium still results in many problems due to the inherent characteristics of aluminium and in general all welds formed in aluminium and aluminium alloys exhibit mechanical properties poorer than those of the base material.

Laser welding has certain advantages when compared to the conventional welding processes. These advantages lead to high cooling rates which were required for this study. The mechanical properties of age-hardenable Al-Si-Mg alloys depend on the rate at which the alloy is cooled after the solution heat treatment. The high cooling rate of laser welding was to be used to eliminate or replace the post-weld solid solution heat treatment for the T6 temper condition. Laser welding was therefore chosen as possible manufacturing process to be investigated.

1.2 Research hypothesis

- Deep penetration laser welding can be successfully applied to SSM rheo-cast F357 aluminium in terms of weld quality and properties.

- Deep penetration laser joining of SSM HPDC F357 aluminium alloy should be able to produce weld seams with mechanical properties of the T6 temper condition without the need for a post-weld solid solution heat treatment. Because of the high processing speed, high thermal conductivity of the metal and low heat input, the cooling rate during LBW should be high enough to obtain sufficient supersaturated solid solution in the weld metal with minimal affect to the parent metal properties (i.e. very small or no HAZ), in order for its T6 mechanical properties to be achieved only with a post weld aging treatment.

- As a result of the high cooling rate, the finer microstructure (although dendritic) of the weld metal, compared to that of the base metal, should be able to contribute to its strength.

- High welding speed and good gas protection should retain the chemical composition of the weld metal. Consequently, the differences in mechanical properties after heat treatment caused by compositional differences between the weld metal and base metal should be negligible.

1.3 Research questions

The following research questions needed to be addressed:

- Can an envelope of permissible parameters be determined for deep penetration laser welding of SSM rheo-cast F357 aluminum which will produce defect-free seams, with acceptable properties?

- Can laser beam welds be produced with mechanical properties virtually indistinguishable from the base material in the T6 temper condition, as opposed to the thermal damage caused by conventional welding processes?

- Does SSM F357 have sufficient quench sensitivity in order to obtain such an increase in strength values during welding, that no post-weld solution heat treatment should be necessary to achieve mechanical properties to the T6 performance specification?

- What are the microstructural characteristics within the optimised area of the LBW window?

- ❖ Are the strengthening mechanisms obtained during laser welding and the different heat treatments, consistent with the expected precipitation hardening processes in Al-Si-Mg alloys?

1.4 Dissertation layout

This research work is presented in five chapters. Chapter one introduces the research topic and the objectives thereof. In Chapter two a literature review of relevant research is presented. The experimental procedures applied during this research are detailed in Chapter three. In Chapter four the results are presented and discussed and the conclusions which were drawn from the results are stated in Chapter five.

CHAPTER TWO

Literature Survey

2 Background

It is now well established that the automobile industries are increasing the use of Al-alloys in order to reduce weight and improve fuel economy. Over the past 18 years the usage of Al almost doubled for cars and tripled for light trucks, resulting in Al castings currently fulfilling the bulk of the automotive and mass transport industry's needs. A large proportion of these castings are produced by the high-pressure die-casting (HPDC) process. However, the porosity, low plasticity and fatigue life of components manufactured by the HPDC process, limits the quality thereof and thus the application of these components in high-safety and pressure tightness systems. HPDC components are not heat treatable and possess poor weldability (5).

New processes, capable of producing aluminium components of high integrity and improved performance, were and still are being developed that compare well with the HPDC process in terms of production cost and efficiency. One such process is semi-solid metal (SSM) casting which is based on the concept of decreasing, or even eliminating porosity. In addition to entrapped gas porosity, SSM processing can also reduce the shrinkage porosity due to much reduced processing temperatures (between solidus and liquidus) and the formation of a specific volume fraction of the primary phase prior to mould filling (2).

A semi-solid metal is a thixo-tropic metal (becoming temporarily liquid when sheared and then turning to a gel when static) used in casting and forging operations. For a metal to be thixo-tropic, it must be heated to the semi-solid region of temperatures and have a globular microstructure at the processing temperature instead of a dendrite one. If these conditions are fulfilled, the metal slurry can be formed in a die by a High Pressure Die Caster (HPDC) or a forging machine (6). Nowadays high pressure die-casting is the most applicable process and casters up to 3000 tons are in operation.

There are two versions of SSM technology which can produce metal slurry with the desirable globular structure in terms of shape and size and at a proper semi-solid casting temperature. These are the Thixo-casting and Rheo-casting processes.

2.1 Thixo-casting

Thixo-casting is a two step process. The molten alloy is at first solidified in billet form which will then be heated to a temperature in the liquid/solid interval so that the material can be injected into a die or subjected to a forming process by means of forging (5).

In the first step, a continuous casting process, upgraded with a stirring device, is used to produce solidified metal with a non-dendritic structure. Rods with diameters from 3" to 6" are cast. There are only a few companies in the world which are specializing in this casting/stirring technology and they are all situated in the Northern Hemisphere. During the second step, the rods are cut to billets prior to being heated in an induction machine to the desired temperature. During the heating process, slurry billets with globular structure suitable for SSM forming are produced. A big disadvantage of the thixo-casting process is that the scrap and returns cannot be recycled on site (6, 7).

2.2 Rheo-casting

Rheo-casting is a one step process. The molten metal is treated by cooling or by cooling/stirring from liquid to semi-solid temperature in order to produce slurry which contains globular solid phase particles and is then injected directly into the die (6, 7).

The big advantage of the rheo-process in comparison with thixo-process is that the slurry with globular structure can be made on demand and "in-house". The stock material can be any standard cast alloy used in other casting methods like squeeze, gravity or HPD casting and therefore does not need to be specially prepared imported material with non-dendritic structure. Scrap and runners can be re-melted in the rheo-casting machine and this fact contributes to a lower production cost (6, 7).

Under optimized conditions, the main technological characteristics of the rheo-casting are as follows (5, 8, 9):

- Very low shrinkage and production of near net-shape parts, due to the small temperature range over which solidification of the castings takes place;
- A fine and uniform microstructure due to enhanced effective nucleation and spherical growth of primary crystals during solidification;

- Very low macro gas porosity due to laminar filling and good venting;
- No inter-dendritic micro porosity due to the non-dendritic crystallization;
- Very good mechanical properties, especially elongation and fatigue, due to elimination of most of the cast defects and globular microstructure;
- Production of thin walled components is possible;
- Long die-life due to low thermal shock as a result of low casting temperatures;
- Components can be joined by welding;
- Heat treatment from T0 - T7 is possible, without compromising surface quality or dimensional control;
- Low production cost due to in-house, tailor-made cast metal and low scrap rate;
- Excellent surface quality;
- Allows for the casting of a wide range of alloys including high strength wrought alloys.

A new Rheo-Casting process has been developed at the CSIR (8) and was recently patented worldwide (9, 10). Process equipment has been designed and constructed and the technology was applied for casting of automotive components. Further development for commercialization is in progress.

2.3 Laser welding

A laser beam, as a controllable, clean, and concentrated high-intensity heat source, can readily heat, melt, and evaporate almost all materials and has therefore been used as a welding heat source. Laser welding is widely used in industrial production owing to the advantages such as (11):

- Low and precise heat input, thus less thermal distortion and greater accuracy;
- Small heat-affected zone;
- Deep and narrow fusion zone with almost parallel fusion boundaries—the aspect ratio (depth/width) of keyhole laser-welded seams is commonly around 4:1;
- High productivity resulting from high welding speed;
- Welding of a wide range of materials (steel, Al, Mg, Ti, superalloys) and dissimilar materials;
- Good process flexibility and reliability;
- Ease of automation.

Laser welding is generally done in either the conduction or deep penetration (keyhole) mode. In conduction welding, the surface of the material is heated to above its melting point but below its vaporization temperature and fusion occurs only by heat conduction through the welding melt pool. A weld bead with a hemispherical cross section with an aspect ratio of 1.2 or less is formed in a similar manner to conventional fusion welding processes. Conduction welds are limited to materials with thin thickness (11, 12). In contrast, keyhole laser welding needs a higher power density to cause local vaporization. Thus, a narrow and deeply penetrated vapour cavity surrounded by molten metal (Figure 1), with an aspect ratio higher than 1.2, is formed by multiple internal reflection of the beam. The basic difference between the two modes is that the surface of the weld pool remains unbroken during conduction welding but opens up to allow the laser beam to enter the melt pool in keyhole welding (12). The conduction mode causes less perturbation of the weld pool and thus provides lower tendency to entrap oxides and gases during welding. In keyhole welding the laser beam is fully absorbed inside the keyhole and the high level of reflection of the laser beam which is characteristic of conduction mode welding is largely eliminated. Keyhole mode welding, therefore, results in better energy coupling, higher penetration, and high welding speed which are necessary for economic justification (12). Therefore, most applications of laser welding utilises the deep penetration process (11, 12).

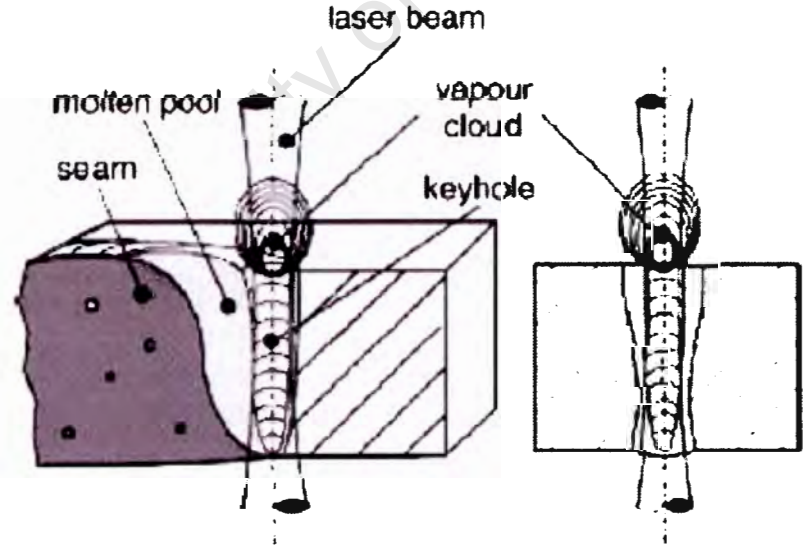

Figure 1: Deep penetration (keyhole) mode laser welding (11), showing the vapour pocket surrounded by liquid metal necessary to produce a deep, narrow weld.

High-power density at the work piece is crucial to achieve keyhole welding and to control the formation of welds, because the energy absorbed should be sufficient to generate and maintain the keyhole. A threshold power density is required to establish the keyhole. The parameters affecting

the threshold power density (irradiance) include the absorptivity of the surface, thermal conductivity and diffusivity of the alloy, heat required to bring the alloy to melting point, heat of melting, beam diameter, travel speed of the beam and joint configuration (trapping of beam will enhance absorption) (11, 13).

Because aluminium is highly reflective and has high thermal conductivity and diffusivity, high laser densities are required for welding of this material. Commercially available laser sources which are capable of producing sufficiently high power output include CO_2, Nd:YAG and fibre lasers. The neodymium-doped yttrium aluminium garnet (Nd:YAG) laser is often the laser of choice for aluminium welding, because the easy manipulation and control of Nd:YAG lasers through optical fibre delivery provides welding opportunities for complex geometries in which overhead, vertical, horizontal, or all-position welding may be carried out (11).

2.3.1 Laser related variables

For a given welding speed the weld penetration depth increases with an increase in the laser power. Similarly for a given laser power the penetration depth decreases with an increase in welding speed. Currently the maximum penetration depth for laser welding is around 25 mm. Excessively high laser power may result in the formation of a laser induced plasma or plume which shields the keyhole from the incident laser beam and reduces penetration (11, 12).

For laser welding the laser beam is focussed onto the workpiece. At the same output power, smaller focus spot size means higher power density but the welds may become too narrow or even not fully fused. Laser welded seams are usually less than one-quarter the width of a tungsten-arc inert gas (TIG) weld for the same material thickness. Joint fit-up and beam alignment are more critical for a small spot size, thus the processing operation window is reduced with the smaller spot size. The high power density associated with a small spot size may also lead to more loss of elements by vaporization as well as spatter which causes undercut and underfill defects. Thus, excessively small spot sizes seldom ensure good welding performance. For a fibre-delivered Nd:YAG laser beam, the spot diameter is dependent on the fibre core diameter and the optical system used for collimating and focusing the beam. Increasing the fibre diameter leads to larger spot diameters and typical spot sizes in industrial laser welding range from about 0.1 to 1.0 mm, with 0.3mm being a common size (11).

The focal plane position is the position of the focal spot, or minimum waist diameter, relative to the workpiece surface. Straying outside the depth of focus (DOF) in relation to the workpiece is unwise because small deviations cause large variations in beam diameter. The focus plane should be set where the maximum penetration depth or best process tolerances are produced. Focusing the laser beam above the workpiece (positive defocusing) produces more plasma which defocuses the beam and reduces the irradiance on the surface, but the keyhole is inherently more stable. The placement of the laser beam focus on or below (negative defocusing) the surface of the workpiece can optimize the laser beam coupling to the material and increase the irradiance inside the weld pool, resulting in lower threshold power density for keyhole formation and therefore a larger weld pool size at negative defocusing compared to the same extent of positive defocusing at a given power and spot size. By slightly focusing the beam below the surface of the material, welding speed could be increased for the same penetration depth than when focusing the beam at the material surface (11, 13).

Different focal lengths are obtainable in laser welding by means of different optical lenses. The focal length determines the laser beam waste diameter, convergence angle and depth of focus. A shorter focal length makes the setting of the focus position more critical, because of less tolerance to the variation in position of the workpiece. A shorter focal length also generates spatter, thermal and vapour damage to the cover- slide glass used to protect the focusing optic and reduces the laser beam's ability to access certain joints and narrow gaps. A longer focal length requires significantly greater power levels to induce keyhole formation and typically, focal lengths of 100 to 200mm are used (11).

Both pulsed wave (PW) and continuous wave (CW) lasers are used for welding of aluminium alloys, but for a first approximation, CW laser welding is used for high speed welding, whereas PW lasers are used for precision welding. Also, either a single beam or multi-beam technique can easily be realised. The term multi-beam or multi-focus is used when more than one spot is produced by combining several beams or by splitting a single beam into several foci. The multi-beam technique originated due to the need for improvement in the process performance and in general can increase the power density of the process, thus increasing the penetration depth or welding speed (11). With single beams, the standard methods to enlarge seam width are to reduce travel speed or defocus the beam. Defocusing the laser beam however results in lower process efficiency, e.g. reduced power density and thus reduced weld penetration depth. The multi-focus technique on the other hand can

bridge larger gap widths and produce less sensitive weld geometry by widening the keyhole opening, keeping the weld pool molten for an extended period of time and thus ensuring an unhindered escape of evaporated material and the flotation of gas / inclusions. As a result, blowholes and cavities of irregular shape and large size can be drastically reduced or even avoided. Multi-focus techniques can also increase flexibility for adapting power density distribution to geometrical requirements of the joints to control the heat input (11, 14, 15). When using only two spots, it is known as "twin-spot" or "twin-beam" method.

The multi-focus spots can be diverted either longitudinally in the laser beam direction or transversely in the horizontal plane. In the longitudinal arrangement, the distance between the beams can be changed by adjusting the focal length. When diverted transversely in the same horizontal plane, the points can be oriented in any direction to the welding direction and with the opportunity to balance the energy distribution between the points. Typical configurations in the horizontal plane include parallel (cross) or tandem (in-line) arrangements. Compared to the single-beam process, the multi-focus technique provides additional controlling parameters such as the number of foci, spot distance, power distribution, orientation angle to the welding direction and beam arrangement. Small distances between the foci lead to deep and narrow weld seams, whereas large spot distances result in shallow and broad seam geometries. An in-line arrangement of foci leads to high penetration depths resulting from the preheating effect of the first beam. By contrast, the cross-arrangement leads to broad seams (11, 15). However, under certain multi-focus conditions and optimum parameters, it was found that there is no great difference in penetration for cross and in-line arrangements. It is also thought that the beam arrangement has less influence on process stability than the beam distance, especially in partial penetration welding (15).

The distance between the multi-focus beams can be changed and can range from zero (i.e. a single spot) up to the maximum value applicable for a specific system set-up. It has been observed that the penetration depth becomes shallower when a longer beam distance is used and it is attributed to the weaker interaction of the dual beams, which can be explained in terms of energy efficiency calculated by the ratio of absorbed energy to input energy. It is therefore important to choose an optimum beam distance that provides both stability and penetration depth (15).

2.3.2 Process related variables

Welding speed is a function of material, laser power, and penetration depth. Penetration is inversely proportional to the speed for a given mode, focal spot size and power and an increase in welding speed at constant laser power therefore results in a corresponding decrease in penetration depth and weld volume, because of the reduction in the heat input applied to the component. The welding speed for a given thickness or depth of penetration increases with power. When the welding speed is too low for a given power and material thickness it leads to excessive melting, sagging, loss of material and weld perforation. Higher welding speeds reduce alloying element evaporation and produce fine microstructures, causing an increase in tensile strength of the weld. The range of welding speeds that produce acceptable welds varies with laser type, material properties and thickness, but the economic objective is always to maintain welding quality at high welding speed (11).

Inert gas shielding is normally applied during welding to prevent face and root oxidation of the weld metal, to prevent degradation of the weld by controlling the convection in the melt pool, to suppress the formation of a plasma plume and to protect the optic lenses from weld spatter and fumes (11). A poorly shielded weld will exhibit porosity, undercut, and bead roughness. In order to prevent oxidation during welding, it is required from the shielding gas to displace all the air / oxygen away from the weld surface (11). Process gas should thus be present in the welding interaction region and close control of the underbead shielding is also required to achieve a smooth underbead. Gas flow is dictated by the shield geometry, type of nozzle, nozzle configuration, nozzle diameter, pressure, and mass flow rate (16).

Most laser welding systems use a small diameter, gas jet tube placed at an angle of 30° - 60° to the metal surface and aiming at the laser beam spot on the metal surface where the metal vapour is coming out of the keyhole (13). The stand-off distance between shielding gas nozzle and the work piece differs from application to application and gas may be delivered coaxially or from a separate nozzle (off-axis). The off-axis gas jet (nozzle) can be either leading (gas flow direction is opposite to the welding direction) or trailing (gas flow is in the same direction as the welding direction.).

Pure helium, a helium–argon mixture or pure argon is often preferred as shielding gas. Helium has higher ionization potential and therefore resists plasma ignition and offers greater weld penetration

and smoother weld surface (17). However, it is much more expensive than argon and helium is lighter than air, thus it tends to rise away from the weld. Argon usually provides better shielding for Nd:YAG lasers (18) and is both cheaper than helium and heavier than air, but is readily ionized by the metal plasma and thus absorbs considerable laser energy. The percentage of absorption rises with increasing power levels, but at lower power levels the energy absorption beneficially slows the solidification rate and yields smoother beads than when produced in helium. The best solution may be a compromise, i.e. a mixture of helium and argon. Welds produced with argon as the shielding gas exhibited root and centerline porosity while helium produced finely distributed porosity (11).

2.3.3 Metallurgy of laser welding

Laser welding is a fusion welding process and therefore also produces three different metallurgical regions, namely fusion zone (FZ), partially melted zone (PMZ) and heat affected zone (HAZ). These regions are categorised according to the temperatures experienced during welding and are generally narrower than those of conventional welding processes. The solid material that surrounds the weld pool acts as a heat sink and leads to high temperature gradients at the interface (19) resulting in solidification rates of up to 10^6 °C/s for high energy density laser and electron beam welding processes. The fusion zone, which is completely melted at temperatures above the liquidus of the alloy, is characterised by fine-grained microstructures due to the high solidification rates (19). The grain structure in laser–welded AA5xxx and AA6xxx Al alloys primarily consist of fine columnar dendrites originating from the fusion line and some equi-axed grains in the weld centre (20), with the amount of equi-axed grains decreasing with increasing travel speed (21).

The columnar dendritic morphology has crystallographic orientation identical to that of the adjoining solid at the fusion line because of epitaxial growth from the adjacent melted substrate (19). The columnar grains grow approximately normal to the welding direction when welded at higher speeds. In contrast, welds produced at lower travel speeds have their columnar grains curve away from the normal to the welding direction and align themselves with the welding direction. The orientation of the grains was reported to have important effects on the ductility of the welds (21).

The PMZ experiences maximum temperatures ranging between the eutectic and liquidus temperatures of the alloy and the low melting point eutectic phases therefore commonly meet at the

recrystallized grain boundaries during laser welding. The partially melted zone in laser-welded Al alloys is very narrow, approximately one or two grains wide (19, 20).

The HAZ has its maximum temperature below the main eutectic temperature of the alloy, thus no bulk metal melting happens in this zone during welding. The softened region is defined as the region where hardness values fall below 90% of the base metal hardness. Thus, although the HAZs of laser-welded joints are very narrow, many solid-state reactions such as grain growth and precipitate coarsening may occur (19, 20).

For the heat-treatable alloys, the thermal cycle associated with the welding process will destroy the temper in the weld and HAZ. Hirose et al. (22) measured the hardness distribution of 2.5kW CO_2-welded 6061-T6 alloy joints in the as-welded condition. It was found that there is a large drop in the hardness of weld metal with minimum hardness occurring in the HAZ. The large drop in WM hardness is mainly due to loss of precipitates (dissolution of strengthening phases and the formation and growth of non-strengthening phases, i.e. full or partial reversion of Guinier-Preston (GP) zones and formation of incoherent precipitates). Loss of hardness in the HAZ is mainly due to overaging. Natural aging can partly recover the loss of hardness in the weld metal and heat-affected zone but not restore the hardness to the same level as that of the base metal. Solution and aging heat treatments after welding can be used to recover the hardness to the level of the base metal. However, it is undesirable to perform solution treatment at high temperatures after welding (19).

The mechanical properties of weld joints are mainly controlled by welding defects, composition, microstructure and metallurgical states of the weld metal and neighbouring base metal. The presence of defects such as undercut, underfill, porosity and cracks will reduce the mechanical properties of the joints. Alloy composition dominates solid solution and precipitation strengthening. Selective vaporization of volatile constituents from the laser-welded fusion zone degrades the mechanical properties of weld metal. In solid solution–strengthened alloys, loss of alloying elements such as Mg has been reported to reduce the strength and hardness of weld metal because of reduced solid solution strengthening (19, 23). The reduction in Mg concentration was, however, reported to be much less pronounced in keyhole mode than in conduction mode. This is because of the smaller surface to volume ratio in keyhole welds compared to conduction welds and vaporization happening on the surface. The reduction in Mg concentration is also much less pronounced at high power levels and high travel speeds (21).

Increased welding speeds results in higher strengths for most aluminium alloys because of decreased losses of alloying elements, finer microstructures, and minimized undesirable microstructural changes in the HAZ. Therefore, the fastest welding speed possible should be used to achieve the highest strengths (23). However, the welding speed is limited by that required for a stable keyhole. At high welding speeds it is more difficult to stabilize the keyhole which could lead to increased porosity.

2.4 Laser weldability of aluminium

Weldability is defined as: "The capacity of a material to be welded under the imposed fabrication conditions into a specific, suitably designed structure and to perform satisfactorily in the intended service" (24). When evaluating the weldability of materials, the following must be considered (25):

- Possible variation in chemical composition of the weld;
- Uniformity of mechanical properties;
- Level of fracture toughness;
- Degree of surface defects;
- Quantification of metallic inclusions;
- Internal soundness;
- Microstructure;
- Joint geometry;
- Any other application-specific implications.

Good weldability, therefore, starts on the foundry floor where the metal is cast, because impurities and porosity must be kept to a minimum.

Laser weldability of a material greatly depends on the physical properties of that material and although laser welding has become a critical joining technique for aluminium alloys, it is far from a mature and reliable process. All aluminium alloys possess certain inherent characteristics, such as low absorptivity to laser radiation, tenacious oxide films, low boiling point elements, high thermal conductivity (as stated above), high coefficient of thermal expansion, relatively wide solidification temperature ranges, high solidification shrinkage, a tendency to form low melting constituents, low viscosity and high solubility of hydrogen in the liquid state (11). All these characteristics lead to many problems like lack of penetration, porosities, blowholes and liquation/solidification cracks in

the weld bead. Laser welding of aluminium is also particularly sensitive to the loss of alloying elements, e.g. Mg and Zn, due to their high vapour pressures, which can have a profound effect on the strength of welds (11, 12, 24). Inconsistent welding performance can thus be encountered in laser welding of aluminium alloys. Industry, on the other hand, will certainly expect a predictable, repeatable, consistent, and reliable laser welding technique before the process is widely accepted. Much work should therefore be done to define parameter operating windows for the different alloys of interest to produce defect-free laser-welded joints and wider welding operating windows are welcomed for wider applications of laser welding processes. Process specifications for laser welding of aluminium alloys should also be built up to assure the reliable production of aluminium joints (11).

Due to the above-mentioned inherent characteristics of Al alloys, typical power densities needed for aluminium keyhole welding are 1 - $2x10^6$ W/cm^2. Power densities close to the threshold may result in inconsistent weld quality or even in no coupling of laser energy-to-workpiece. Power density that is too high may cause spatter, undercut, underfill, and "drop out" (11, 13). In practice, it is generally advisable not to exceed 10^7 W/cm^2 to avoid heavy ejection of molten material (12). It has also been shown that the threshold power density is reduced with the increase of volatile alloying elements (e.g. Mg, Zn and Li), because these elements help to establish and stabilise keyholes when vaporising because of their high vapour pressures and lower vaporisation temperatures (20, 26).

The surface condition of the material also has a great influence on the energy absorption of incident laser light and hence on the threshold power density required for keyhole welding. A polished surface has lower absorptivity, indicating higher reflectivity of the smooth surface while a sand-blasted surface has twice the absorptivity than a typical as-received surface, indicating that rough surfaces absorb more energy than do smooth ones (27).

Laser welding can be performed with or without filler material and in various environments. However in autogenous laser welding where no filler material is used tolerance to fit-up is low. Butt welding usually requires a machined joint to minimize the gap between the parts. Part fit-up must be good enough to maintain the alignment between the beam and the joint and to avoid bead concavity caused by air gaps. The typical joint fit-up tolerance is 10% of the material thickness with a maximum tolerable gap width of 0.3mm for dual beam laser welding (11).

There are also stringent requirements for the clamping and fitting of workpieces, because the small laser beam diameter leaves little tolerance for the variation of workpiece positions. Compared to traditional welding, the laser process produces a very narrow weld bead, with minimum thermal distortion, but excessive heat input during aluminium welding can cause considerable distortion, particularly in thin sheets. Aluminum components, therefore, should be carefully fixtured before welding to assure the repeatable accuracy of welding joints in a production environment (11).

Aluminium usually has continuous oxide layers on the workpiece surface because of its high chemical affinity for oxygen. A high-power Nd:YAG beam can easily penetrate the surface oxides and produce consistent welds of aluminium alloys in the as-received condition, but the porous oxide films contains moisture which is absorbed especially over extended periods in high humidity and fluctuating temperature environments. The presence of the oxide layer will cause porosity in the welds due to the dissociation of moisture which will induce hydrogen porosity (20). Therefore, some traditional techniques such as mechanical scraping / wire brushing, or chemical etching are recommended to remove such oxides in preparation for welding. In addition, workpiece surfaces may also contain some lubricants, such as oils, or may be specially treated. Little is known about the effects of these surface conditions on the absorptivity of laser beams and the welding performance of Al alloys (11), but it is known to produce hydrogen porosity (20).

The porosity in aluminium laser welds can also be caused by a variety of other factors, including the welding speed, focusing conditions and keyhole instability. It seems that the collapse of the keyhole during welding plays an important role in the production of pores, because pore-free welds can be produced at higher welding speed and high beam intensity, which are keyhole stabilizing conditions. Vaporization of Mg or Zn during welding also plays a significant role in cavity formation (19).

Hydrogen is the only gas that is appreciably soluble in aluminium and its alloys. All gas porosity precipitated in aluminium alloys is thus attributed to hydrogen because hydrogen is highly soluble in molten aluminium and is therefore readily absorbed during welding. During the cooling and solidification of molten aluminium, dissolved hydrogen in excess of the extremely low solid solubility is rejected at the solid–liquid interface, resulting in the formation of bubbles. Unless these bubbles can escape to the melt surface, gas porosity will be present in the solidified metal. No tolerable hydrogen content limit has been reported for laser-welded joints in aluminium alloys (19).

High cooling rates are unfavourable for the growth and flotation of hydrogen bubbles because of the decreased time available for the diffusion or flotation of hydrogen. Thus, the high cooling rates experienced in laser welding lead to the formation of small bubbles (micropores) and lower pore number densities and volume fractions (28). Hydrogen in aluminium is mainly formed by the release of hydrogen through the reaction of molten aluminium and water vapour. This may originate from porous oxide layers containing moisture. Grease, oil, dirt, paint or other contaminated surface layers on the workpiece contain carbohydrates and/or water which also release hydrogen in the weld pool (19).

Even with proper surface preparation, aluminium alloys are still susceptible to random macro-porosity caused by the collapse of keyholes or turbulent flow within the weld metal. Keyhole stability during laser welding depends to a high degree on the balance of forces active inside the keyhole. Upon the establishment of the vapour cavity, the fluid forces of the molten pool are balanced by the vaporization pressure within the cavity (29). The inherent instability of keyholes may lead to periodic collapse of the liquid metal surrounding the vapour cavity and thereby causing the formation of periodic voids. They are large enough to be visible with X-ray analysis and are usually located in the keyhole path, whereas hydrogen pores are more or less equally distributed with slight enrichment at the fusion line (29, 31). One way to reduce this type of porosity is to keep the keyhole stable, but this is only achievable in high-speed welding (30). Another approach relies on the "shaping" of the keyhole geometry with multifoci Nd:YAG systems (19).

Laser-welded joints are characterized by high degrees of anisotropy and the inhomogeneity of the joints will have important effects on their mechanical properties and service. The condition of the material before welding has also been shown to be critical for the strength obtained after laser welding. If welded in T4 condition, the tensile strength of heat-treatable alloys is lowered to between 65% and 85% of that of the base metal but the yield strength remains unchanged, whereas aluminium alloys in T6 condition show reduction in tensile and yield strengths of between 65% and 85%. The autogenous butt joints usually fail in the weld metal, whereas the joints with addition of filler metal fail in the parent material/HAZ (19, 31).

In general, all laser welds performed in aluminium and aluminium alloys exhibit mechanical properties which are poorer than those of the base metal (12, 32). However, some claims have been made that welding wrought aluminium in the solution heat-treated temper (T4) condition followed

by only a post-weld artificial aging treatment will recover the hardness of the entire weld, almost to the same level as that for the base metal (22, 33, 34).

2.5 F357 aluminium alloy

Al-Si-Mg casting alloys are being used in automotive applications, aerospace applications and other uses requiring heat-treatable permanent mould castings that combine good weldability with high strength and toughness (1). These alloys are also known for their excellent castability, corrosion resistance and, in particular, a range of mechanical properties in the heat-treated condition. A357 aluminum alloy has been extensively used for semi-solid processing for more than three decades, and a large amount of components like fuel rails, engine mounts, engine brackets and suspension parts have been produced (2). This alloy is also included in the Statement for Work between CSIR and Boeing Co, USA (3, 4).

F357 aluminium is an Al-7%Si-0.55%Mg alloy which in this study also contains 0.025%Sr as a microstructural modifier. The difference between alloys F357 and A357 is in their beryllium content, with F357 containing no Be. The addition of beryllium to this alloy system (A357) leads to a change in the morphology of the iron rich intermetallics, which results in slightly better ductility. Alloy A357 is gradually being phased out in many applications due to the carcinogenic effects of beryllium, particularly at higher concentrations used during the preparation of the alloy (35).

F357 is a heat-treatable alloy with a relatively high eutectic content and due to the normally low porosity no distortion and/or blistering of the components are obtained. These castings are usually heat-treated to obtain the desired combination of strength and ductility. Age hardening has been recognized as one of the most important methods for strengthening aluminium alloys and involves strengthening by coherent precipitates that are capable of being sheared by dislocations (36).

The heat treatment of age-hardenable aluminium alloys involves solution treatment followed by quenching and then either aging at room temperature (natural, T4 temper) or at an elevated temperature (artificial, T6 temper). In the solution heat treatment, the alloy is heated to a temperature just below the eutectic temperature of the alloy for sufficiently long times to produce a nearly homogenous solid solution. The alloy is then quenched to room temperature at a rate sufficient to inhibit the formation of Mg–Si precipitates, resulting in a non-equilibrium solid

solution which is supersaturated. During age hardening, the alloy is heated to an intermediate temperature (below a meta-stable miscibility gap called Guinier-Preston (GP) zone, solvus line) where nucleation and growth of the Mg–Si precipitates can occur. The precipitate phase nucleates within grains and at grain boundaries as uniformly dispersed particles. The holding time governs the extent to which precipitate growth occurs and the mechanical properties that are attained (37). It is well accepted that the precipitation sequence responsible for age hardening of Al-Si-Mg alloys is based on the Mg_2Si precipitates, represented by the following stages (38, 39):

$\alpha_{SSS} \rightarrow$ GP zones$\rightarrow \beta'' \rightarrow \beta' \rightarrow \beta$

where α_{SSS} stands for α supersaturated solid solution, β'' and β' are the meta-stable precursors of β, and β is the equilibrium Mg_2Si phase.
AK Gupta, et.al. describe it as follows (40):

$SSS \rightarrow (Mg+Si)_{clusters} / GP(I)_{spherical} \rightarrow \beta'' / GP(II)_{needles} \rightarrow \beta'_{rods} + Si + others \rightarrow \beta_{plates} + Si$

The strength of the alloy is determined by the size and distribution of precipitated particles as well as the coherency of the particles with the aluminium matrix (41). The natural aging response of these alloys is considered to be due to (Mg+Si) clusters/particles and GP zones, whereas peak hardening with artificial aging results from the precipitation of the meta-stable and coherent β''.

Mg is thus intentionally added in these castings to induce age hardening and thus strengthening. An increase in Mg content results in an increase in strength, due to the formation of a higher density of hardening β'-Mg_2Si precipitates (42). However, the increased Mg content decreases the ductility and fracture toughness of the material. This suggests that, while Mg achieves the aim of making the aluminium matrix age-hardenable, it might also influence the microstructure and particularly the type and morphology of brittle phases (5, 32). It was however observed that the ductility was also affected by the combination of Mg and Si concentration. Higher silicon level led to a reduced ductility even after a long solution treatment, which resulted from the increased amount of Al-Si eutectic. Thus, solution heat treatment of the foundry alloys leads to two more-or-less competing changes in the microstructure. On the one hand, micro-stresses from the formation of meta-stable β'-Mg_2Si precipitates lead to an overall reduction in ductility in the aluminium; on the other hand, the solution heat treatment leads to changes in the silicon's morphology, hence increasing the ductility (42).

The mechanical properties of age-hardenable Al-Si-Mg alloys depend on the rate at which the alloy is cooled after the solution heat treatment, because the precipitation hardening effect is proportional to the level of super-saturation after solution treatment and quenching. Quenching is thus a crucial step in the suppression of the precipitation, the retention of the super-saturated solid solution, the control of the distortion and the minimization of the residual stress in aluminium alloys (43).

2.6 Effect of solution heat treatment and quench rate on F357 aluminium

Ma, S. (41) did an in-depth literature study on the effects of quench rates on the mechanical properties of cast aluminium alloys. It is stated that the optimum solution treatment time and temperature depend largely on the casting method, the extent of modification and the desired level of spheroidization and coarsening of silicon particles. A solution treatment of cast Al-Si-Mg alloys in the range of 400-560°C (with dissolves the hardening agents (Mg_2Si particles) into the α-Al matrix, reduces the micro-segregation of magnesium, copper, manganese, and other alloying elements in aluminium dendrites and spheroidizes the eutectic silicon particles to improve the ductility (Figure 2) (44, 45). The amount and rate of dissolution increase with increasing solution treatment temperature, which in turn is limited by the solidus temperature (41).

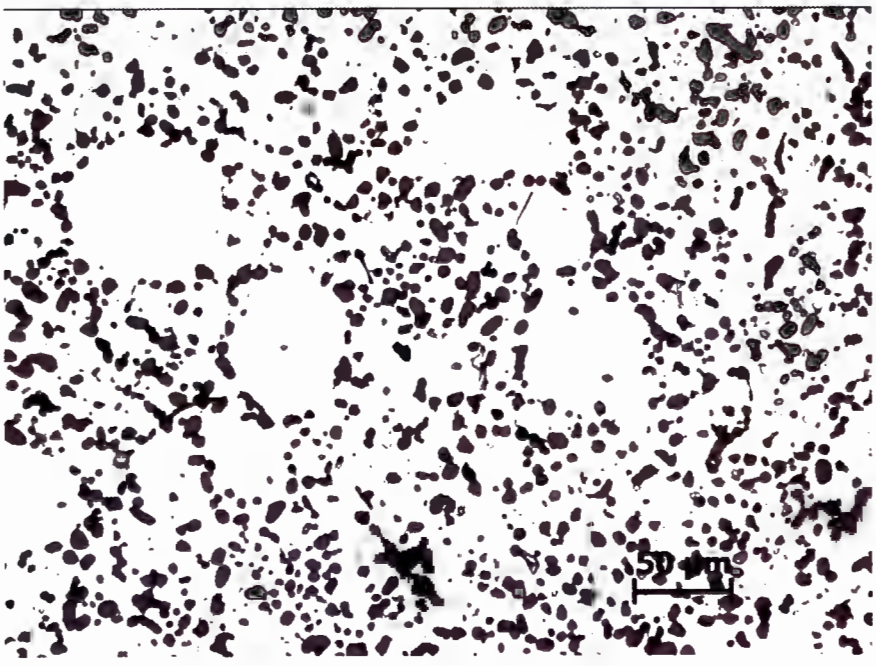

Figure 2: Optical micrograph showing the typical microstructure of a rheo-diecast (RDC) A357 alloy after T6 heat treatment. The dark particles are spheroidised eutectic Si and the fine, light-grey particles are Mg_2Si (5).

The objectives of quenching are to suppress the precipitation during quenching as well as to retain solute atoms and quenched-in vacancies in solution (43). Cooling rates should be selected to obtain the desired microstructures and to reduce the duration time over certain critical temperature ranges, e.g. regions where diffusion of smaller atoms can lead to precipitation at potential defects (44).

The best combination of strength and ductility is achieved from a rapid quenching. However, although a high quench rate is essential to achieve high strength, in many cases such a quench rate can not be used due to problems with high internal stress and distortion. This is especially true for cast components with complex shapes and thin sections. To ensure that the minimum required strength is obtained throughout a cast component, the effects of quench rate on the strength of casting alloys need to be understood (46, 47, 47).

In a study done on cast Al-7%Si-0.4% Mg alloy, it was reported that the average quench rate within the temperature range of 200°C to 450°C was the most critical in influencing the strength. Quench rates in the range of 0.5°C/sec to 250°C/sec were investigated after the samples were solution treated at 540°C for 14 hours and subsequently aged at 170°C for 6 hours. From Figure 3 it can be seen that the peak hardness wasn't affected by the quench rate when the quench rate was higher than 110°C/ sec., but when the quench rate was reduced to 0.5°C/ sec, the peak hardness decreased to only about 78% of the peak hardness obtained with 250°C/ sec. (43).

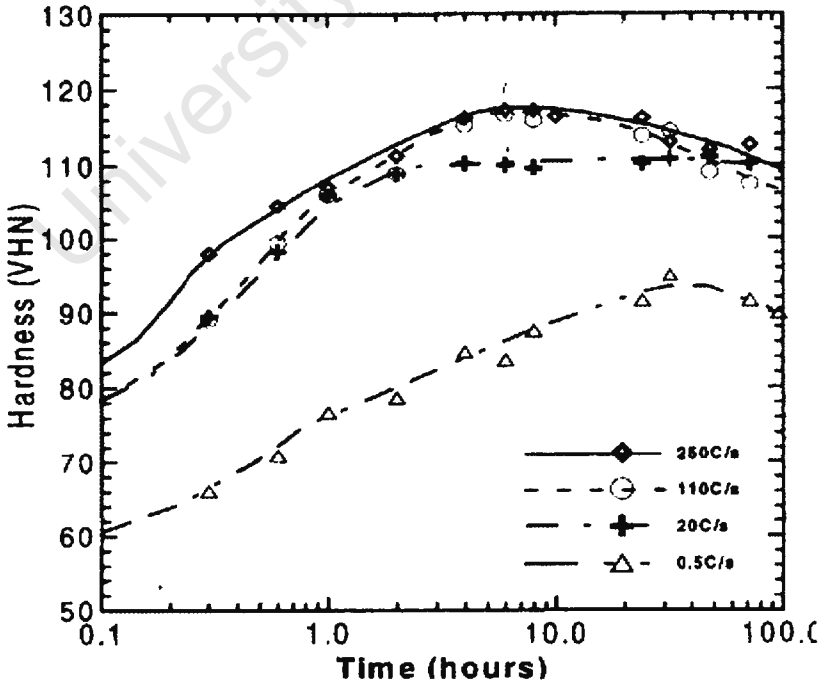

Figure 3: Hardness profile of cast aluminium alloy A356 vs. aging time at 170°C for different quench rates (43)

From the microstructure analysis, it was observed that the quenching condition only influenced the nature of Mg_2Si-type precipitates in the α-matrix produced during the subsequent artificial aging and did not influence the size and shape of eutectic silicon. TEM examination of the peak-aged samples showed only β"-Mg_2Si precipitates (3-4nm diameter, 10-20nm length) to be present in the matrix if samples were quenched at 250°C/sec. The number of precipitates decreased and the size increased slightly when the quench rate was lowered to 110°C/ sec. and a further decrease in quench rate down to 0.5 °C/sec resulted in more areas containing coarse rods of β'-Mg_2Si precipitates (15nm diameter, 300nm length) and surrounding precipitate-free zones (PFZs) in the α-Al matrix (Figure 4). The yield strength and UTS of the peak-aged cast aluminium alloy A356 decreased respectively by 33% and 27% as the quench rate decreased from 250°C/sec to 0.5°C/sec (41, 43, 43, 48).

L. Pedersen and L. Arnberg (42) showed that the UTS of AlSiMg alloys is strictly related to the Mg level whereas the combination of Mg and Si determines the ductility. It has also been observed that a reduction in the quenching rate leads to a reduced strength and an increased ductility in Al-Si-Mg alloys with a high Mg concentration, while the ductility of low Mg alloys was relatively unaffected. The reduction in strength was related to the lower density of hardening precipitates Mg_2Si, which in turn can be related to the amount of vacancies present. A reduced quenching rate allows vacancies to move, partly cluster within the α-Al, and partly move out of the α-Al by diffusion to surfaces and probably also to areas near the silicon particles. An increase in ductility with decreasing cooling rate for high-Mg alloy was attributed to the lower level of excess silicon in the matrix due to the formation of Mg_2Si, resulting in the formation of silicon precipitates of smaller size during the quenching. While for rapid quenching the entire growth of the Si precipitates took place during the subsequent aging and the relatively low temperature resulted in Si precipitates of moderate size, which decreased the ductility. However, for a low-Mg alloy, either an increase in the number of Si precipitates or an increased coarsening of the silicon precipitates was expected. The effect of a reduced amount of hardening precipitates thus was "neutralized" by the increased amount of brittle silicon precipitates and the expected overall increase in ductility wasn't observed (42).

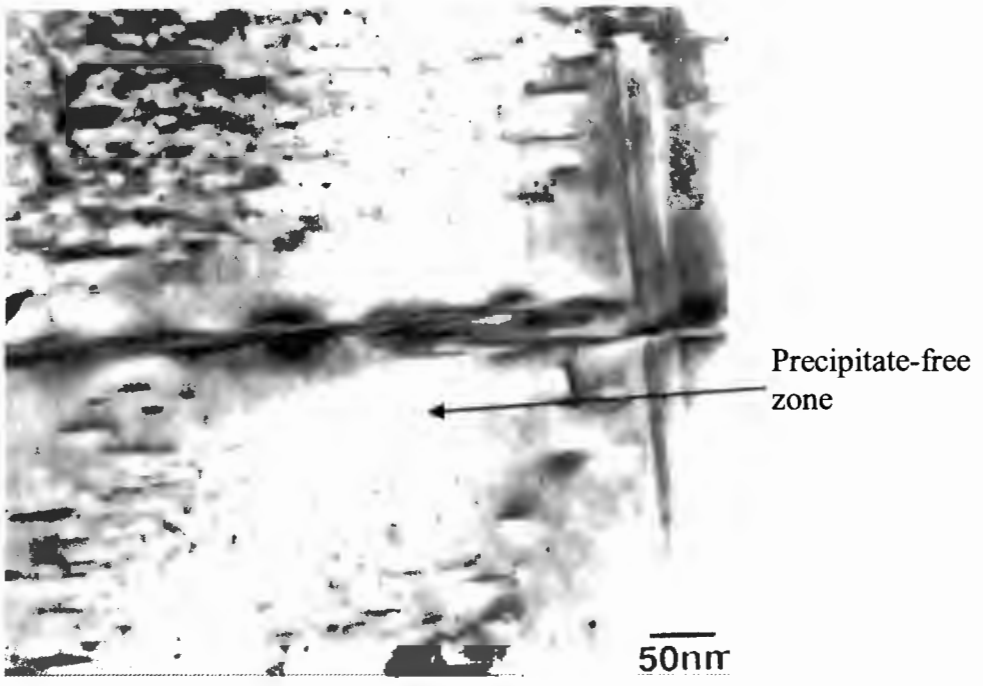

Figure 4: TEM micrograph showing fine β"-Mg_2Si and coarse β'-Mg_2Si precipitates and precipitate-free zones in the α-Al matrix of peak-aged A356 alloy corresponding to an average quench rate of 0.5°C/s (43).

2.7 Quench Factor Analysis (QFA)

Depending on the cooling rate during the quenching process, the precipitates heterogeneously nucleate at the grain boundaries or any available defects present in the α-aluminium matrix. This kind of precipitation can result in the reduction in the super-saturation of the solid solution, which decreases the ability of an alloy to develop the maximum strength attainable with the subsequent aging treatment. In order to strike a balance between the mechanical properties and distortion/residual stress, quantitative measurement of the strength resulting from different cooling rates is needed for the quenching process design (41, 49, 49).

The dependence of the mechanical properties on quench rate is called quench sensitivity. The development of Quench Factor analysis makes it possible to quantitatively determine the variation in attainable mechanical properties due to heterogeneous precipitation during continuous cooling. Thus, the Quench Factor analysis quantifies the quench sensitivity of aluminium alloys. However, in order to employ this analysis for the property prediction in industrial practice, the transformation kinetics during quenching needs to be obtained for generating the Time-Temperature-Property (TTP) curves for the alloy of interest. A variety of methods have been used over the years to

estimate the kinetic parameters of wrought aluminium alloys during quenching, but these parameters are not available for most of the cast aluminium alloys and therefore Quench Factor data for aluminium castings is still rare in the literature (41).

Quench Factor analysis is therefore a tool for predicting mechanical properties of an alloy with a known quench path and precipitation kinetics described by the applicable TTP curve. The advantage of this method is that it provides a single number to correlate the cooling rate during quenching with the strength attainable from the subsequent aging. The QF analysis, developed by Staley (49), is able to successfully predict yield strength and hardness of wrought aluminium alloys (41).

The Quench Factor is typically calculated from a cooling curve and a C_T function. TTP curves for aluminium alloys, which are analogous to TTT diagrams for steels, are graphical representations of transformation kinetics of an alloy and a C_T function is an equation that describes these transformation kinetics. The first Time-Temperature-Property (TTP) C-curves for aluminium alloys were developed by Fink and Willey (50) and the C_T function was defined by Evancho and Staley (51). The assumptions behind the analysis are that the precipitation reaction during quenching is additive/iso-kinetic and the reduction in properties can be related to the loss of super-saturation of the solid solution during quenching.

The C_T function could be expressed using the following equation (49, 52, 53, 54, 55):

$$C_T = -K_1 * K_2 * Exp\left[\frac{\left(K_3 * K_4^{\,2}\right)}{RT\left(K_4 - T\right)^2}\right] * Exp\left[\frac{K_5}{RT}\right] \qquad (1)$$

C_T is the critical time required to form a constant amount of a new phase or reduce the strength by a specific amount; K_1 is a constant which equals the natural logarithm of the fraction untransformed during quenching (typically 99%: Ln (0.99)= -0.01005); K_2 is a constant related to the reciprocal of the number of nucleation sites; K_3 is a constant related to the energy required to form a nucleus; K_4 is a constant related to the solvus temperature; K_5 is a constant related to the activation energy for diffusion; R is the universal gas constant, 8.3143 J/K*mole; T is the absolute temperature (K).

The incremental Quench Factor, q_f, is calculated for each time step on the cooling curve (Figure 5 and Figure 6) and represents the ratio of the amount of time the alloy was at a particular temperature, Δt_i, divided by the critical time required for a certain fraction of precipitation or certain reduction in strength to occur at a temperature (C_{Ti}) (55). The incremental Quench Factors are summed up over the entire transformation temperature range (T_1 to T_2) to produce a cumulative Quench Factor, Q (49, 54, 57, 58, 59):

$$Q = \sum q_f = \sum_{T_1}^{T_2} \frac{\Delta t_i}{C_{Ti}} \tag{2}$$

Lower Quench Factor values are associated with rapid cooling and high attainable strength. The critical Quench Factor value is the maximum value that can result in the desired strength and this value can be defined in terms of the maximum amount of transformation during cooling (55). With a known Quench Factor, the as-aged strength can be predicted using the following improved formula, based on the strengthening theory (54):

$$\frac{\sigma - \sigma_{min}}{\sigma_{max} - \sigma_{min}} = \left[Exp(k_1 Q)^n\right]^{1/2} \tag{3}$$

where σ_{max} is the maximum value of strength which is obtained by solution heat treating a thin specimen of the alloy followed by an instantaneous quench to room temperature and a subsequent age-hardening, and σ_{min} is the strength obtained by very slow, controlled cooling.

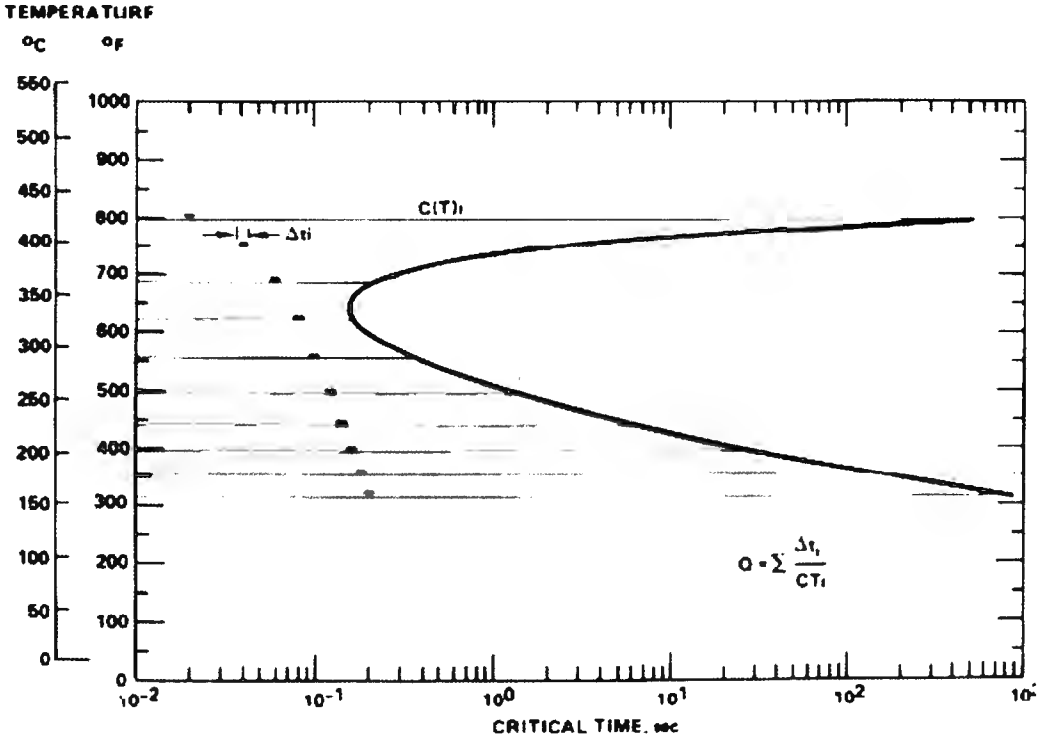

Figure 5: Schematic illustrations on plot of C_T function to calculate the quench factor (55).

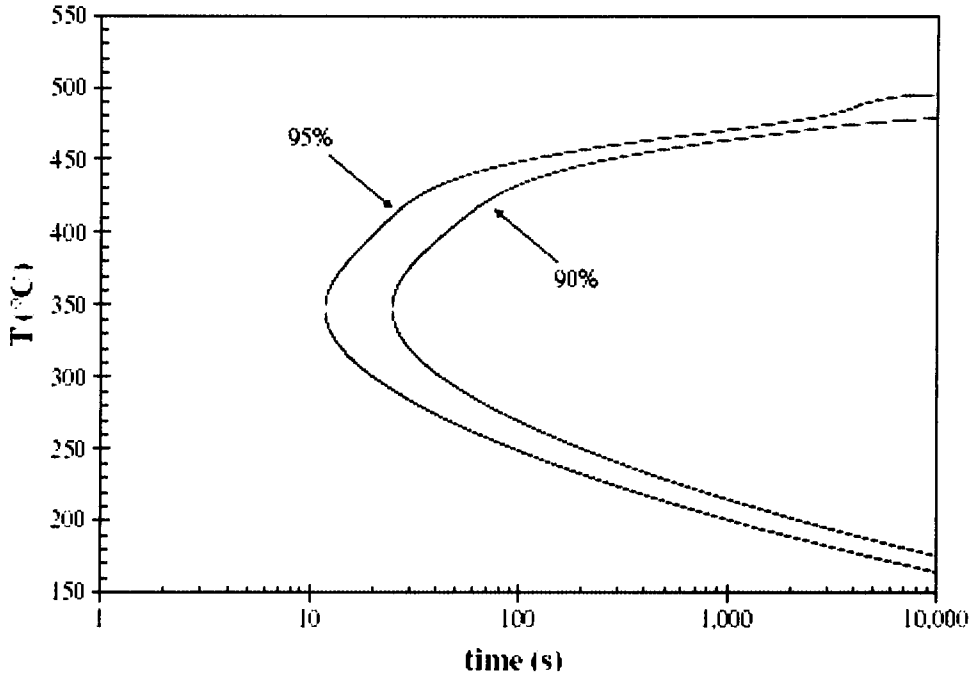

Figure 6: 95 and 90 pct iso-yield strength contours (56)

Quench Factor analysis has been applied to a wide range of wrought aluminium alloys to predict properties and/or optimize industrial quenching procedures (41, 48, 55, 57, 60, 61, 62, 63, 64). It has also been applied to steels and aluminium castings and is now recognized as an important technique for modelling property loss during continuous cooling (53).

CHAPTER THREE

Experimental Techniques

3.1 Rheo-casting of F357 aluminium

The well-known A357 aluminium was cast without Be, therefore the notation F357. The molten aluminium was degassed with Ar for an hour before casting, in order to obtain a non-porous product (Verified by tests – Figure 7). The CSIR rheo-process utilizes a shear dispersive mixing action which is provided by an induced electromagnetic field supplied by an AC induction coil, together with air cooling to obtain the desired semi-solid temperature (Induction Heating /Stirring Process). The metal in the mushy state is transferred to the shot chamber of the 50ton High Pressure Die Casting (HPDC) machine for casting of the plates required for this project. The chemical composition was closely controlled and the process was carried out according to the CSIR procedure (10). F357 aluminium samples were cast into 90mm×100mm plates with 6mm thickness.

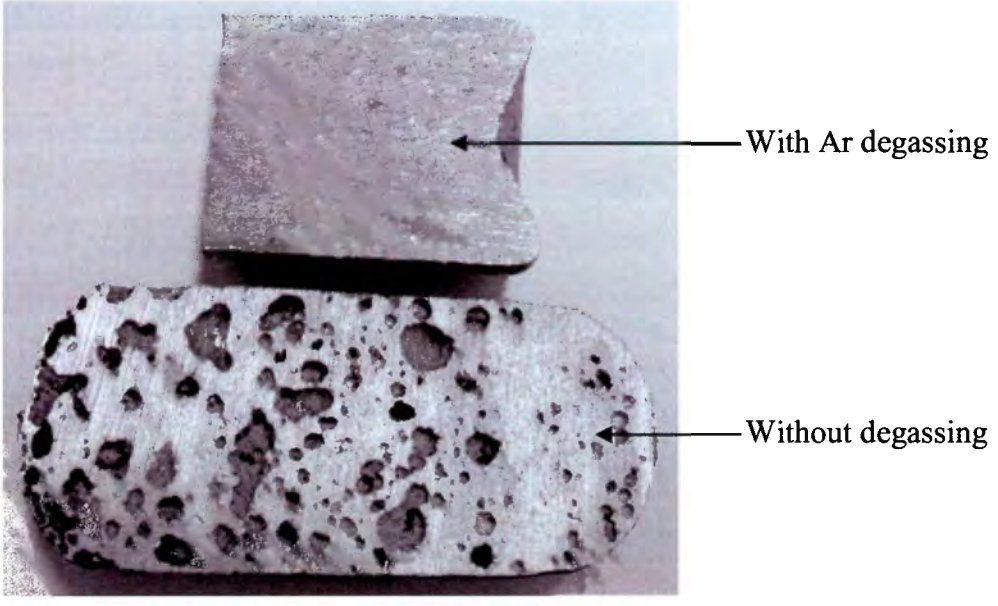

Figure 7: F357 aluminium billet without Ar degassing and with degassing for an hour (top)

3.2 Chemical analyses

All the chemical analyses in the project were done by means of a ThermoFischer Quantris Optical Emission Spectrometer. From each cast batch, randomly selected plates (including the first and last

plate) were chemically analysed and the compositional ranges of the cast material used in this study are given in Table 1.

Some laser welded joints were also chemically analysed in order to determine the compositional variation between the weld metal and base metal after heat treatment. The weld fusion zone (± 4mm width) were mechanically separated from the surrounding base metal and cut into pieces. The thickness of each weld joint was reduced by 50% by compression, followed by annealing at 450 °C for 30 minutes. Some of the remaining base metal along the weld was cut off before the weld sample thickness was compressed again by 50% and annealed. This procedure of pressing and annealing was repeated three times before the weld metal area was big enough (± 12mm width) for spectrometry to be performed (Figure 8).

Table 1: Chemical specification (a) and obtained composition of (b) first batch and (c) second batch F357 rheo-cast aluminium for this study

Element (wt%)	Al	Si	Mg	Fe	Ti	Sr
Min.[a)]	Bal.	6.5	0.4	-	0.04	-
Max.[a)]	Bal.	7.5	0.7	0.2	0.2	-
Min.[b)]	Bal.	6.79	0.65	0.071	0.10	0.010
Max.[b)]	Bal.	7.41	0.72	0.075	0.15	0.035
Min.[c)]	Bal.	6.52	0.70	0.08	0.12	0.020
Max.[c)]	Bal.	6.96	0.71	0.10	0.14	0.030

Figure 8: Flattened F357 weld sample showing the circular positions of the spectral analyses with reference to the weld

3.3 Heat treatments

The cast plates were either left in the as-cast (F) condition, heat treated to the T4 (naturally aged after solution treatment) or T4+ condition or heat treated to the T6 condition (artificially aged after solution treatment) – Parameters given in Table 2. T4+ condition refers to the plates being heat treated to the T4 condition before welding and only artificially aged after welding (no post-weld solution treatment) to reach the T6 condition. This was done in order to compare the effect of welding on the microstructure and properties of F357 in the T4+ and T6 conditions.

The natural aging time period (T4 condition) was set at a minimum of 5 days which is generally accepted in the literature as appropriate for age-hardenable aluminium alloys (1) since no significant increase in hardness is observed thereafter. This assumption was confirmed for F357 aluminium by measuring the Vickers hardness of the material in the T4 condition after different time intervals as is shown in Figure 9.

Table 2: Temper heat treatment parameters applied to the F357 aluminium before welding (pre-weld heat treatments)

Temper condition	Solution treatment	Aging
T4	540°C x 6h → water quenched	Room T for a minimum of 5 days
T4+	540°C x 6h → water quenched	Room T for a minimum of 5 days followed by post-weld annealing at 170°C x 6h after 20hrs at room T
T6	540°C x 6h → water quenched	170°C x 6h after 20hrs at room T

The heat treatment and welding cycles were thus as follows:

T4 : 540 °C / 6h → quenching → natural aging (NA) 5 days → welding

T4+ : 540 °C / 6h → quenching → natural aging 5 days → welding → natural aging 20h → artificial aging (AA) 170 °C / 6h

T6 : 540 °C / 6h → quenching → natural aging 20h → artificial aging 170 °C / 6h → welding (The 'traditional' T6 heat treatment for A356)

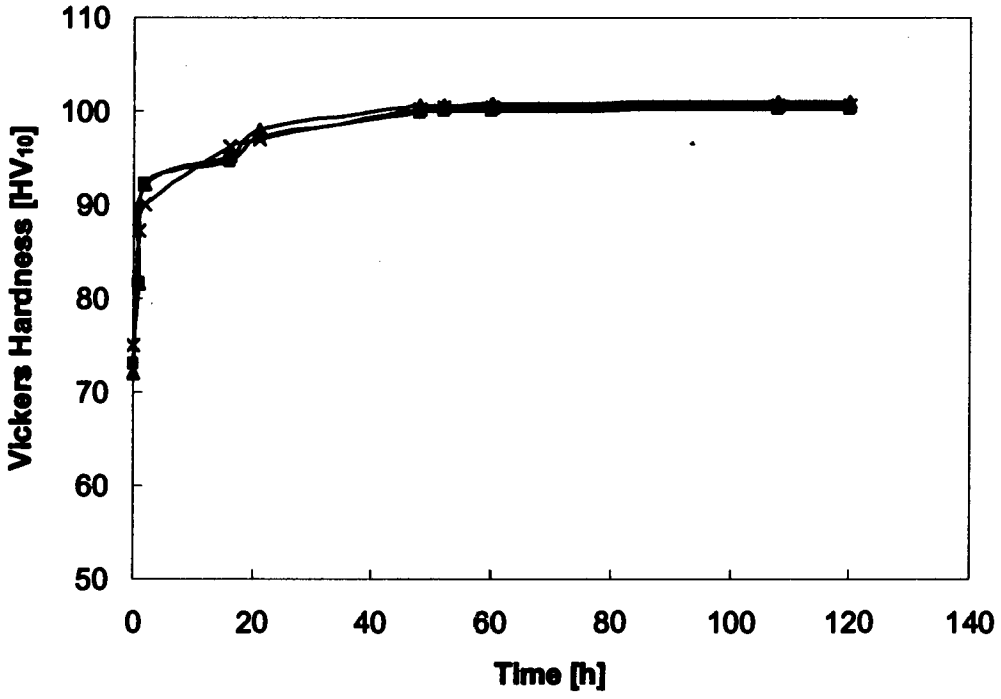

Figure 9: Hardness results of SSM cast F357 aluminium during natural aging (room temperature) at different time periods after solution treatment at 540 °C for 6 hrs.

3.4 Sample preparation

After heat treatment, all plates were skimmed down (both sides) from the as-cast thickness to 3.5mm in order to eliminate possible surface defects or irregularities as well as the deformation obtained during the heat treatments. Machining of edges was also performed (Figure 10) to optimize the fit-up which is important for laser welding. Poor fit-up will produce underfill and may also cause porosity resulting from air that is trapped between the butt faces. This machining was done within 1 hour before welding and after all the applicable surfaces had been wire-brushed (stainless steel brush – Figure 11) to remove the oxide layer. One of the main aims of the steps taken during sample preparation was to remove possible causes of hydrogen induced porosity. This involves the removal of the oxide layer and precautions to prevent contamination of surfaces, which are to be welded, by moisture or hydrocarbons such as oils and grease.

Autogenous butt welding of the F357 aluminium in the F, T4, T4+ and T6 conditions was then executed.

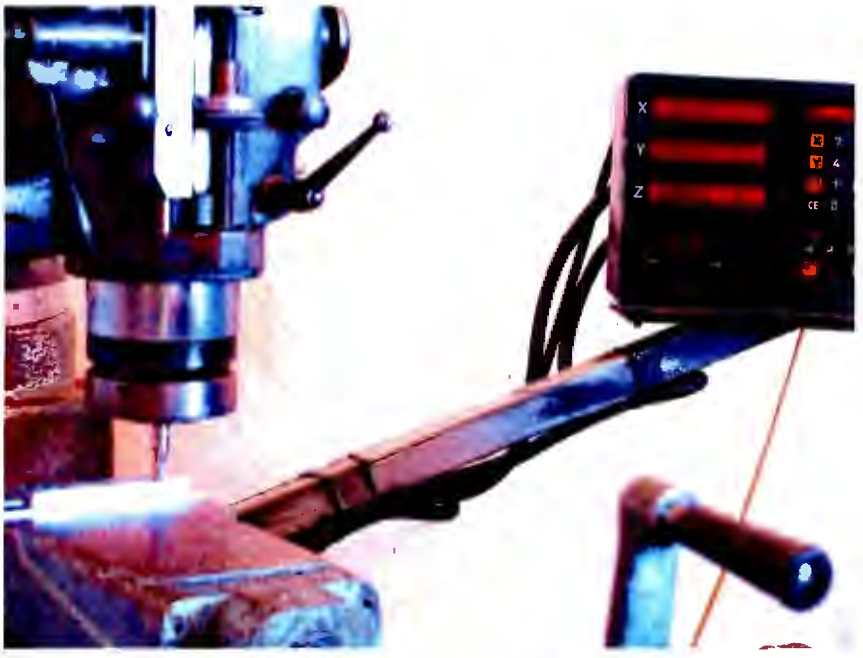

Figure 10: Machining of the sample faces to be butt welded

Figure 11: Stainless steel wire brushing of the sample sides to be butt welded

3.5 Optimization of laser welding parameters

According to the literature (65, 66) hydrogen and keyhole induced porosity and hot cracking are the major problems associated with the welding of aluminium alloys. However, cracking was not found to be a problem when welding F357 aluminium. The determination of a process parameter window

which eliminates porosity and optimizes weld bead geometry was therefore required. The task required the simultaneous optimization of laser power, welding speed, shielding gas composition, shielding gas flow rate and focal condition to produce a weld which is both free of hydrogen / keyhole induced porosity and has an acceptable weld bead geometry. The latter is important since both excessive root formation and weld face under-fill will reduce the mechanical properties.

A HIGHYAG ASK aluminium welding head coupled to a 6-axes KUKA KR60L30HA articulated arm robot was used with a 4.4kW CW (continuous wave) Rofin Sinar RS DY044 diode pumped Nd:YAG laser which was delivered through a 400 micron step index fibre. The combination of a 200mm focal length collimator and a 200mm focal length lens produced a magnification of 1.0 which in turn delivered a minimum single spot size of 0.4mm. However, by means of the variable double-focus forming module of the ASK welding head, a longitudinal twin spot (double focus) configuration could be produced in which the relative intensities of the two spots as well as the spot separations (centre-to-centre) could be adjusted.

Because of the relatively low viscosity of molten aluminium the keyhole is less stable since the molten metal that flows around the keyhole from the front to the back of the keyhole is reflected back towards the keyhole by the solidification front and can close off the keyhole if the keyhole is too small. This will give rise to porosity. The application of a twin spot welding configuration is therefore beneficial for aluminium welding due to a stabilising effect on the weld pool, resulting in smoother beads compared to single spot welding, and a key-hole opening that is less narrow and less prone to closure. This allows the Mg gas that is vaporised during the melting process, to escape and not to generate occluded gases resulting in porosities (65).

First trial laser welding bead-on-plate (BOP) tests were executed in order to determine the best operating window for this material. It was observed that the maximum available power of 3.8kW to the workpiece and a travel speed of 4m/min were the best to obtain deep penetration welding on this plate thickness. Consequently experimentation focused on the optimization of the twin spot parameters, namely spot separation distance and power intensity distribution (Table 9 – Appendix A). However, due to the effect of the twin spot parameters on the depth of penetration, it was necessary to change the welding speed in some instances in order to obtain through-thickness penetration.

In order to obtain a single spot with the dual-focus ASK welding head, the applicable micrometer setting of the ASK unit must be set to 16.0mm. However, because a twin spot configuration was required in this study, the micrometer setting was varied between 16.83 and 17.10mm, corresponding to a centre-to-centre spot separation of 0.38 and 0.53mm respectively. The power intensity distribution was varied by adjusting the applicable micrometer setting between 12.3 and 12.5mm. The 12.3mm setting produces a power intensity distribution consisting of a leading spot with slightly higher power intensity (52 %) than the trailing spot (48 %). The 12.35mm setting produces a 50/50 % power distribution (Figure 12(a)) and a 12.5mm setting produces a leading spot with slightly lower power intensity (45 %) than the trailing spot (55 %) (Figure 12(b)). The power intensity distribution between the two spots should be close to 50/50 % so that both spots contribute to the formation of a keyhole (deep penetration welding), but a slight off-set to approximately 45/55 % (leading/trailing spot power) seemed to result in a more stable keyhole.

Independently from the power intensity micrometer setting (within the range investigated), a 0.38mm centre-to-centre spot separation distance produces a twin spot configuration where the spots slightly overlap each other, with a slight power peak in the overlap region (Figure 12(b)). A 0.48mm distance results in the twin spots being closely next to each other (Figure 12(c)). In order to retain the advantages of twin spot welding and higher welding speeds, the spot separation should be limited since increased spot separation results in an effective reduction in laser intensity.

X-ray radiographic testing was done on all these preliminary welds and the only defect observed, was porosity. A porosity count was done on each sample in order to determine the optimum set of welding parameters and the results are shown in Figure 13. From these results a general trend of decreasing porosity with decreasing spot separation distance (SSD) can be observed. It is suspected that a spot separation distance lower than 0.38mm (closer to single spot) will result in an increase in porosity again due to a less stable weld pool. This was however not investigated. The minimum level of porosity (indicated by arrow on graph) was obtained at a power intensity distribution (PID) of ± 45/55 % leading/trailing spot power ratio. The optimum parameters of 0.38mm SSD, ± 45/55 % PID and 4m/min were therefore used for the laser welding of the F357 samples investigated.

All laser welds were performed in the 1G position (flat groove weld) with the incident laser beam perpendicular to the surface of the aluminium plate. The sample plates were clamped in a butt joint configuration with a specially made jig which provides both perpendicular and transverse clamping, thus limiting distortion and preventing the butt joint from opening up during welding (Figure 14).

The welding jig also allows for a root purge to be applied. For the first batch, Helium (He) at a flow rate of 20 l/min was applied as shielding gas via the ASK off-axis nozzle (7.8mm ID). For the second batch, He at 10 l/min was supplied via a self-manufactured off-axis nozzle (based on a concept used by A. Haboudou, et.al. (65)). This nozzle had a similar diameter, but a much smaller stand-off (2mm) was used and it was inclined at 30° to the horizontal (Figure 15 – Recommendations made by M. Dahmen (Dipl.-Ing.) from Fraunhofer ILT, during a technical visit). Argon (Ar) at a flow rate of 5 l/min was applied as root purging gas. Experiments were conducted with different shielding and purging gasses. Various mixtures of Ar and He were investigated at different flow rates and it was observed that Ar as shielding gas resulted in the most severe weld porosity. He + Ar caused less porosity while He shielding gas produced the lowest levels of weld porosity. The effect of the type of root purging gas on weld porosity was however found to be negligible and Ar was therefore the preferred option due to lower cost.

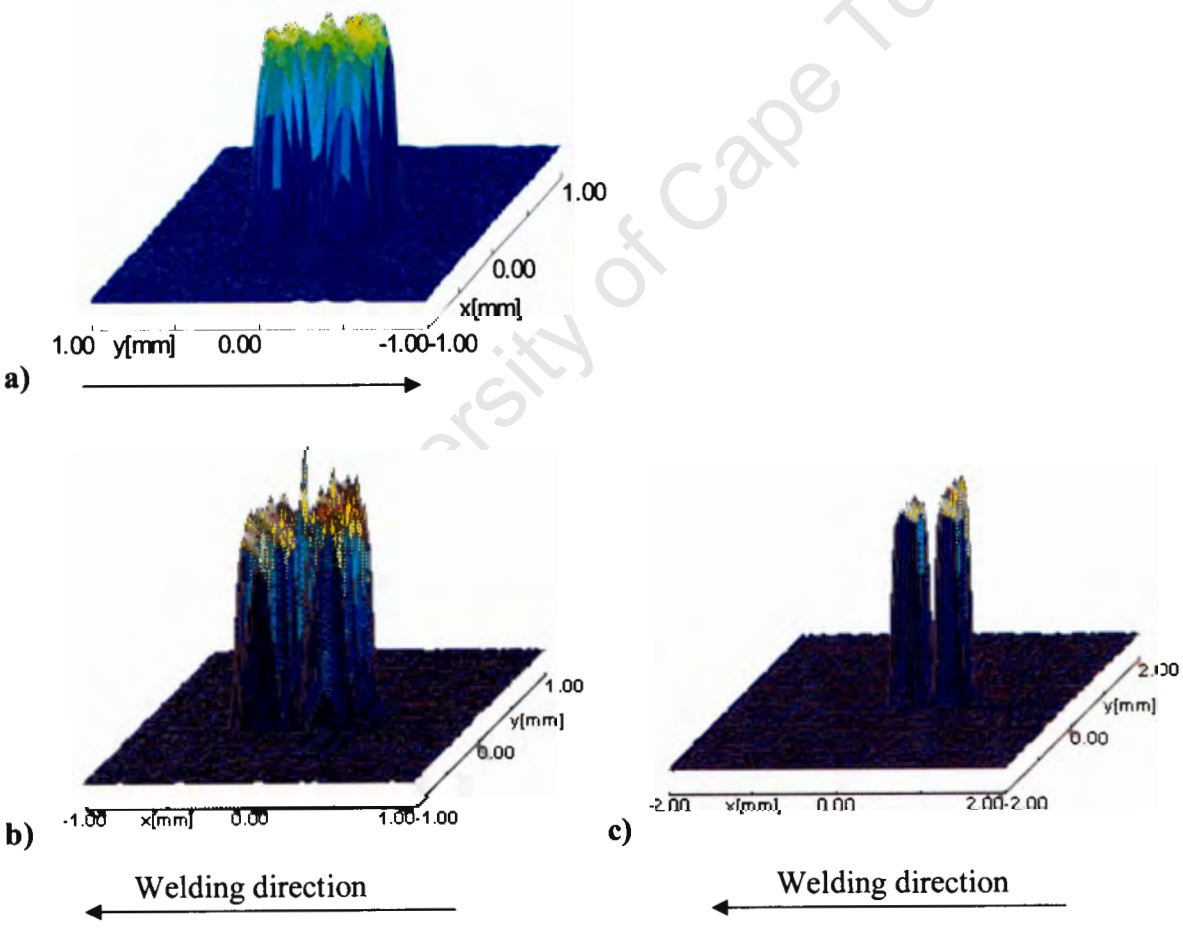

Figure 12: Beam analyses of the ASK welding head twin spots: a) 0.38mm centre-to-centre spot separation and 50/50 % power intensity distribution, b) 0.38mm spot separation and 45/55 % power intensity distribution and c) 0.48mm spot separation and 45/55 % power intensity distribution.

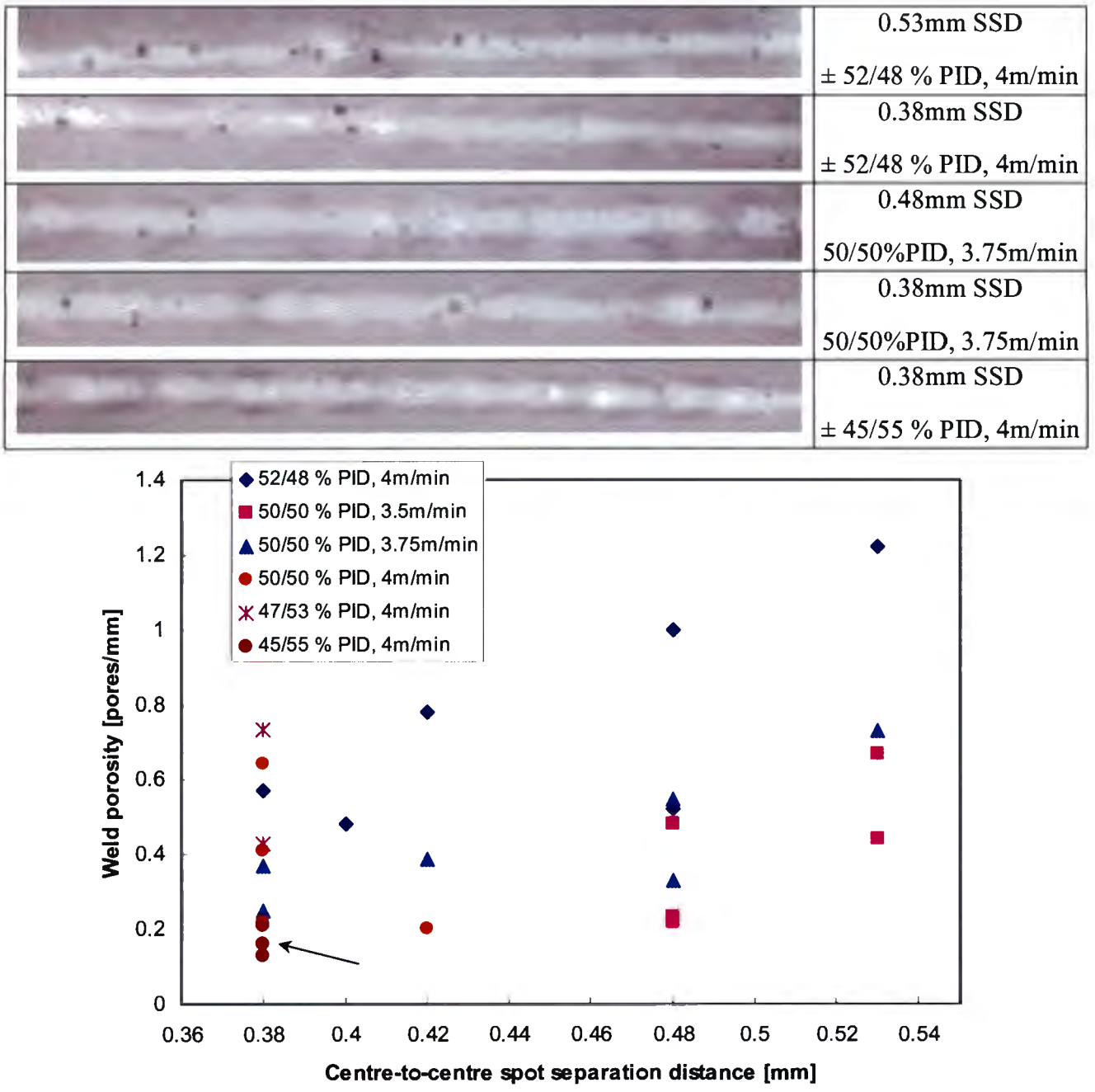

Figure 13: Some radiography results and the matrix of experimental parameters changed during the first trial of laser welding bead-on-plate tests done at 3.8kW power at workpiece, 14 l/min He + 6 l/min Ar shielding gas (leading nozzle) and 5 l/min Ar root purging gas.

The butt welds were performed with the focal plane at the top surface of the plates and centered along the contact line of the plates. All welding was performed in the 1G position (flat groove weld) with the long axis of the dual focal spot orientated in the welding direction (Figure 14). The welding parameters used in this study consisted of a speed of 4m/min, 3.8kW laser power to the workpiece, ± 45/55 % leading/trailing spot power distribution (12.5mm setting) and 0.38mm centre-to-centre

spot separation distance (16.825mm setting). All welds were performed with a leading shielding gas nozzle.

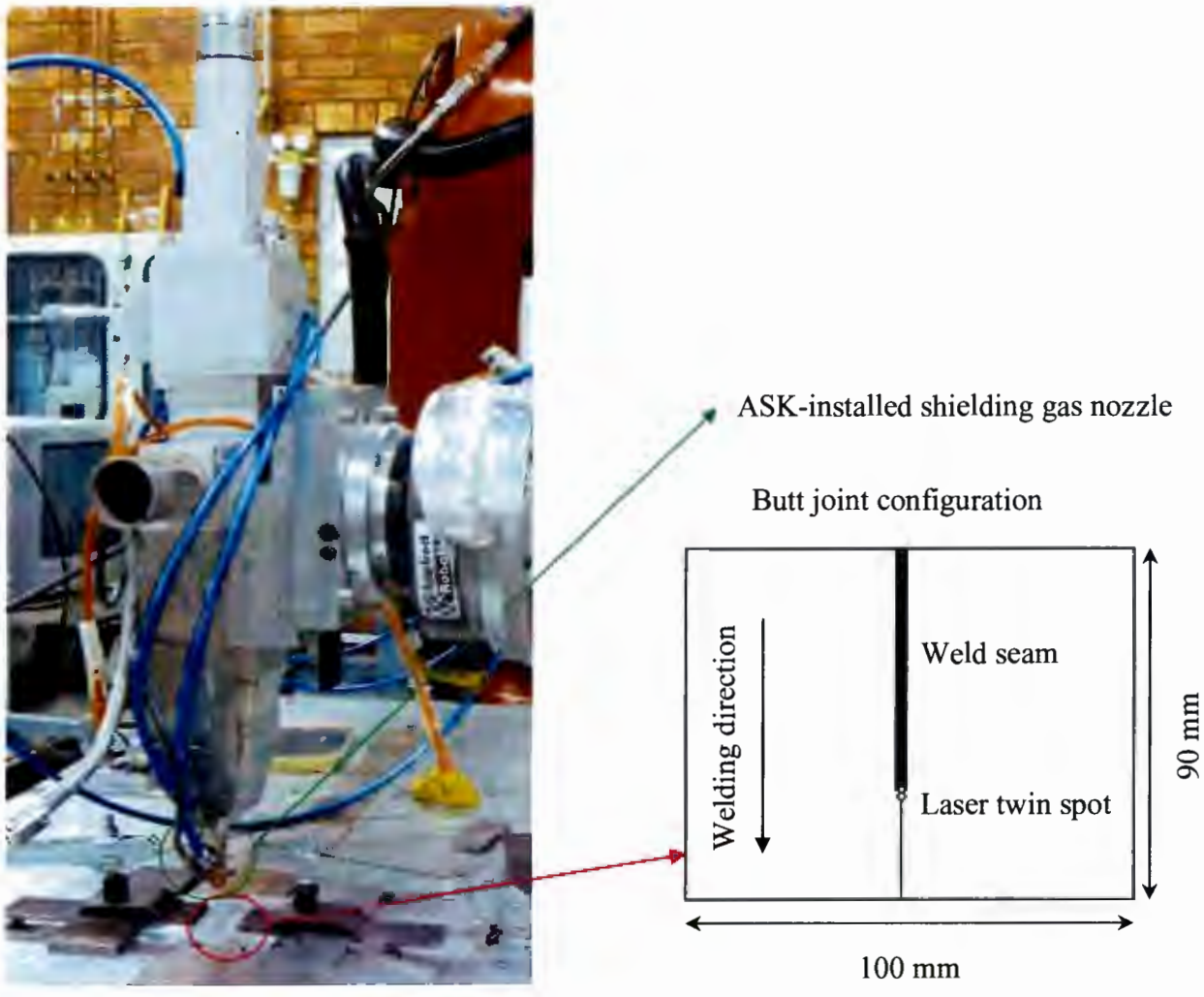

Figure 14: Experimental laser welding set-up, with the HIGHYAG ASK welding head and nozzle, for the first batch of F357 aluminium samples

The welding standard applicable to laser welding of aluminium and its weldable alloys is ISO 13919-2 (68). Weld imperfections in this welding standard are quoted in terms of the actual dimensions, but the standard does not include details of recommended non-destructive methods for detection and sizing, because the examination, inspection and testing requirements should come from the application standard. It is stated that the latter standard should ensure that the specified method(s) of non-destructive examination will be able to give the detection, characterisation and sizing necessary for use within certain classes of imperfections. Due to the absence of a specific customer at this stage and thus an application standard, the F357 butt welded samples were subjected to X-ray radiography testing. Since X-rays are not easy to focus, this method produces

low-resolution images which limits its usefulness to some extent, but it was chosen because it is a well-known non-destructive testing method for welds. The possible limitations are constant in this project and weld porosity is the only internal defect of interest.

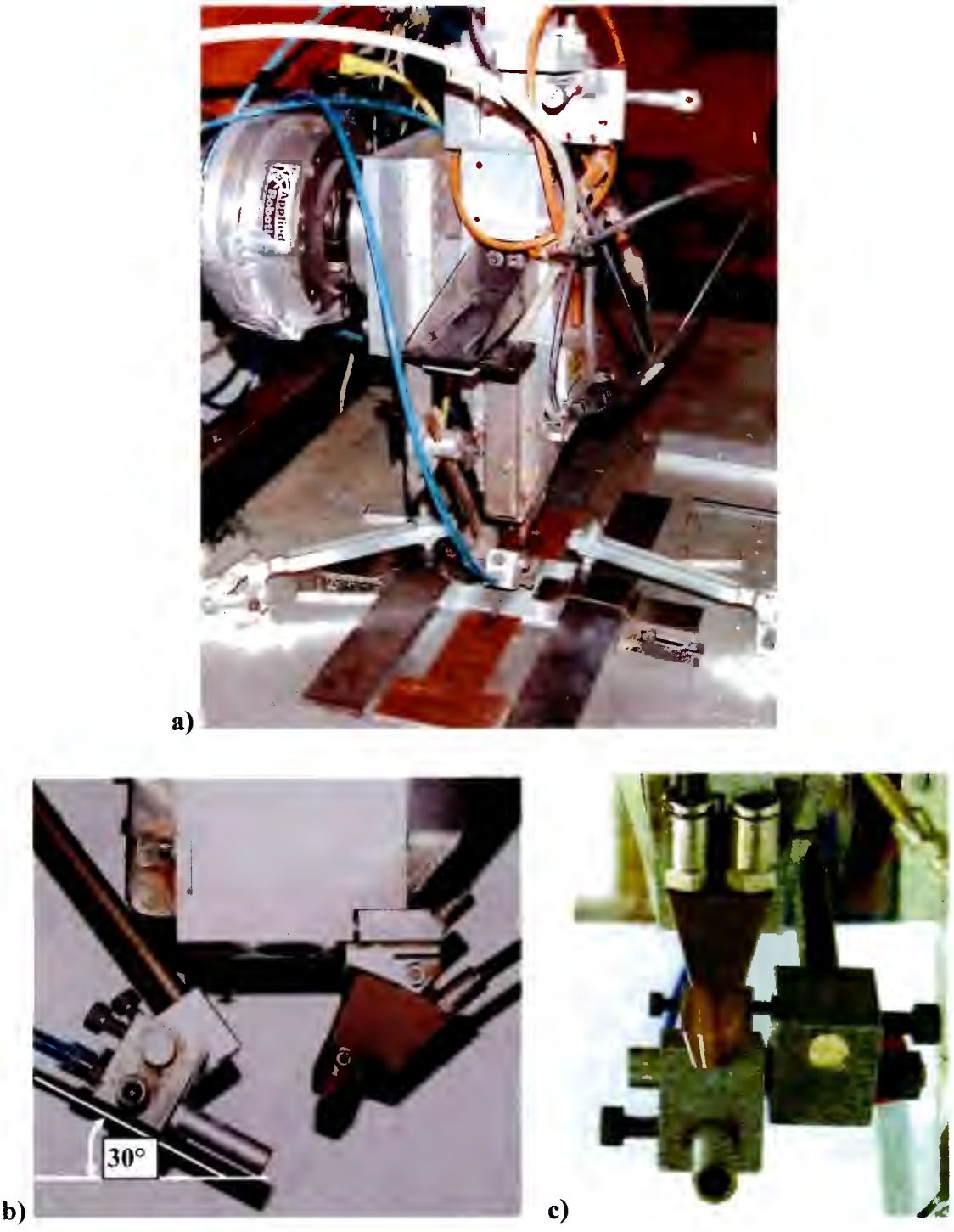

Figure 15: a) Experimental laser welding set-up for the second batch of F357 aluminium samples, with the HIGHYAG ASK welding head but using the self-manufactured off-axis nozzle at an angle of 30° to the horizontal (b) and centred the same as the ASK nozzle towards the twin spot (c).

3.6 Quench rate measurement

In order to establish the quenching effect of laser welding on F357 aluminium, the cooling rate of the material during quenching after solution treatment and the cooling rate during welding had to be determined and compared.

The same sample sizes were used for the cooling rate determination of both the solution treatment (ST) quenching and welding. For the ST quenching, a 1mm Ø hole was drilled into a 100x50mm F357 sample, down to mid-thickness of 1.75 mm. A K-type wire thermocouple (Chromel-Alumel: Ni/5% Al and Si, with a T range of -200 to 1250 °C) was press-fit into the hole with Al wire to ensure good contact. The thermocouple was coupled to a Tektronix TDS 744A oscilloscope for the logging of the cooling data (logging rate of 2500 readings per second). The sample was heated in a muffle furnace to the solution temperature of 540 °C and then quenched in water (room T) during which the cooling data was captured. This was repeated a few times to obtain representative cooling data and to ensure repeatability.

The same K-type thermocouple was at first used for measuring the cooling rate during welding by press-fitting (with a vice-grip) the wire ends into one of the butt faces before setting the samples up for butt welding. However, the welding temperature was found to be too high and the thermocouple, bent 90° upwards towards the face of the weld, was burnt off. The procedure was repeated, but with the thermocouple facing downwards as well as with the thermocouple embedded in a hole drilled at an angle at the bottom of the plate. However, the thermocouple burnt off in the latter two cases as well.

A small C-type thermocouple (W/5% Re-W/26% Re, T range of 0 – 2320 °C) was sourced and used for the next batch of cooling rate experiments. The two ends of the thermocouple were again pressed into one of the butt faces (between the jaws of a milling machine) and bent 90° with the thermocouple facing upwards (Figure 16). Butt welds could be successfully performed with the thermocouple in the weld and the cooling data was recorded by means of the oscilloscope.

All the cooling data was recorded over time as millivolt output readings that were converted to temperatures by means of standard reference tables (ASTM E-230) applicable to either the K or C-type thermocouple. These reference tables are all based on a reference or cold junction temperature

of 0°C, which is the freezing point of pure water, so the effect of the sample being at room temperature, had to be taken into account.

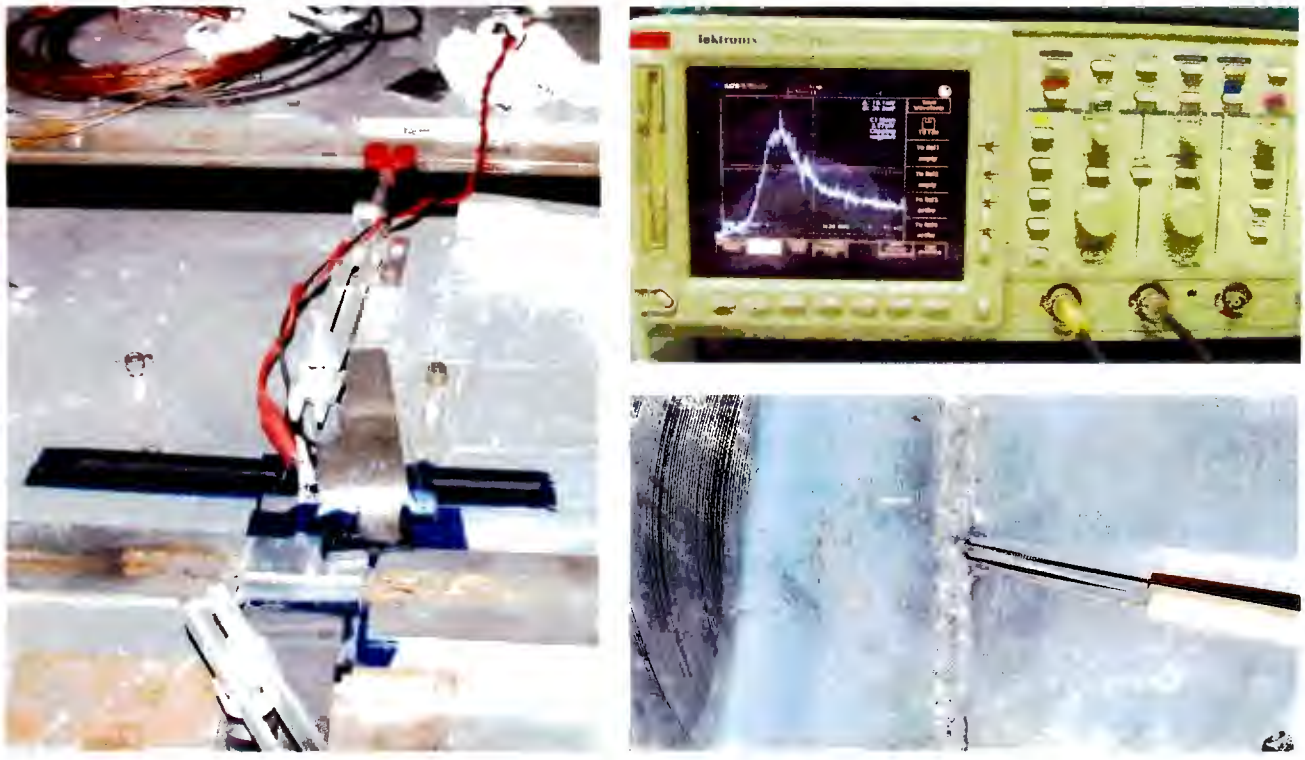

Figure 16: The experimental set-up for measuring the weld cooling rate and electronic isolation of the weld sample (left) in order to obtain a cooling curve with least electronic noise (right top). Bottom right shows the butt weld with the C-type thermocouple pressed into the right-hand side butt face.

3.7 Radiographic testing

All cast plates were radiographically tested before weld preparation and only the plates that passed the ASTM E155 specification for Al castings (67) were used for welding. After butt welding, all the plates were again radiographically tested in order to evaluate the possible internal weld defects.

3.8 Stereo and optical microscopy

Transverse, through-thickness sections of all the base material and weld joints of both F357 sample batches were cut, mounted, polished, etched with Keller's reagent and microscopically analyzed. The weld profile was studied by means of stereo microscopy on an Olympus SZ-CTV microscope from Japan coupled to a CDX Baxall camera. The general microstructure of the base metal and

weld metal was studied by means of optical microscopy in order to also characterise possible internal defects. This work was done on an Olympus BX51M microscope coupled to an Altra 20 Soft Imaging system. The typical microstructure present through the whole cast plate was also characterised.

3.9 Micro-hardness testing

Mounted and polished transverse, through-thickness sample sections were used for hardness measurements. Vickers micro-hardness traverses were done across the weld joints (from base metal to base metal) at mid-thickness for both F357 sample batches and for all the different heat treatment conditions in order to determine the differences in hardness of the base metal and weld metal in all conditions. A load of 300g was used for all micro-hardness measurements, except for base metal hardness determinations, for which a 1kg load was used.

On each sample, hardness traverses were repeated to obtain general representative hardness trends for the material in every heat treatment condition. Between hardness traverses the samples were reground and polished.

3.10 Tensile testing

Transverse sub-size tensile specimens (Figure 17) were machined from the base metal in all heat treatment conditions as well as all the F357 weld seams. The tensile specimens conformed to ASTM B557M: Standard Test Methods of Tension Testing Wrought and Cast Aluminum- and Magnesium-Alloy Products [Metric]. For these weld metal tensile specimens, all the excess weld metal was removed (machined off) so that the thickness of the welds was the same as that of the base material and thus no strengthening effect was obtained from weld build-up. The strength of the weld metal was therefore tested against the strength of the base metal. Weld joint tensile specimens were also machined and tested (on a 1342 Instron machine) for comparison with the weld metal properties. For the weld joint specimens, the weld joint was not altered in any way and the strength of the joint was tested against that of the base metal. Where applicable, no undercut was removed from the tensile specimens, in order to comply with ISO 13919:2 specification requirements (68).

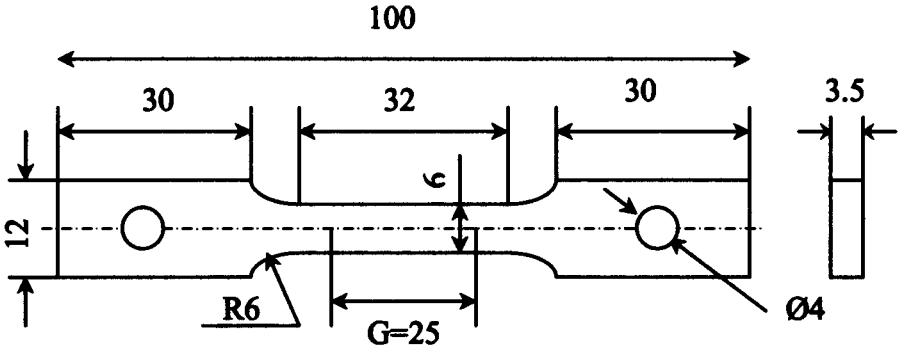

Figure 17: Dimensions (mm) of sub-size tensile specimens machined from the F357 base material and weld joints

3.11 Transmission electron microscopy (TEM)

TEM work was done on the F357 base material, HAZ and weld metal in order to characterise and verify the strengthening mechanisms. The TEM foils were prepared by milling the butt-welded plates down to ± 1mm thickness, cutting off 20 x 20 mm samples and grinding these samples down to ± 0.1 mm thickness (ending with paper grade 800). By using a special tool (die and punch) 10 to 15 disks with 3 mm diameter were cut from each 0.1 mm thick sample. These foils were subjected to double jet electrolytic thinning using a Struers Tenupol-2 apparatus (Figure 18(a)). An electrolyte of 40% CH_3COOH-30% H_3PO_4-20% HNO_3-10% H_2O at ambient temperature was used. The apparatus was set to 8V and pump position at 7 for electrolyte speed. After completion of the thinning process the samples were cleaned in an ultrasonic bath for 2 s. The foil was then removed from the electro-polishing sample holder (Figure 18(b)), cleaned with alcohol and put in a TEM foil sample holder (Figure 18(c)) in order to keep track of the specific sampling position and heat treatment condition.

This TEM foil electro-polishing technique differs from the conventional technique where the process is stopped as soon as a first centre hole is pierced. This is due to the large difference in electrochemical properties of the Si and Al phases of Al-Si alloys that prevents thin foils of good quality from being obtained by the conventional electro-polishing technique. Nowadays ion milling is recommended for thin foil preparation of Al-Si alloys, whereas earlier TEM replicas had to be used (69).

Figure 18: a) Struers Tenupol-2 apparatus used for electro-polishing thin foils from F357 aluminium b) Electro-polishing sample holder and thin foil c) Thin foil organising sample holder

It was found in this work that the "first hole" criterion is thus not applicable for our hyper-eutectic alloy. However, with the above-mentioned double jet technique, it was still possible to obtain good quality thin foils for the TEM investigation on F357 aluminium alloy by using another criterion. The process was carried out until a big hole, about 30-40 % of the polished area of the foil, was eroded (Figure 19(a)). At this stage some α-crystals on the edges of the hole became very thin and transparent. The thinness of the α-Al globules is marked by the visible lineage which might be attributed to polygonisation effects. This is a good indication that the α-crystals are well thinned and suitable for TEM investigation, Figure 19(b).

The foils were studied on a JEM 1011, production of JEOL, Japan, operated at 100 kV accelerating voltage.

a)

b)

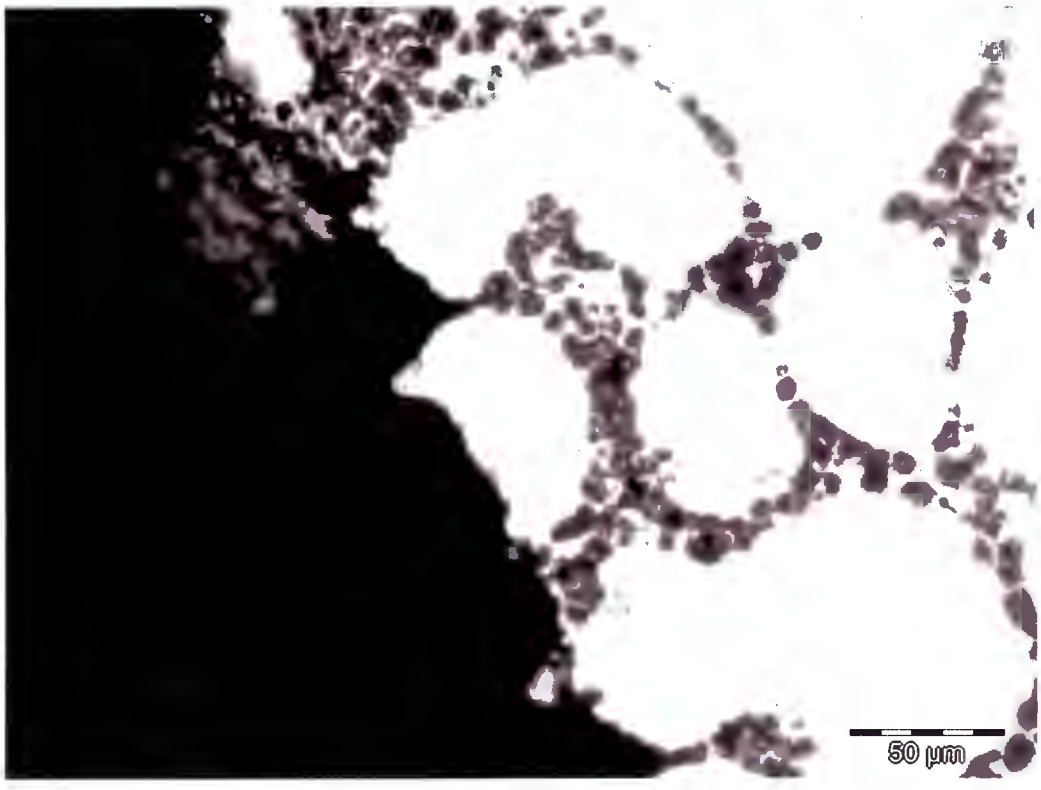

Figure 19: Microstructure of electrolytic thinned F357 foil, showing α-primary crystals surrounded by Al-12%Si eutectic. Perforation of approximately 30-40% of the foil area (a) in order to obtain sufficiently thinned α-Al globules (b) for the TEM investigation.

CHAPTER FOUR

Results and Discussion

4.1 Radiographic observations

Porosity, shrinkage cavities and entrapped dirt/oxide were typical defects which were detected by radiographic testing in some of the cast plates. These defects typically constituted less than 5% by volume. It was not always possible to distinguish between the different defects by means of X-rays. The only internal defect observed in the welds was porosity. All welds were analysed according to the stringent quality level of the ISO 13919-2:2001 specification. Although all welds met the requirements in terms of maximum porosity size allowed, some of the first-batch welds (ASK nozzle used) did not comply with the specification in terms of the localised (clustered) / linear porosity (Figure 20 and Table 6). In general the second batch welds, welded with the custom-made nozzle, revealed less porosity (Figure 24).

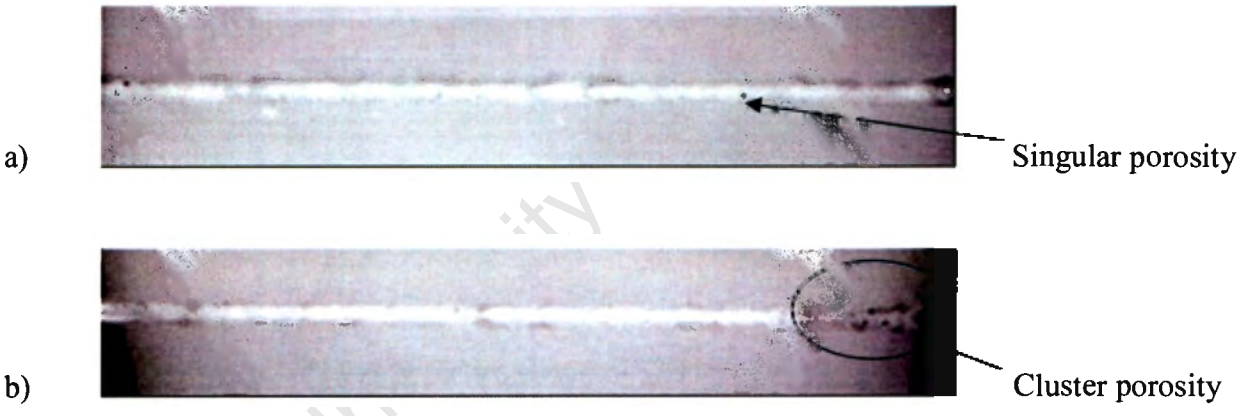

Figure 20: Example of a laser butt weld a) complying with the porosity specifications and b) not complying with the cluster (localized) porosity specification.

4.2 Chemical analyses of the welds

Chemical analyses by means of spectrometry were done on six welded samples which had been prepared as discussed in the chapter on experimental techniques. The results are given in Table 3. From these results it can be concluded that the Mg content of the welds is the same as that of the base metal and has therefore been retained in the fusion metal. It is known that Mg, because of its

low boiling point, tends to evaporate during laser welding and a lower Mg content was thus expected. This was however found not to be the case.

Table 3: Comparison of Mg content in the base metal and weld metal of six F357 butt welds

Sample		Mg [wt%]
F condition	Base metal	0.73
	Weld metal	0.65
	Base metal	0.61
	Weld metal	0.66
	Base metal	0.75
	Weld metal	0.71
	Base metal	0.66
	Weld metal	0.71
T6 condition	Base metal	0.77
	Weld metal	0.78
	Base metal	0.67
	Weld metal	0.67

4.3 Quench rate determination and Quench Factor Analysis

The cooling rate during quenching after solution treatment and during laser welding of F357 aluminium was determined as discussed in the chapter on the experimental techniques. Typical cooling curves obtained during these quenching processes are shown in Figure 21 and depicts the temperature curve from the oscilloscope (via voltage) as well as a calculated moving average curve. The average quench rate of these processes was determined from the graphs and the results are given in Table 4.

Figure 21(a) shows some extreme noise peaks on the temperature-time graph, which resulted from the sample being shaken during quenching (loss of good thermocouple-sample contact) to prevent a steam blanket from forming around it which might have had an inhibiting effect on the quenching. Noise peaks were also observed with data-plotting during laser welding (Figure 21(b)) in spite of good isolation precautions being taken (Figure 16). The average cooling rates could, however, still be determined with relatively good accuracy.

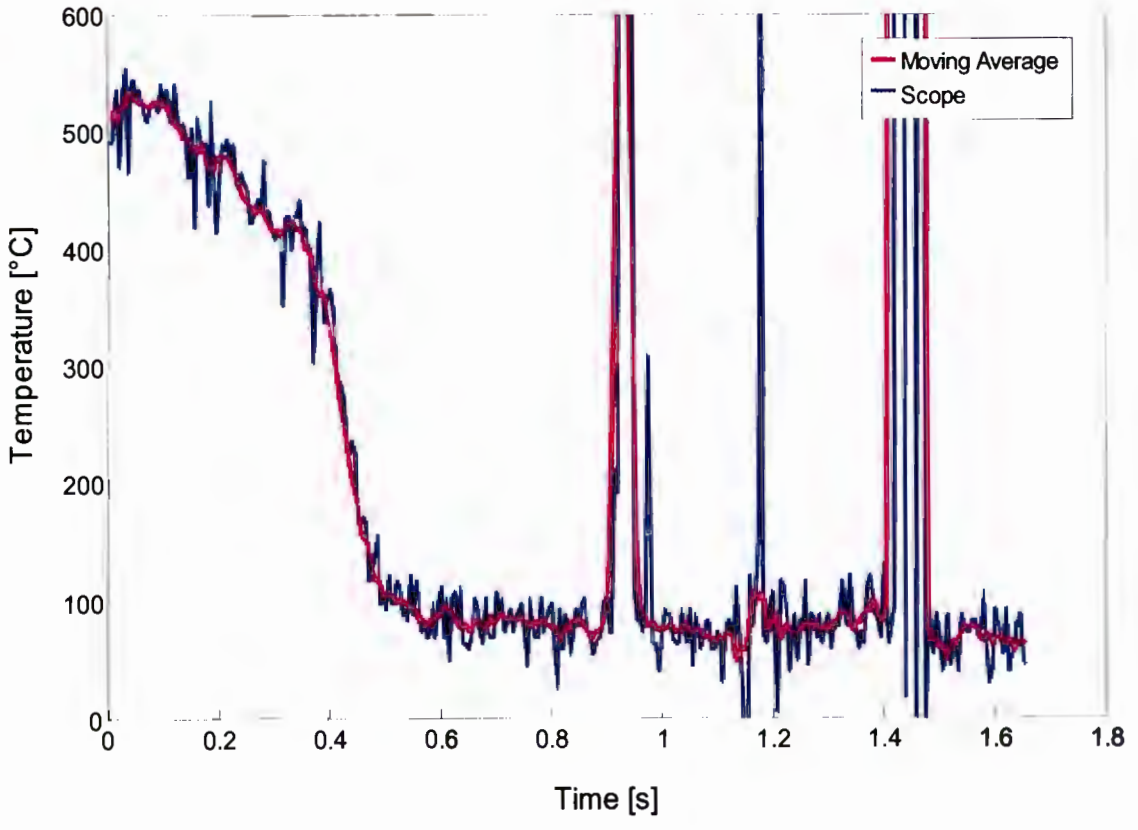

a)

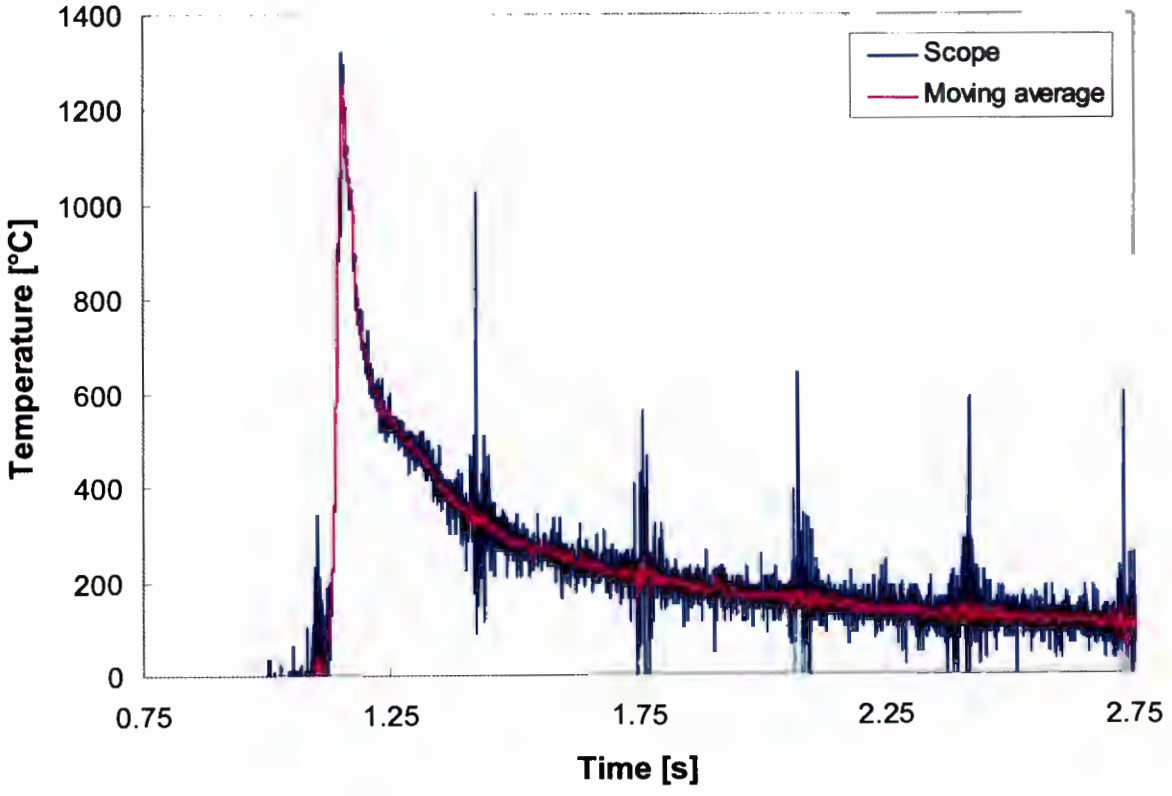

b)

Figure 21: Typical cooling curves for F357 quenching after a) solution treatment at 540 °C and b) during laser welding.

From Table 4 it is clear that there is no significant difference in average quench rate over the whole temperature range (540 to 30 °C) after solution treatment and laser welding, although a range of cooling rate values were obtained. For the quench rate between 450 and 200 °C, which is according to literature (43, 43) the critical temperature range for solid solution treatment of aluminium, a larger range of average cooling rate values were obtained with the laser welding quench rate being slightly lower than that of the solution treatment quenching. However, the latter was determined on sample sizes similar to the weld samples, which is relatively small. This resulted in higher quench rates than that which would be obtained during industrial quenching of big components. In contrast to this, industrial laser welding will result in higher quench rates (much bigger samples, more material to facilitate self-quenching) than was obtained in this study. There is thus a good possibility of the difference between the two average quench rates becoming very small in practice.

Table 4: Average quench rate results obtained after solution treatment at 540 °C and laser welding of F357 aluminium

Process	Average quench rate: 450 to 200 °C [°C/s]	Average quench rate: 540 to 30 °C [°C/s]
Solution treatment	524	353
	700	433
	726	381
Laser welding	430	367
	450	374
	451	257
	529	317
	584	363
	585	331
	595	317
	604	337
	615	344

It should also be noted that the study done by D.L. Zhang and L. Zheng (43) has shown that the peak hardness for Al-7Si-0.4Mg material was not affected by the quench rate when the average

quench rate between 450 and 200 °C was higher than 110°C/s. The measured quench rate after laser welding is thus more than four times higher than the quench rate required for solid solution treatment of this type of aluminium and would therefore explain the good mechanical properties obtained in the T4+ condition.

The procedure for determining the quench factor (Figure 22), presented by Kim, Hoff and Gaskell (73), was followed to calculate the overall quench factor (Q) for F357 aluminium from Figure 23 and Equation 2 ($Q = \sum q_f = \sum_{T=170^0C}^{T=500^0C} \frac{\Delta t_i}{C_{Ti}}$) with temperature intervals of 10 °C. The quench factor technique approximates an actual quench (measured experimentally in the present study) as a series of isothermal quenches, thus allowing transient transformations to be predicted from the isothermal precipitation kinetics.

It has been shown by Razaghian et.al. (74) that the maximum strength of A357 aluminium is only modestly improved by Sr modification, which leads to the assumption that the C-curve for D357 (unmodified) will be similar to that for F357 (modified) and may therefore be used for the calculations. The obtained Q values for solution treatment quenching and laser weld quenching of F357 aluminium are given in Table 5.

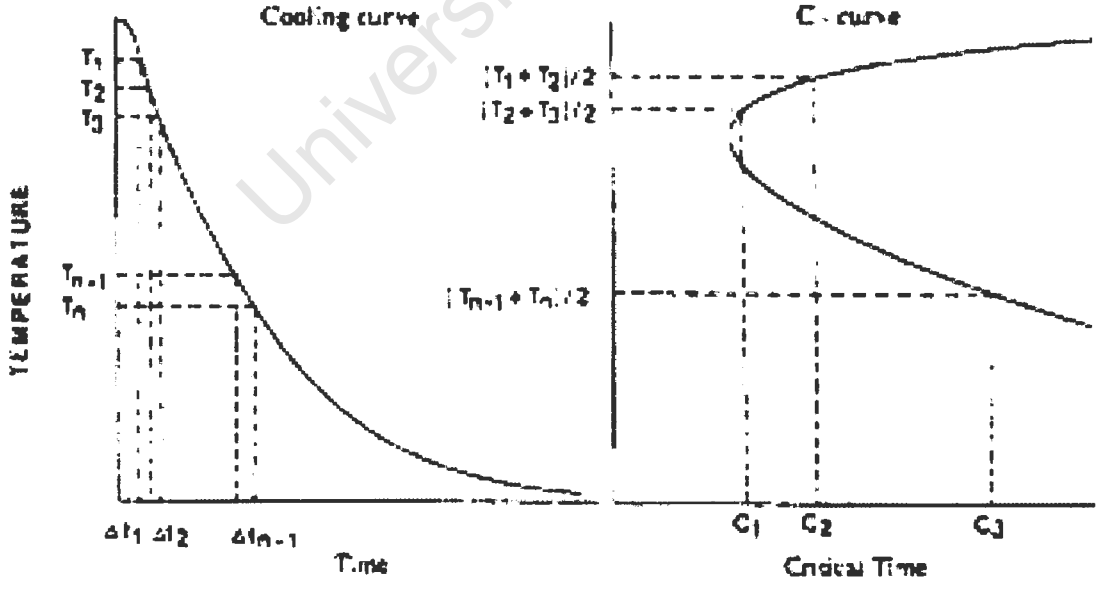

Figure 22: Determination of quench factor by the combination of a quenchant cooling curve and a C-curve (73)

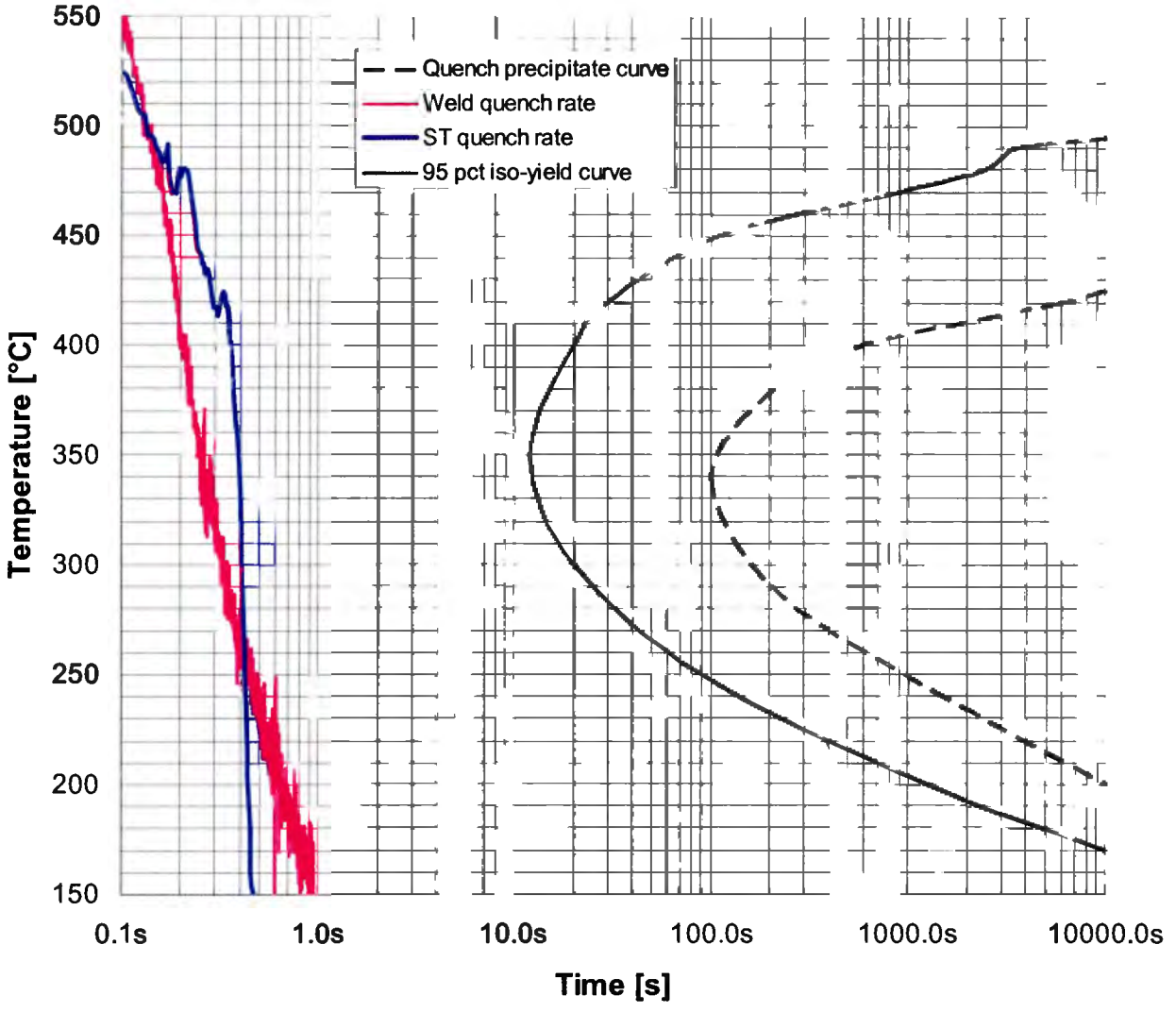

Figure 23: Measured quenching curves after laser welding and solution treatment superimposed onto a reconstructed 95 pct iso-yield strength contour (TTP curve) for D357 (no Sr modification) presented by M. Tiryakioğlu and R.T. Shuey (56). The cast D357 was solution treated at 540 °C x 8hrs, natural aged for 24hrs and artificially aged at 170 °C x 8hrs.

As stated in the literature background, if the Quench Factor is known, the as-aged strength can be predicted using Equation (3) ($\frac{\sigma - \sigma_{min}}{\sigma_{max} - \sigma_{min}} = \left[\exp\left(k_1 Q\right)^n\right]^{1/2}$). Based on data obtained by Tiryakioğlu and Shuey (56) and Möller et.al (35), the value of σ_{min} (T6 yield strength) equals 220 MPa and σ_{max} equals 315 MPa. As stated previously, k_1 is a constant which equals the natural logarithm of the fraction untransformed during quenching (typically 99%) (75), thus k_1 = -0.01005 and n = 1.5 (54), resulting in the predicted as-aged yield strength (σ) being equal to 315 MPa for Q_{Weld} and 315 MPa for Q_{ST} as well.

4.4 Optical microscopy

4.4.1 Weld joint characterization

Some weld spatter was obtained during laser welding, but in general the welds were smooth with regular flow patterns (Figure 24(a)) as is claimed to be the advantage of the twin spot welding of aluminium. The maximum degree of porosity observed in the welds as well as the bead profile and geometry of the first-batch welds is represented in Figure 24(b) and that of the second-batch welds in Figure 24(c). The bead profiles were similar for almost all of the welds and was in general characterised by a small degree of undercut (first-batch welds) and protruding weld roots (excessive penetration). The latter is ascribed to the sagging of low viscosity weld metal when welding is performed in the 1G position.

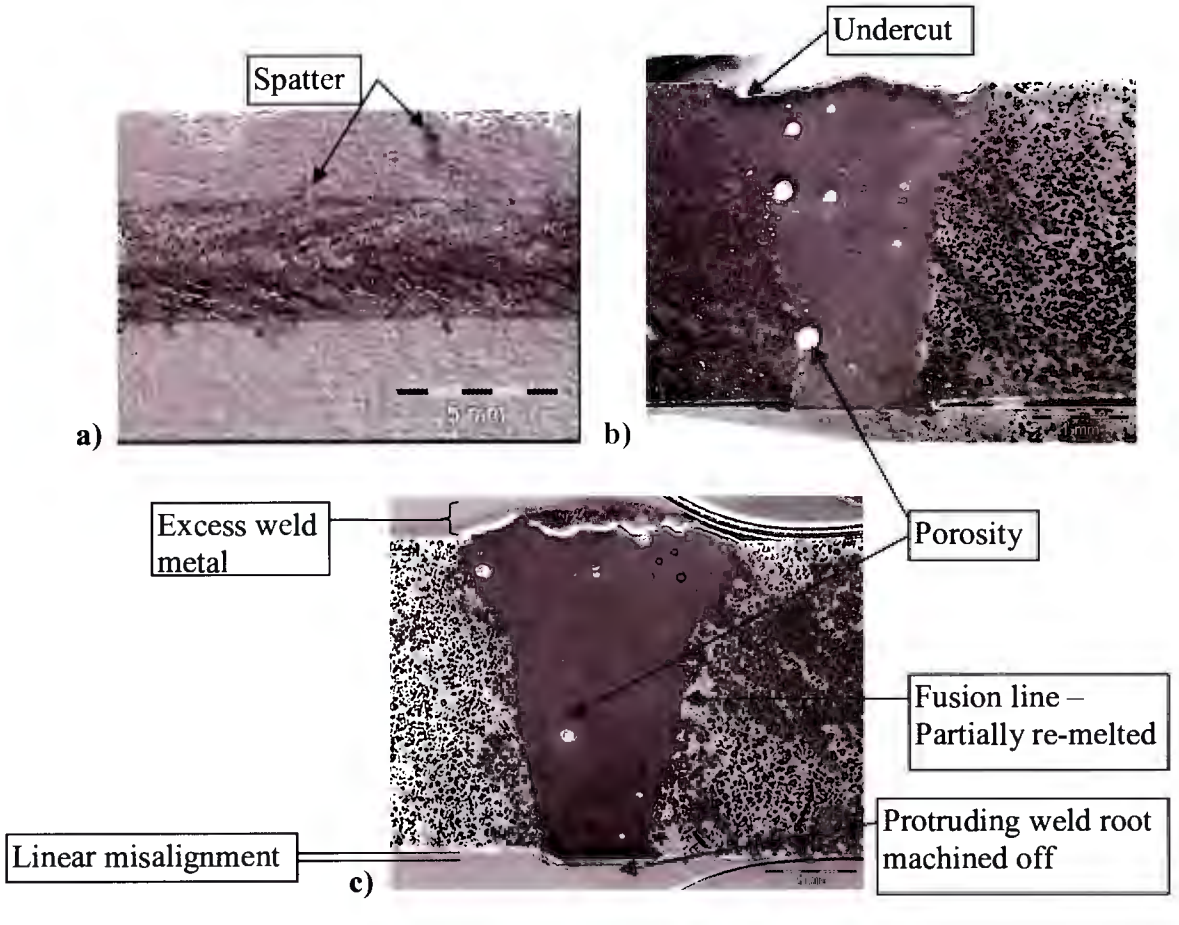

Figure 24: Stereo micrographs of typical F357 laser butt weld faces (a) and bead geometry / porosity level of first-batch welds (b) and second-batch welds (c).

Weld imperfections in the ISO 13919-2:2001 welding specification is quoted in terms of the actual dimensions and was therefore measured on the X-ray films (porosity) or on the transverse through-thickness samples which were prepared. The measured imperfections are listed in Table 6.

Table 6: ISO 13919-2:2001 specification for weld imperfections (Level B: Stringent) and compliance / non-compliance of the F357 butt welds therewith

Imperfection	Specification	First-batch	Second-batch
Undercut	h ≤0.05t (h ≤0.175mm)	0 – ***0.26***mm	0 – 0.07mm
Excess weld metal	h ≤0,2mm + 0,15 t (h ≤0.725mm)	0 – 0.2mm	0.09 – 0.39mm
Excessive penetration	h ≤0,2mm + 0,15 t (h ≤0.725mm)	0.2 – 0.5mm	0.13 – 0.37mm
Linear misalignment	h ≤0,1 t (h ≤0.35mm)	0 – 0.28mm	0.04 – 0.15mm
Porosity and gas pores	L or h ≤0,3 t (L or h ≤1.05mm) f ≤3%	0.9mm max. 2.5% max.	0.8mm max. 1% max.
Localised (clustered) and linear porosity	L or h ≤0,3 t (L or h ≤1.05mm) f ≤2% ΔL ≥ 0.5t L_c ≤t	***Some non-compliance***	Full compliance

L, h ≡Size of imperfection (length, height/width) ΔL ≡ Distance between 2 pores

f ≡Summation of projected areas of pores or cavities L_c ≡Clustered porosity length

t ≡Thickness of plate

4.4.2 Base material characterization

The general microstructure of SSM cast F357 material consists of globular α-primary crystals and Al-12%Si eutectic. The F357 base material in the various heat treatment conditions was microscopically investigated and an example of a defect-free cast material is shown in Figure 25(a), whereas some typical defects and inhomogeneous SSM cast structures that can be obtained, are

shown in Figure 25(b) to (f). All these defects are tolerated to some extend within the ASTM E155 specification, except the solidification cracking. A typical through-thickness microstructure along the length of a cast plate is shown in Figure 26.

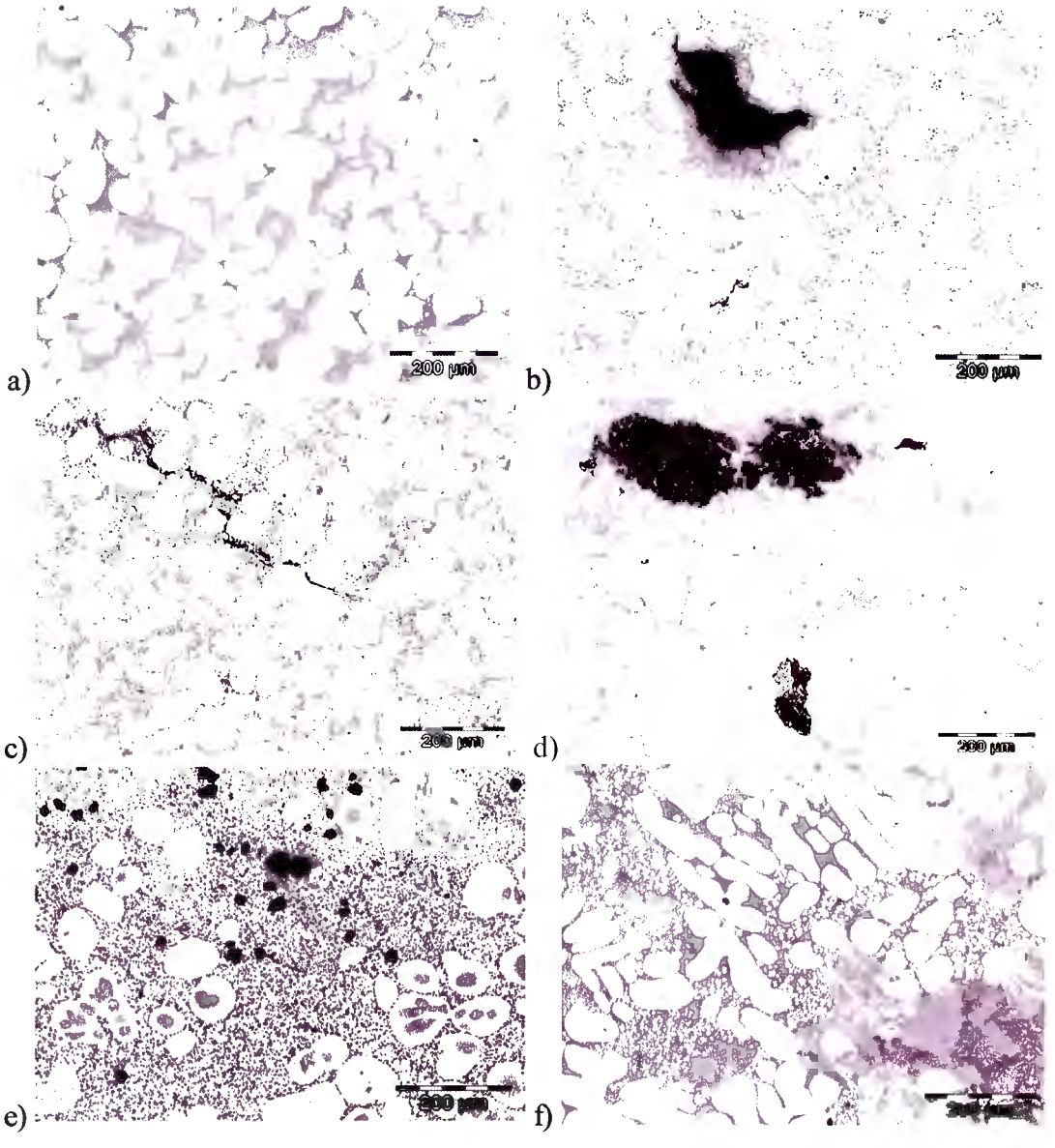

Figure 25: SSM cast F357 material with the following characteristics: a) Typical defect-free SSM cast structure b) shrinkage cavity c) solidification cracking d) entrapped dirt/oxide e) porosity + inverse coring and f) inhomogeneous SSM cast structure.

The applied solid solution treatment at 540°C/6h for T4 and T6 heat treatments causes changes of the eutectic by coagulation of the platelike eutectic Si phase from the F condition to an 4.5µm average spherical particle size in the T4 and T6 condition. The shape and sizes of primary crystals are almost the same for all three conditions, namely globular with mean size of 60-90 µm, Figure 27(a, b and d).

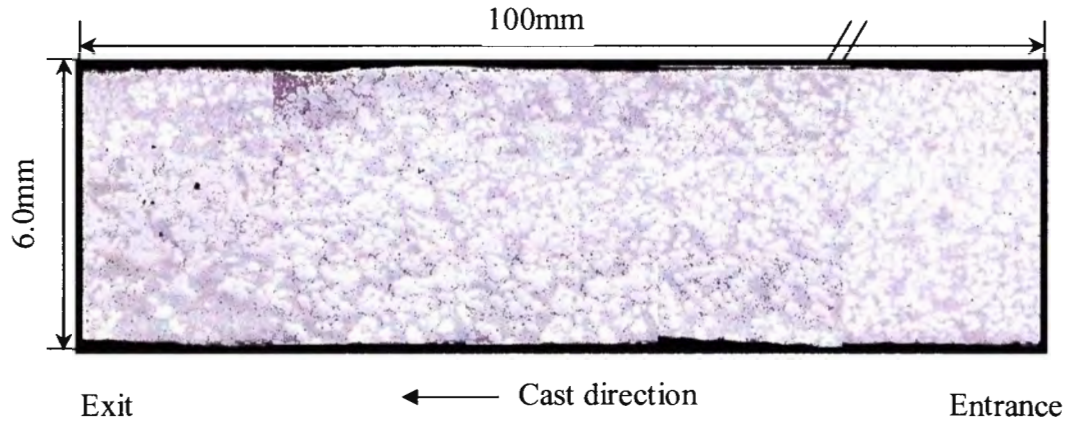

Figure 26: Typical transverse through-thickness microstructure along the length of a cast plate

4.4.3 Weld metal characterization

The microstructure of the F357 base metal in F condition consists of globular α-primary crystals with mean size of 60-90 µm and Al-12%Si eutectic. The butt weld metal has the same structure, but the primary crystals are much finer (dendritic) with a mean size of 6 µm thickness and 19 µm length, Figure 27(a). All weld centerline microstructures consist of this dendritic structure due to the fact that all welds experienced the same solidification conditions. Figure 27(a) to (d) shows the typical SSM F357 base metal microstructure in the F, T4, T4+ and T6 condition respectively on the left. Fusion line microstructures are shown in the centre and enlarged weld metal microstructures on the right. The typical Al globules and Al-Si eutectic of the base metal can be clearly observed, as well as the modified Al-Si eutectic after the T4, T4+ and T6 heat treatments.

4.5 Transmission Electron Microscopy (TEM)

4.5.1 Weld metal characterization of pre-weld T6 treated material

For the pre-weld T6 treated material, the weld metal undergoes remarkable changes during the welding (re-melting) process as stated previously in the optical microscopy of the weld microstructure. The shape of eutectic silicon crystals changes from round to plate-like, the size of WM α-grains is strongly reduced compared to BM α-grains and all secondary phases that have been present in the α-grain volume before welding (in F, T4 or T6 condition) are dissolved (Figure 28(a)).

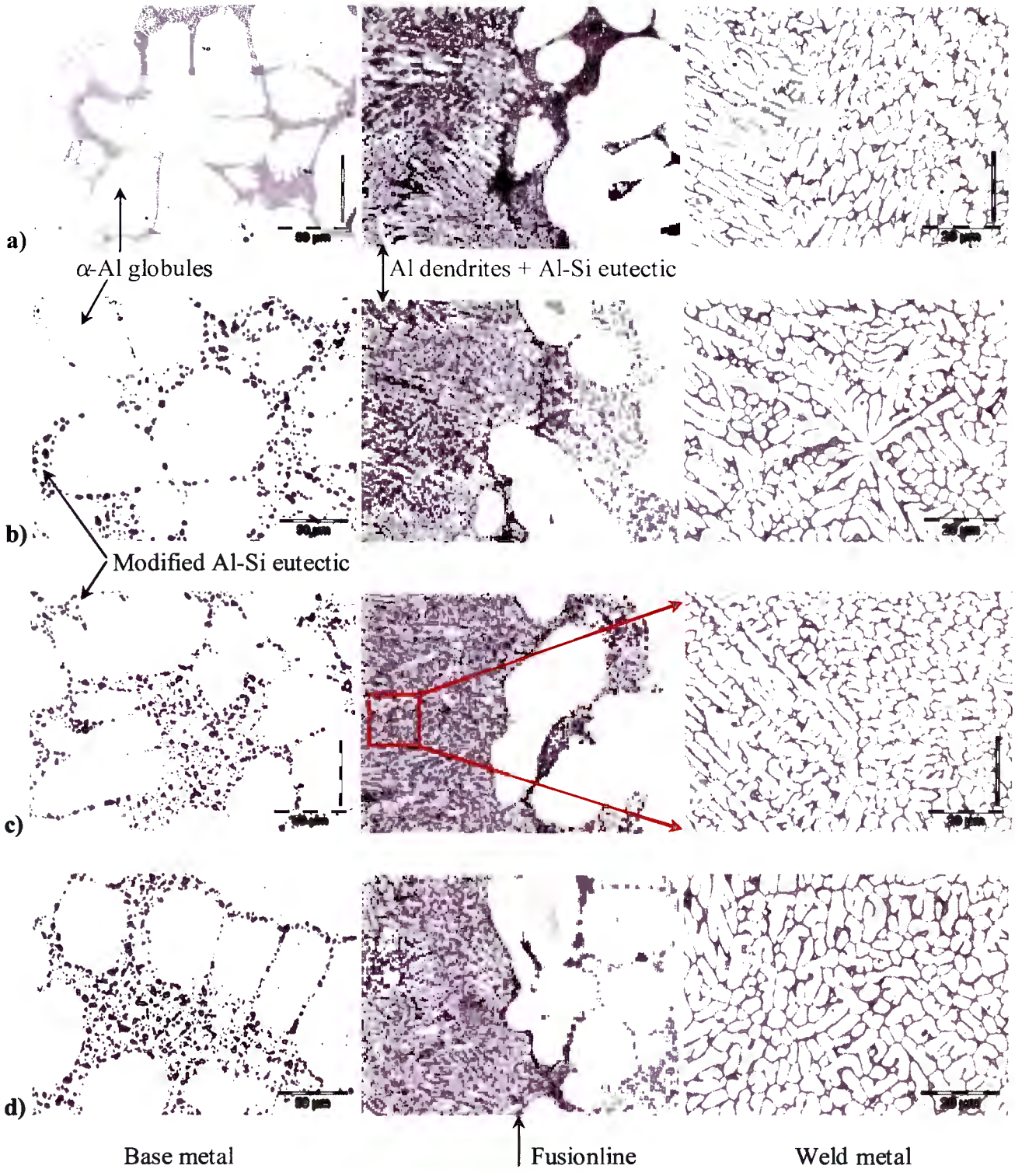

Figure 27: Typical microstructures of the SSM F357 base metal (left) in the a) F condition, b) T4, c) T4+ and d) T6 condition and a corresponding as-welded mid-thickness fusion line microstructure in the centre and weld metal on the right.

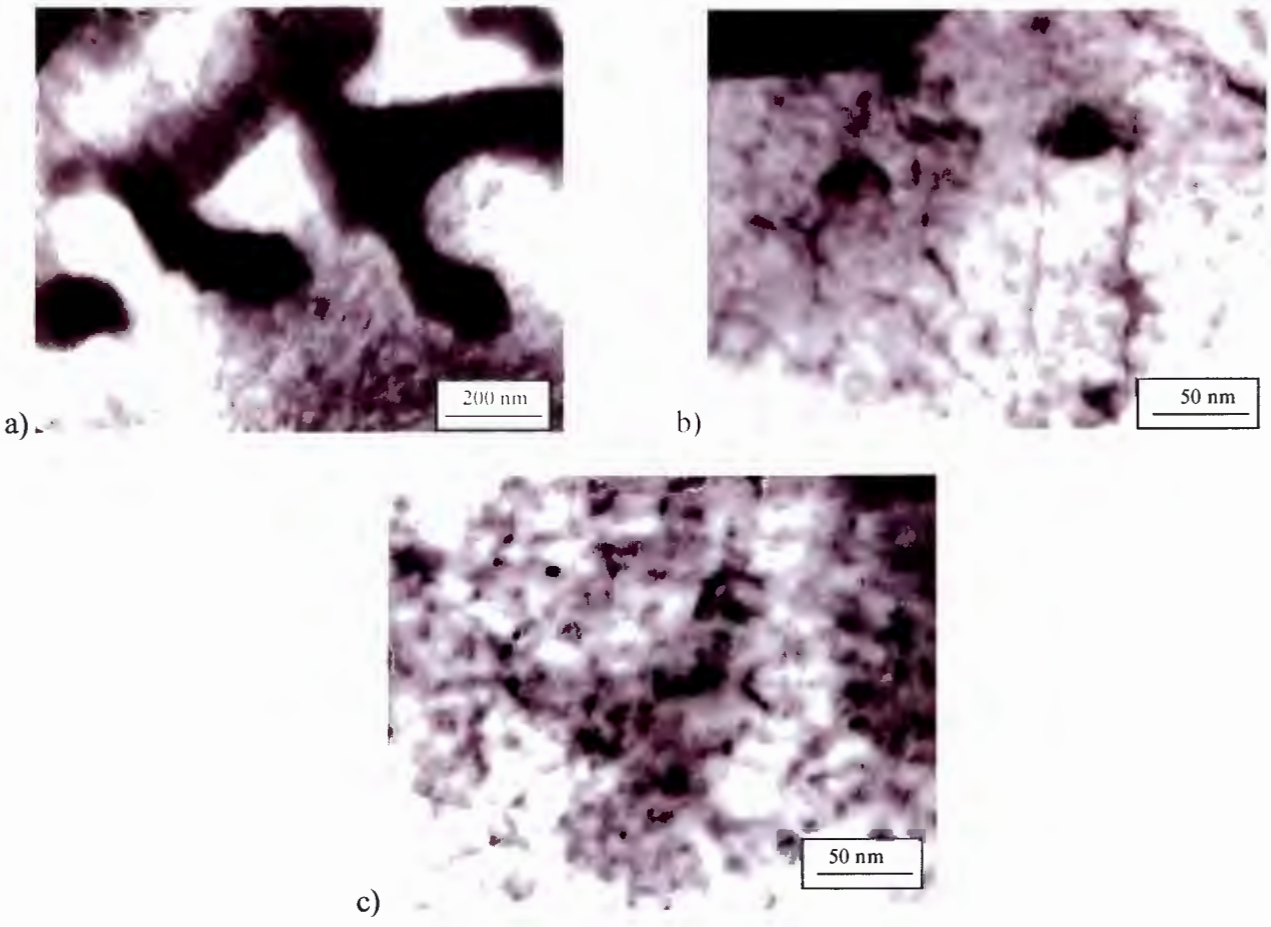

a) b) c)

Figure 28: TEM micrographs of F357 weld metal after butt-welding of T6 base material, revealing features like curling dislocations (b) and spherical precipitates surrounded by stress fields (c).

The appearance of the α-grains is typical for a decomposed solid solution. The characteristic features in this case are the spotted surface (Figure 28(a)) and the curling dislocations (Figure 28(b)), which have to overcome obstacles in their movement. At higher magnification one can discern separate spherical precipitates smaller than 10 nm, surrounded by stress fields (dark shadows, Figure 28(c)). The morphology and size of these precipitates and especially the presence of stress fields are typical for the zone aging stage with GP zones formation. The zone formation has probably occurred during the natural aging of the weld metal and not during the cooling after welding, because of the high cooling rate in laser welding that prevents the solid solution from decomposition.

The similar structures of the weld metal (Figure 27) and similar microhardness values for samples welded in the F, T4 and T6 conditions (Figure 30) confirm the above conclusions. The rapid cooling after laser welding results in similar structures which does not retain any properties of the initial

state or heat treatment due to the re-melting and solidification process. The WM structure and the properties depend therefore only on the degree of solid solution decomposition during the subsequent natural aging.

4.5.2 Weld metal characterization of T4+ treated material

The state of the weld metal before the last step of artificial aging in T4+ regime is similar to the state of the T6 WM described above. The artificial aging of the naturally aged (5 days) weld metal causes further decomposition of the supersaturated solid solution. The TEM observations showed two types of precipitations after artificial aging: round or faceted with diameters up to 30 nm and rod-like with lengths up to 30 nm and thicknesses in the range of 5 to10 nm (Figure 29). No signs of strain fields could be observed around particles, which indicate that the aging has reached the phase stage where semi-coherent or maybe coherent precipitates have formed.

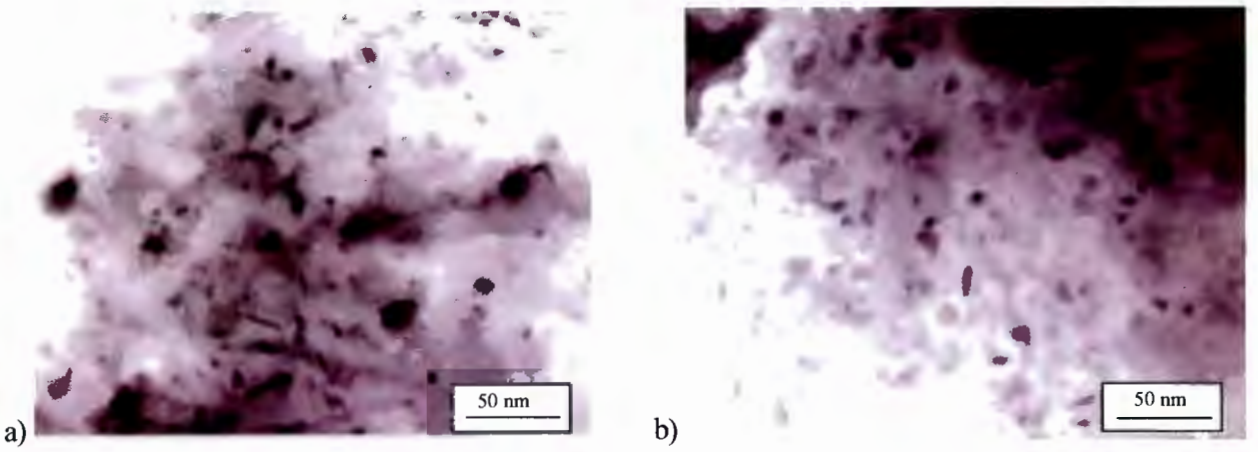

Figure 29: TEM micrographs of artificially aged F357 weld metal after butt-welding of T4+ base material, revealing rod- and disc-like Mg_2Si particles.

The expected strengthening phase in the Al-Si-Mg system is Mg_2Si, which develops in two morphologies depending on the aging stage: needle-like β'' or rod-like β'. The full absence of strain fields around particles indicates that the rod-like particles in Figure 29 probably are β'. The round particles with diameters up to 10 nm are cross-sections of the rod-like β', but the diameter of the coarser particles is too large to match the rods' thicknesses. Our experiments with different orientations of the TEM thin foil led us to the conclusion, that the faceted particles are actually discs. The non-typical shape (discs instead of rods or needles) and the large size of the precipitates, as well as the slightly lower hardness of WM in T4+ condition (115HV instead of 122HV measured

for the BM in T6) suggest that the artificial aging regime was probably not optimal for the weld metal and that a slightly higher temperature and/or longer time should have been used.

4.6 Micro-hardness

The hardness of the F357 base material in all the heat treated conditions was measured and found to be 75 $HV_{0.3}$ in the as-cast condition, 95 $HV_{0.3}$ in T4 condition, 120 $HV_{0.3}$ in the T6 condition and almost 130 $HV_{0.3}$ in the T4+ condition. The reason for T4+ hardness being slightly higher than T6, might be due to the added effect of 5 days natural aging before artificial aging for the T4+ condition compared to only 20 hrs natural aging before artificial aging for the T6 condition.

From Figure 30 it can be seen that there are substantial variances in hardness values at specific positions, especially for the material in the F condition, but the general trend for each material condition can clearly be observed and was the same for both sample batches. The scatter in hardness, however, was less for the second material batch than for the first material batch, especially over the weld. This might indicate that a more stable welding process was obtained with the custom-made nozzle (2^{nd} batch).

The properties after heat treatment of Al–Si–Mg alloys shows a cumulative effect due to an increase in the precipitation hardening (Mg_2Si), reduction in the segregation of alloying elements, spheroidization of the silicon crystals and improvement in the bonding between the second phase particles and matrix aluminium (70). Therefore, heat-treated alloys show enhanced hardness from the F to T4 to T6 condition (Figure 30). The BM hardness obtained in the T4+ condition was similar to that of the T6 material.

The reason for variance in hardness values of the BM / HAZ might be attributed either to the position of the hardness indentation coinciding with either α-aluminium or Al-Si eutectic or partly on both. Additionally it could be ascribed to possible differences in microstructure as was seen in Figure 25, e.g. inhomogeneous SSM structure.

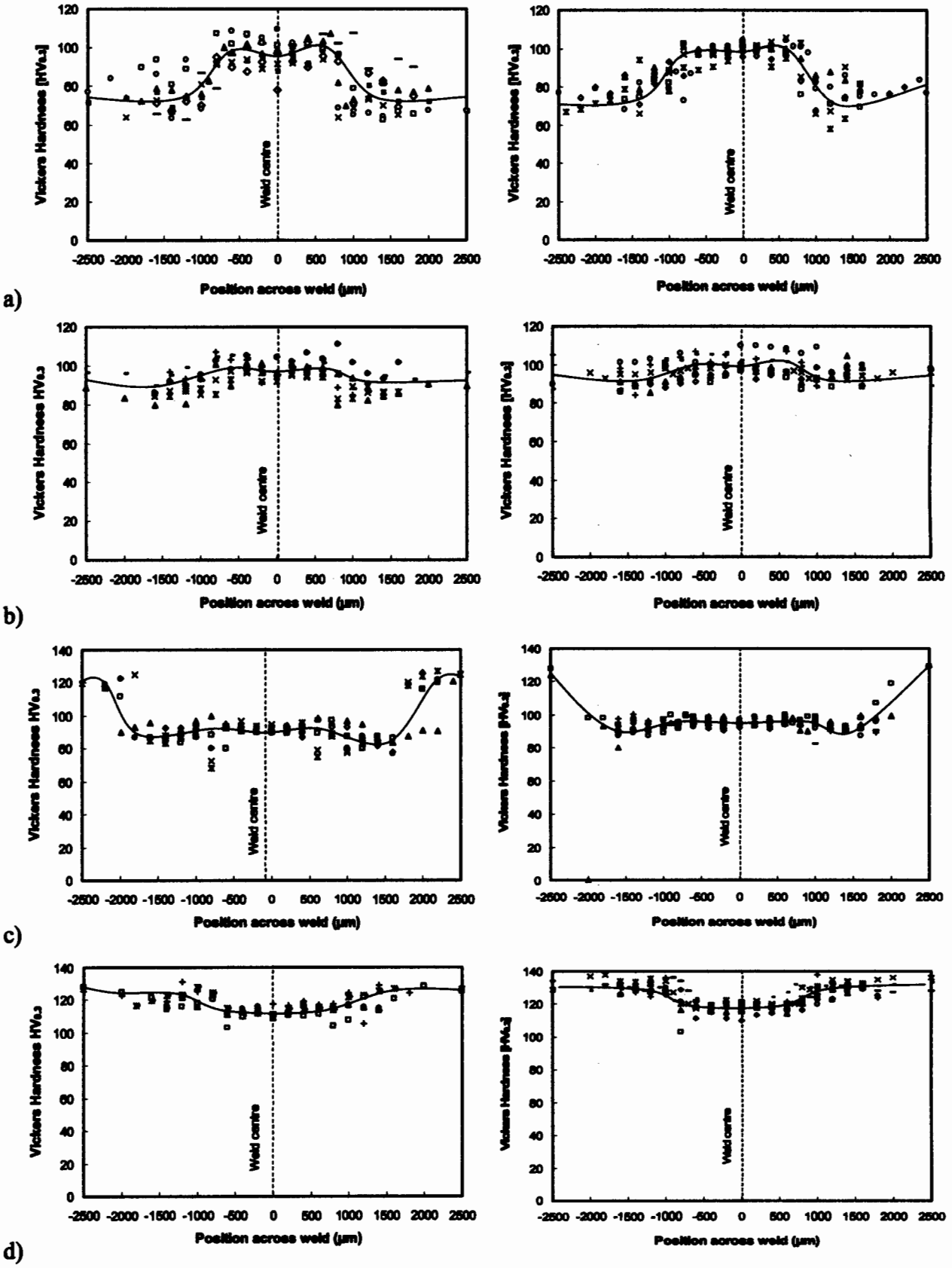

Figure 30: Mid-thickness micro-hardness traverses across the welds, for all the 1st batch samples (left) and 2nd batch samples (right) in the a) F condition, b) T4, c) T6 and d) T4+ condition.

It can also be seen that the weld metal hardness traverses of F357 in F, T4 and T6 conditions are very similar and just below 100 HV average. This is expected due to the as-welded condition of all these joints. The base metal hardness in the F condition is lower than that of the weld metal (WM) hardness, in the T4 condition it is similar and in the T6 condition it is higher than the weld metal. This can be attributed to the fine weld microstructure and solid solution strengthening obtained during the rapid cooling after laser welding, which is sufficient to contribute to a weld metal hardness, after natural aging, similar to the T4 base metal, but not sufficient to reach the T6 base metal hardness. This is in accordance with literature (19, 22). It has been stated that for heat-treatable aluminium alloys, the thermal cycle associated with the welding process will destroy the temper in the weld and HAZ. This will result in a large drop of hardness from T6 base material to the weld metal, with minimum hardness in the HAZ.

The large drop in WM hardness is mainly due to the loss of precipitates, namely dissolution of strengthening phases and the formation and growth of non-strengthening phases, e.g. GP zones. The latter has been confirmed through TEM work in this study, Figure 28. The drop in HAZ hardness is mainly due to over-aging, with the effect decreasing with distance from the fusion zone. Natural aging partly recovered the loss of hardness in the weld metal and heat-affected zone but only to that of the T4 base metal and not to that of the T6 base metal.

In the T4+ condition, the weld metal hardness is only slightly lower than that of the T6 BM and suggests that the conditions of laser welding might be sufficient to replace the T6 solution treatment after welding. This has been confirmed by the TEM investigation (Figure 29) which showed that the same strengthening mechanisms are obtained in the T4+ weld metal (without a post-weld solution treatment) as in the T6 base metal, although it appears as if the artificial aging treatment was not optimal for the T4+ WM.

4.7 Tensile properties

The tensile property specification requirements according to the Aluminium Association* for Permanent Mold Cast A357.0-T61 aluminium are given in Table 7, together with average tensile properties that have also been reported (71) for A357-T6 rheo-cast components.

Table 7: Specified and typical tensile property values for A357-T6 aluminium alloy (permanent mold- and rheo-cast respectively)

	UTS [MPa]	Yield strength [MPa]	Elongation [%]
Specification requirements*	≥310	≥248	≥3.00 % in 50mm
Literature values (71)	350	302	5.4

* Standards for Aluminum Sand and Permanent Mold Castings (14th Edition, 2000)

Figure 31 shows the results of the tensile testing done on the base metal as well as the welded samples (1st and 2nd batch). It can be observed that the T6 base material and the T4+ welded material conforms very well to the tensile specification requirements, with values well above the minimum required. The obtained strength property values of the F357-T6 base material are higher than the reported values whereas the values of the welded T4+ material are exactly the same or slightly higher than the reported values.

Only slight scatter was observed in most of the property values for all heat treated conditions and for both sample batches. However, material properties revealing significant scatter, could in all instances be attributed to either weld geometry (1st batch) or casting defects/porosity in the BM or WM for both batches (see Figure 32). 86% of the tensile samples in the 2nd batch failed in the BM during testing. The few samples that failed in the WM/HAZ revealed mainly micro-porosity on the fractured surfaces (Figure 32).

From Figure 31 it can also be observed that the UTS and yield strength obtained from the 2nd batch of weld samples is similar or slightly higher than that of the 1st batch for all heat treatment conditions, except for the T4+ condition which is similar or slightly lower. In general, the higher values might be attributed to the elimination of undercut in the 2nd batch with the custom-made nozzle used for welding, because the undercut was the cause of failure in most instances for the 1st sample batch. However, in the case of the welded T4+ samples, the BM and not the WM seems to have been the limiting factor in the 2nd batch, because the strength properties are slightly lower than that of the 1st batch although all samples failed in the BM (Figure 32 and Figure 33).

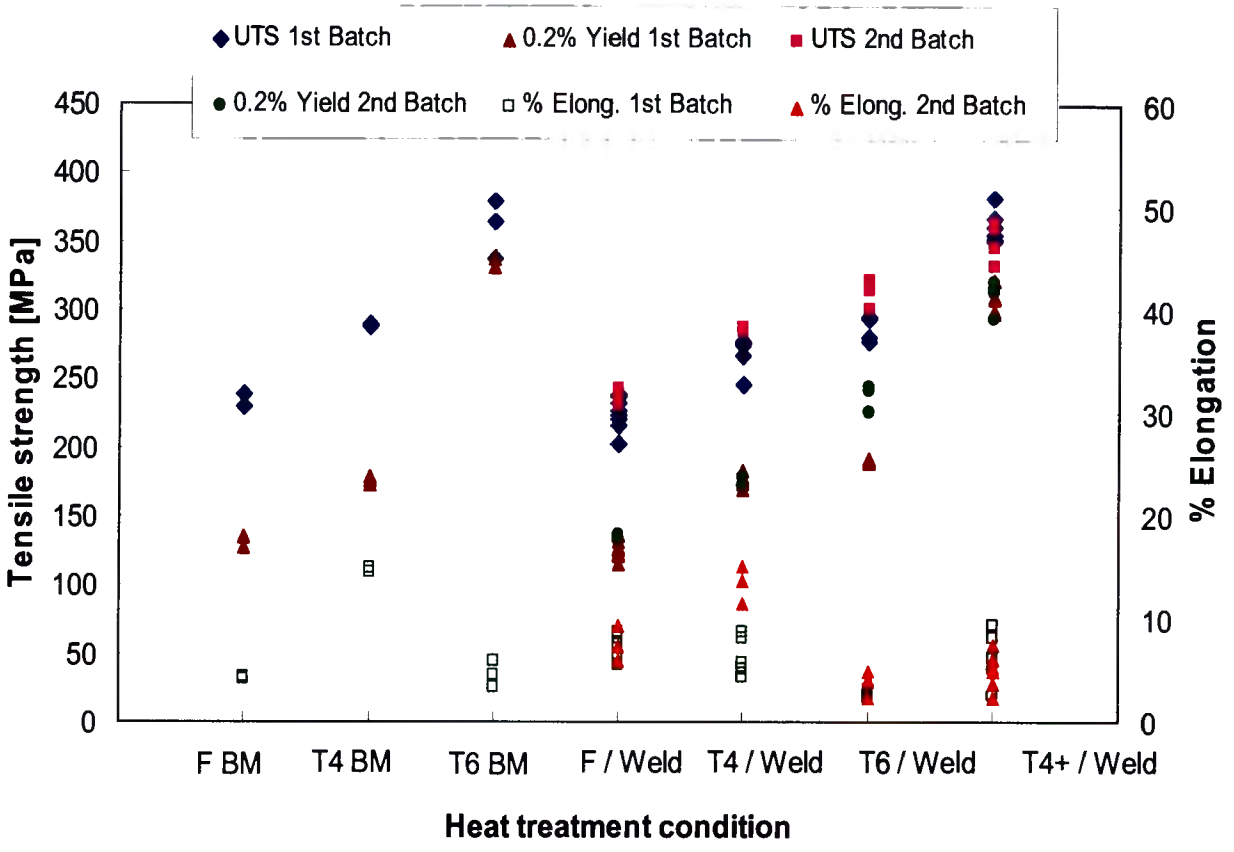

Figure 31: Tensile properties of the F357 base metal in all three pre-weld heat treated conditions and as-welded joints of all four BM heat treatment conditions (only T4+ has a post-weld aging treatment). First and second batch value comparison is also shown.

All tensile fractures of the welded samples occurred in the base metal for condition F (both batches), because the WM hardness for condition F is higher than that of the BM, which indicates the UTS of the WM to be higher than that of the BM. Due to the similar hardness of the fusion zone and BM in the T4 and T4+ welded samples, the fractures mainly occurred on the fusion line, due to the weld undercut present in the 1st batch (Figure 32(a)), but only in the BM in the 2nd batch (no weld undercut). Tensile fractures of the T6 welded samples only occurred on the fusion line of the 1st sample batch, due to the lower WM hardness and the presence of weld undercut. However, in the 2nd sample batch, the fractures occur either in the WM itself or in the HAZ due to the absence of weld undercut (Table 10 – Appendix A).

Because almost all fractures in the 1st batch of samples occurred on the weld fusion line, slightly higher tensile properties of T6 samples compared to T4 samples might be related to weld geometry or porosity variations. However, almost all fractures in the 2nd batch occurred in the BM and therefore explain the increasing tensile properties from F condition to T4+ condition (Figure 31).

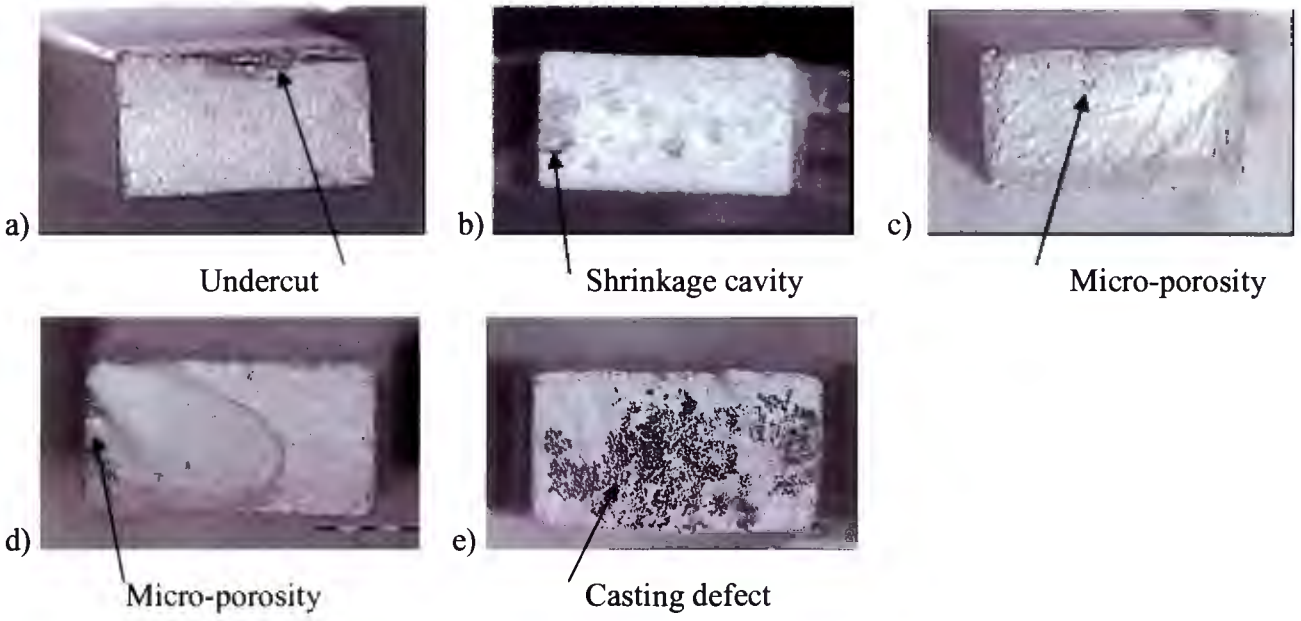

Figure 32: Examples of tensile fracture surfaces obtained with butt welds of the F357 material: a) Fusion line fracture due to undercut b) Base metal fracture due to shrinkage cavities c) Weld metal fracture revealing micro-pores d) Weld metal fracture (revealing micro-pores) propagating into the HAZ e) Base metal fracture revealing severe casting defect (only on this one sample)

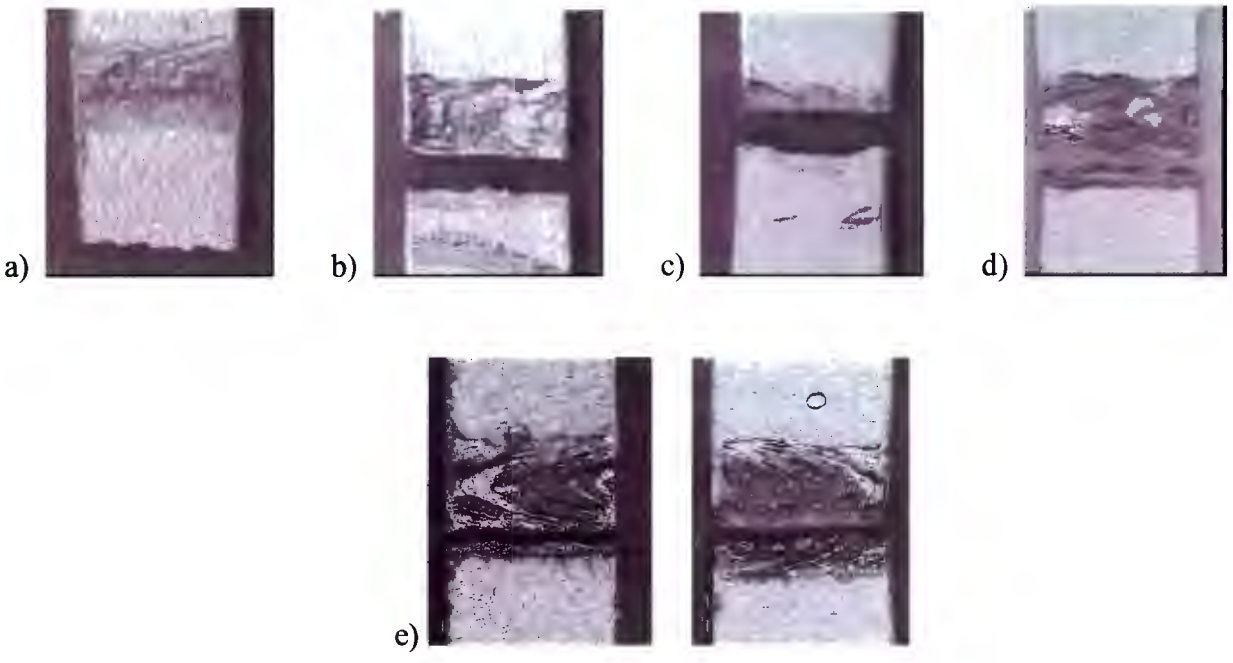

Figure 33: Typical positions of fracture during weld metal (excess weld metal removed) tensile testing of F357 butt welds in a) F condition of BM, b) T4 condition of BM, c) T6 condition of BM and d) T4+ condition and e) Two of the five weld joint (unmodified) tensile fractures from the 2nd batch that occurred on the fusion line (left) and in the WM (right).

In the 1st batch, the weld metal hardness and strength, without any post-weld heat treatment (PWHT) of the welded joint, was found to be similar for the T4 and T6 conditions, as was expected and reflected in Figure 30 and Figure 31. Fracture occurred mainly on the weld fusion line for both conditions. However, in the 2nd batch there are differences because fracture of the samples in the T4 condition occurred in the BM whereas the fracture of the samples in the T6 condition occurred in the HAZ. The T4+ condition weld metal entailed a post-weld artificial aging treatment and resulted thus in higher hardness and strength than that of the as-welded T4 strength. Although the F357 T4+ weld metal resulted in slightly lower strength and hardness than that of the base material in the T6 condition, it compares very well with the T6 material and the most important design property, namely yield strength, is still excellent.

The average BM elongation in the T6 condition is similar to that of the as-cast material (between 3 and 6%), with the T4 base metal elongation being the highest, namely 15%. The T4+ weld metal elongation is similar to that of the T4 weld and slightly higher than that of the T6 weld (Figure 31).

As stated in the chapter on experimental techniques, tensile tests were also done on unmodified weld joints (all other tensile tests done on modified weld joints) on which no excess weld metal was removed (Figure 34). These tests were only done on the 2nd batch of material and the comparison of the tensile properties between these two sample conditions is shown in Figure 35. For all practical purposes the tensile properties of the modified, as-welded samples and that of the unmodified weld joint samples are the same, except in the T6 condition. In the T6 condition the unmodified joint properties are slightly lower than that of the modified joint samples. Although all the T6 tensile samples of both the modified and unmodified joints failed in the WM or HAZ, the slightly lower properties of the unmodified joints might be attributed to the presence of micro-porosity that is revealed on the fracture surfaces of these samples. This could have caused the lower strength compared to that of the modified weld joints which did not show any visible defects.

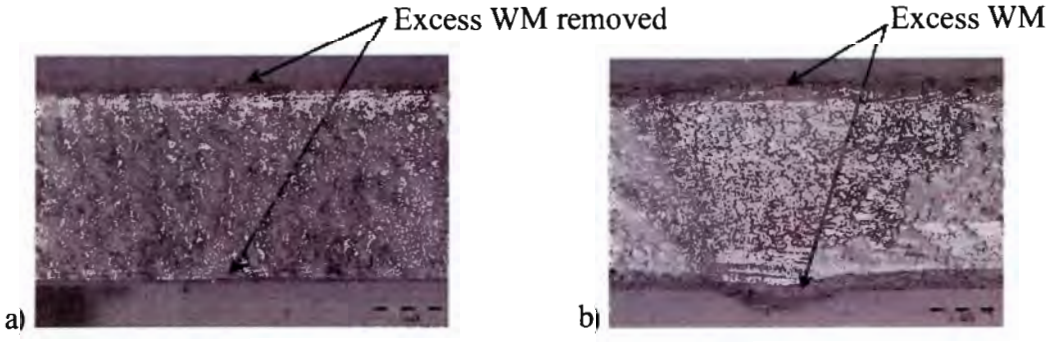

Figure 34: a) Side-view of a transverse modified weld joint tensile sample and (b) unmodified weld joint tensile sample.

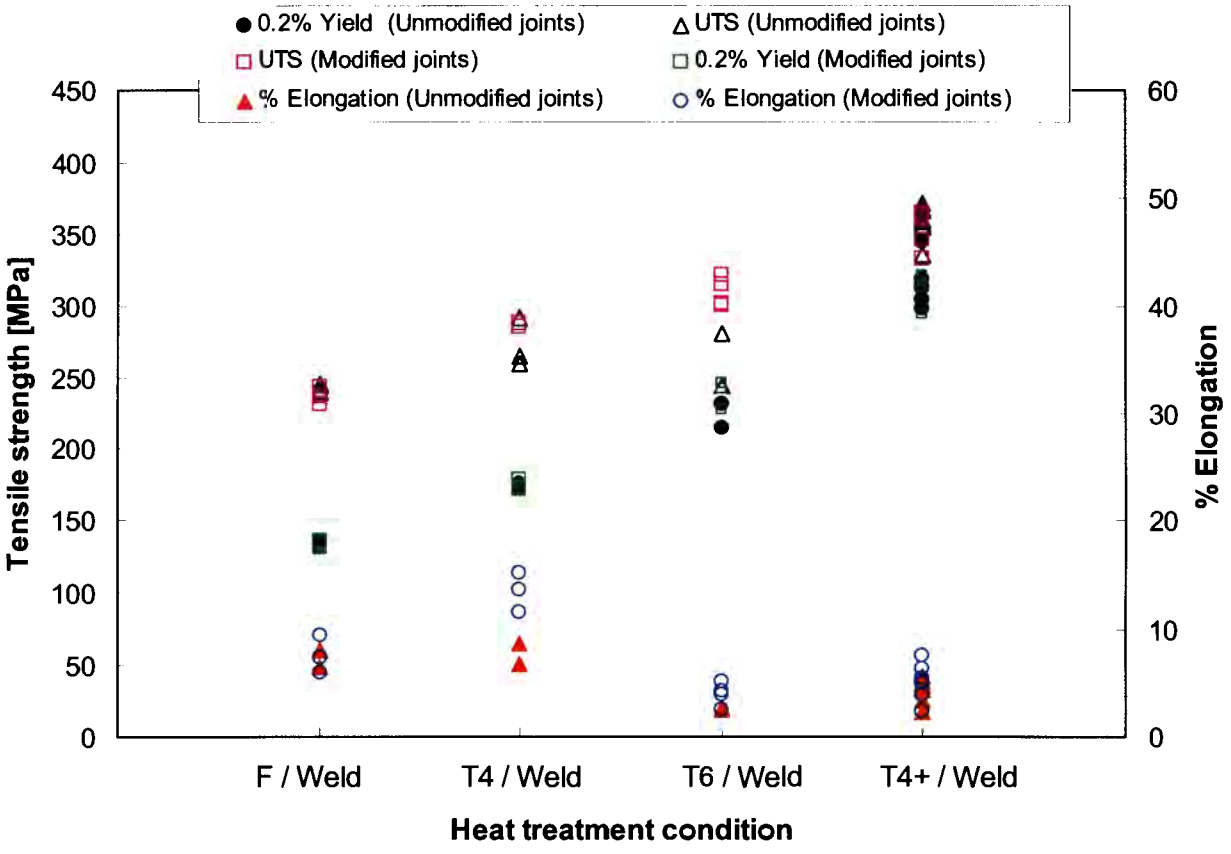

Figure 35: Tensile properties of as-welded, modified and unmodified weld joint samples for the second batch of material.

A few welded samples in the pre-welded T6 condition were also post-weld heat treated to the T6 condition again and subjected to tensile testing. The results are given in Table 8 and indicate a significant increase in all tensile properties if the welded samples are subjected to a post-weld T6 heat treatment. The reason for the latter can be explained by the difference in WM microstructure for the two heat treatment conditions (Figure 36). The WM microstructure of the pre-welded T6 material is dendritic and reveals only GP zone strengthening (Figure 28) due to natural ageing. These tensile samples failed in the WM or HAZ. The WM microstructure of the post-weld T6 treated material, however, consists of very fine α-Al globules and modified Al-Si eutectic (Figure 36(b)) together with all the hardening precipitates obtained from artificial aging. This resulted in much higher strengths and tensile test failures in the BM. This is in agreement with literature (72) which states that an additional T6 post-weld heat treatment (PWHT) applied to material that has been welded in the T6 condition, could be beneficial for the fusion zone, although it does not change the precipitation dispersion of the base material much.

Table 8: Comparison of modified versus unmodified weld joint properties in the pre-weld T6 treated condition and pre-weld + post-weld T6 treated condition

Weld joint condition	Heat treatment condition	0.2% Yield strength [Mpa]	UTS [Mpa]	% Elongation
Modified	T6	232	280	2.5
		215	244	2.8
	T6 + post-weld T6	312	356	6.3
		322	364	6.4
Unmodified	T6	227	302	5.1
		227	301	4.3
	T6 + post-weld T6	321	361	5
		303	306*	3.8*

* Much lower values due to severe casting defect (Figure 32(e))

In the pre-weld T6 treated condition, significantly higher UTS and % elongation were obtained with the unmodified weld joint samples than with the modified weld joint samples. The reason for this was probably the strengthening effect that the excess weld metal had on the unmodified samples and the fact that all the samples (modified and unmodified) failed in the WM or HAZ. However, this was not the case for the samples that were post-weld treated to the T6 condition again. Both the unmodified and modified weld joint samples in the post-weld T6 treated condition failed in the base metal. This indicates that the WM is stronger than the BM, possibly due to a high volume fraction of strengthening precipitates in the WM.

The question was raised whether the increase in mechanical properties of the T4+ material might not be attributed mainly to the fine grain size obtained in the fusion zone. A test was therefore conducted in which a welded F357 sample in the F condition and one in the T4+ condition were both annealed at 320 °C for 15 hrs. This was done to eliminate any possibility of precipitate strengthening and therefore only determine the strengthening effect of the smaller WM grain size. Transverse Vickers micro-hardness measurements were done across the weld on both samples in both heat treatment condition and the traverses are shown in Figure 37.

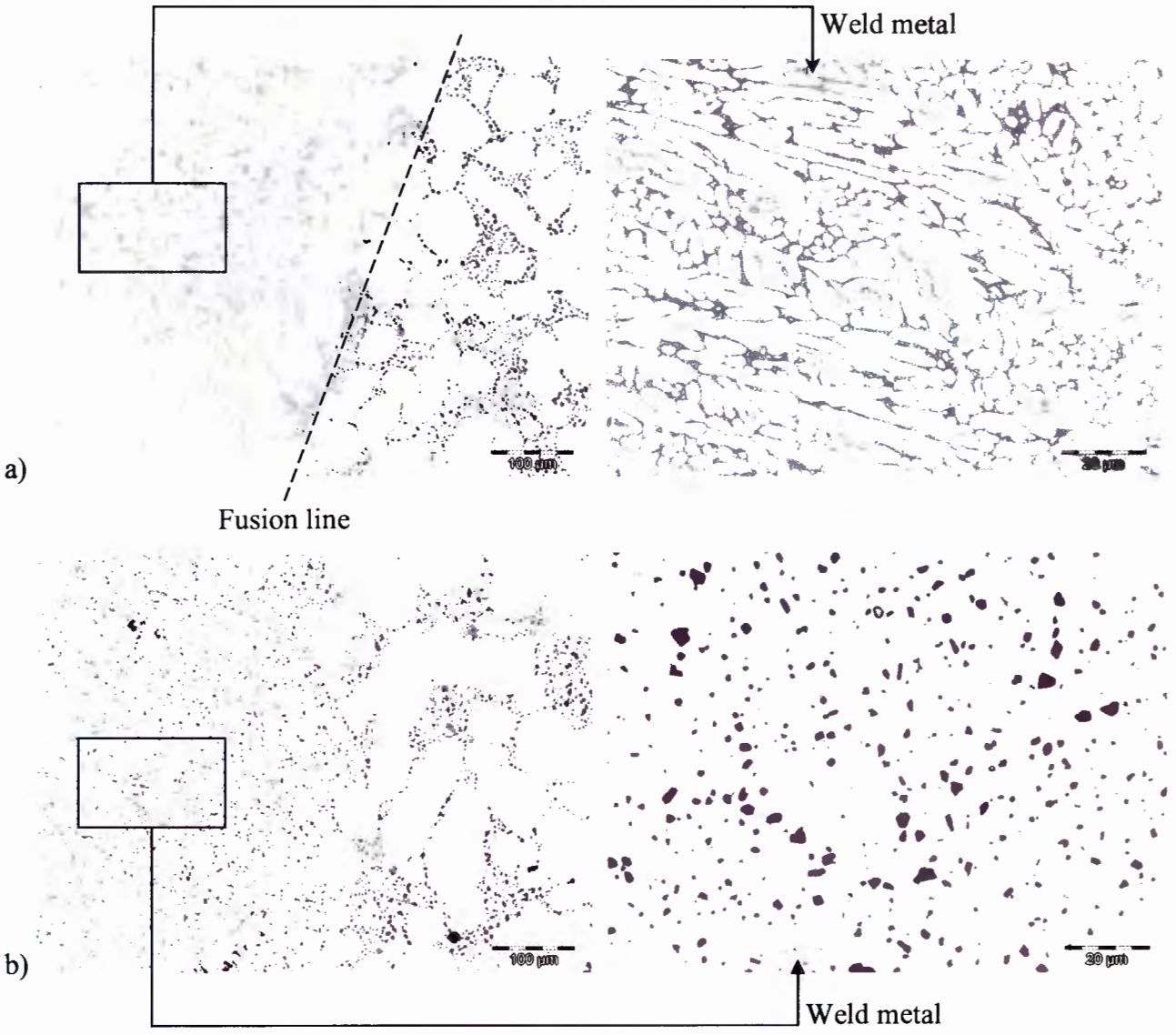

Figure 36: Microstructure of autogenously welded F357 material in the pre-weld T6 treated condition (a) and the pre-weld + post-weld T6 treated condition (b). The fusion line interfaces are shown on the left and the weld metal centre microstructures are shown on the right.

The same hardness trends were obtained as previously shown for the welded material in the F and T4+ condition (Figure 30) and a drastic overall drop in hardness occurs after annealing. After annealing, the average BM hardness of both the samples is 50 VHN, whereas the average WM hardness is 56 VHN. These results indicated the smaller WM grain size to have a hardness increase (strengthening effect) of approximately 10%. The increase in mechanical properties of the T4+ heat treated material can, therefore, not be attributed mainly to the fine grain size obtained in the fusion zone.

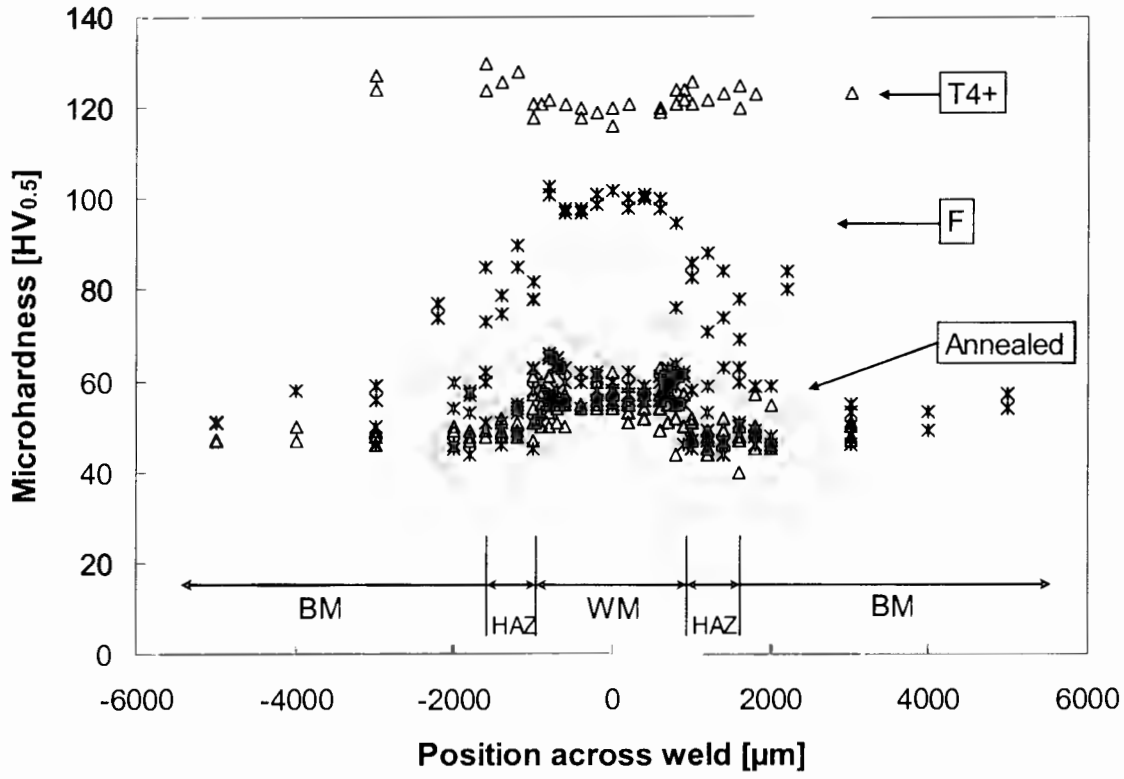

Figure 37: Transverse micro-hardness traverses of welded F and T4+ samples before and after annealing at 320 °C for 15 hrs.

CHAPTER FIVE

Conclusions

The first objective of the study was to apply deep penetration laser welding to SSM Rheo-cast F357 aluminium and to develop an envelope of permissible parameters for defect-free seams with acceptable properties. Autogenous Nd:YAG laser welding with a longitudinal twin spot configuration was applied and trials were run with various spot intensity distributions, centre-to-centre spot separation distances, shielding gas combinations and flow rates, various purging gasses and also two types of nozzles. From the findings of the study, the following main conclusions were drawn in terms of deep penetration laser welding of SSM F357 aluminium:

- By means of laser welding bead-on-plate (BOP) trials, it was possible to obtain a welding parameter window and to optimize the welding parameters for autogenously welded SSM F357 material.

- The welding parameters, weldability of SSM F357 aluminium and the mechanical properties of the welds were verified by means of a 2nd batch of weld samples. The degree of porosity obtained in the welds was within specification (ISO 13919:2) for all of the samples in the 2nd batch. No weld cracking occurred in any of the samples and the use of a custom-made nozzle resulted in welds that were 95% free of undercut and therefore had very good weld geometries.

- The lower degree of scatter in hardness values across the welds and higher tensile properties obtained with the 2nd batch of samples are indications of a more stable welding process with the custom-made nozzle than with the ASK nozzle.

- With the current laser welding parameters it was possible to produce welds with similar tensile properties to that of the base metal in both the as-cast and T4 conditions. The tensile properties of the welded joint which was performed on pre-weld T6 heat treated material were however lower than that of the base material, as expected.

- The chemical analyses done on weld metal samples revealed almost no variation in Mg content between the base metal and the weld metal. Therefore, with a relatively high welding speed and good gas protection during laser welding it was possible to retain the chemical composition of the weld metal.

- A suitable method for measuring quench rate after laser welding has been successfully set up. The measured quench rates obtained after the solution treatment and laser welding showed a somewhat lower quench rate after laser welding, but were found to be sufficient for the retention of the solid solution in the Al-Si-Mg alloy. Therefore, the quench rate during laser welding is higher than the critical quench rate required.

- Deep penetration laser welding can be successfully applied to SSM Rheo-cast F357 aluminium in terms of weld quality and properties.

The second objective of the study was to produce laser weld seams with mechanical properties of the T6 temper condition without the need for a post-weld solid solution heat treatment. It had to be shown that the quench rate during laser welding is sufficient for the retention of the WM solid solution, because only then the mechanical properties to the T6 performance specification could be achieved with only a post-weld aging treatment. The usefulness of the Quench Factor Analysis in predicting the as-aged yield strength of F357 aluminium was also investigated. With regards to this objective and the findings of the study, the following main conclusions were drawn:

- Similar hardness and tensile properties to that of the T6 base material were obtained with T4 material which was welded and then artificially aged at the same temperature and time as that of the T6 heat treatment (T4+ condition). This has been verified by means of a 2nd batch of welding samples and thus does suggest that the degree of solid solution obtained during laser welding, together with the fine weld microstructure, is sufficient to eliminate or replace the solution heat treatment required to acquire T6 temper properties.

- Due to the elimination of undercut in the 2nd batch welds, almost all the samples (F, T4 and T4+ heat treated conditions) fractured in the base metal.

- No significant difference in tensile properties could be observed between modified and unmodified weld joint samples, because most of the samples failed in the base material. The base metal therefore seems to be the limiting factor (weaker link) in terms of tensile properties and not the weld metal.

- The tensile properties of pre-weld T6 heat treated samples were found to be much lower than that of pre-weld + post-weld T6 heat treated samples due to the modified WM structure obtained after post-weld T6 treatment. This is known to provide an immediate means to

improve the strength, since it leads to the formation of a significant amount of β'' precipitates in the weld, but it is not recommended due to residual stress formation and distortion accompanied by the treatment.

- The Quench Factor Analysis is useful in predicting the as-aged yield strength of autogenously welded F357 aluminium alloy.

The third and final objective of the study was to characterise the microstructures within the optimised area of the laser welding parameter window and to verify the strengthening mechanisms obtained during laser welding of the T4+ treated material. In this regard, there were only two main conclusions:

- The centreline WM microstructures of all pre-weld treated material consist of a dendritic structure due to the fact that all welds experienced the same solidification conditions and the fine WM grain size contributed about 10% to the weld metal hardness.
- It has been confirmed through the TEM study that the thermal cycle associated with the laser welding process is responsible for the dissolution of strengthening precipitates in the weld metal of F357 aluminium. Also, it has been confirmed that the same strengthening mechanisms applicable to T6 heat treatments are invoked through the T4+ heat treatment.

REFERENCES

1. DAVIS, J. R. *ASM Specialty Handbook: Aluminium and aluminium alloys.* 4th ed. United States of America: ASM International, 1998. ISBN 087170496X.

2. DASGUPTA, R. *Industrial applications - The present status and challenges we face.* , September 21 - 23, 2004.

3. AKHTER, R., et al. Laser Welding of SSM Cast A356 Aluminium alloy Processed with CSIR-Rheo Technology. *Journal of Materials Processing Technology*, 1999, vol. 94, no. 1. pp. 151-156.

4. AKHTER, R.; IVANCHEV, L. H. and BURGER, H. P. Effect of pre/post T6 heat treatment on the mechanical properties of laser welded SSM cast A356 aluminium alloy. *Materials Science and Engineering A*, 2007, vol. 447, no. 1. pp. 192-196.

5. FAN, Z.; FANG, X. and JI, S. Microstructure and mechanical properties of rheo-diecast (RDC) aluminium alloys. *Materials Science and Engineering A*, 2005, vol. 412. pp. 298-306.

6. IVANCHEV, L. H., et al. *Rheo-processing of semi-solid metal alloys: A new technology for manufacturing automotive and aerospace components.* South-Africa: CSIR, 27 - 28 February, 2006.

7. BASNER, T. *Rheocasting of Semi-Solid A357 Aluminum.* SAE, 6 - 9 March, 2000.

8. IVANCHEV, L. H.; WILKINS, D. and GOVENDER, G. *Method and apparatus for rheo-processing of semi-solid metal alloys.* , September 21-23, 2004.

9. BRUWER, R., *et al. Method and apparatus for rheo-processing of semi-solid metal alloys.* USA: 7,225,858 B2. , 2007.

10. IVANCHEV, L. H. and WILKINS, J. D. *Processing of a molten alloy.* USA: 2007/0079949 A1. , 2007.

11. CAO, X., et al. Research and Progress in Laser Welding of Wrought Aluminum Alloys. I. Laser Welding Processes. *Materials & Manufacturing Processes*, 01, 2003, vol. 18, no. 1. pp. 1. ISSN 10426914.

12. DULEY, W. W. *Laser welding.* 1st ed. United States of America and Canada: Wiley-Interscience, 1999. ISBN 0-471-24679-4.

13. LEONG, K. H., et al. *Laser Welding of Aluminum Alloys.* USA: U.S. Government. , 1997.

14. NAEEM, M. *Welding of aluminium alloys with continuous wave Nd:YAG Laser up to 5 kW.* Laser Institute of America, 15 - 18 November, 1999.

15. IWASE, T., et al. *Dual focus technique for high-power Nd:YAG laser welding of aluminum alloys.* , 2000 [cited 22 October 2009]. Available from <http://www.scopus.com/inward/record.url?eid=2-s2.0-0033897480&partnerID=40> SCOPUS.

16. BLAKE, A. and MAZUMDER, J. Control of magnesium loss during laser welding of Al-5083 using plasma suppression technique. *Journal of Engineering for Industry*, 1985, vol. 107, no. 3. pp. 275-280.

17. YOSHIKAWA, M., et al. YAG laser welding of aluminum alloys. *Journal of Light Metal Welding and Construction*, 1994, vol. 32, no. 9. pp. 15-23.

18. CLARKE, J. A. Laser welding aluminum alloys. *Industrial Laser Solutions Articles*, 2000, vol. 15, no. 6. pp. 17-22.

19. CAO, X., et al. Research and Progress in Laser Welding of Wrought Aluminum Alloys. II. Metallurgical Microstructures, Defects, and Mechanical Properties. *Materials & Manufacturing Processes*, 01, 2003, vol. 18, no. 1. pp. 23. ISSN 10426914.

20. ZHAO, H.; WHITE, D. R. and DEBROY, T. Current issues and problems in laser welding of automotive aluminum alloys. *International Materials Reviews*, 1999, vol. 44, no. 6. pp. 238-266.

21. RAMASAMY, S. and ALBRIGHT, C. E. CO_2 and Nd:YAG laser beam welding of 6111-T4 aluminum alloy for automotive applications. *Journal of Laser Applications*, 2000, vol. 12, no. 3. pp. 101-115.

22. HIROSE, A., et al. Evaluation of properties in laser welds of A6061-T6 aluminum alloy. *Keikinzoku Yosetsu/Journal of Light Metal Welding and Construction*, 1999, vol. 37, no. 9 [cited 21 December 2009]. pp. 1-9. Available from <http://www.scopus.com/inward/record.url?eid=2-s2.0-0012257534&partnerID=40> SCOPUS.

23. WESTON, J. and WALLACH, R. *Mechanical properties of laser welds in aluminum alloys.* , 15 - 17 April, 2000.

24. CONNOR, L. P. *Welding Handbook: Welding Technology.* 8th ed. United States of America: American Welding Society, 1987. ISBN 0-87171-281-4.

25. READY, J. F. and FARSON, D. F. *LIA Handbook of Laser Materials Processing.* 1st ed. United States of America: Magnolia Publishing, Inc., 2001. ISBN 0-912035-15-3.

26. BOISSELIER, D. and LENOIR, R. *Weldability and manufacturing of YAG laser welds on aluminum alloys.* , 4 - 5 February, 1999.

27. FORSMAN, T., et al. Nd:YAG laser welding of aluminum: Factors affecting absorptivity. *Lasers in Engineering*, 1999, vol. 8. pp. 295-309.

28. PASTOR, M., et al. Porosity, underfill and magnesium loss during continuous wave Nd:YAG laser welding of thin plates of aluminum alloys 5182 and 5754. *Welding Journal*, 1999. pp. 207S-216S.

29. MARTUKANITZ, R. P. and SMITH, D. J. *Laser beam welding of aluminum alloys.* American Welding Society, 1995.

30. MATSUNAWA, A.; KATAYAMA, S. and FUJITA, Y. *Laser welding of aluminum alloys - Defects formation mechanisms and their suppression methods.* , 15 - 17 April, 1998.

31. DAUSINGER, F., et al. *Laser beam welding of aluminum alloys: State of the art and recent developments.* , 30 September - 2 October, 1997.

32. WANG, Q. G. and DAVIDSON, C. J. Solidification and precipitation behaviour of Al-Si-Mg casting alloys. *Journal of Materials Science*, 2001, vol. 36. pp. 739-750.

33. YAMAOKA, H. Microstructural control of laser-welded aluminum alloys. *Journal of Light Metal Welding and Construction*, 2001, vol. 39, no. 5. pp. 1-7.

34. KATOH, M. Factors affecting mechanical properties of laser welded aluminum alloys. *Journal of Light Metal Welding and Construction*, 1996, vol. 34, no. 4. pp. 42-48.

35. MÖLLER, H., et al. Comparison of heat treatment response of semi-solid metal processed alloys A356 and F357. *International Journal of Cast Metals Research*, 2009, vol. 000, no. 000.

36. KANDIL, H. M. *Recent Developments in Age Hardening Behavior of Aluminum Alloys - A Review Article: Heat Treating.* ASM International, 2001.

37. CALLISTER, W. D. An Introduction. *Materials Science and Engineering A*, 1994. pp. 783.

38. DAVIS, J. R. *ASM specialty handbook: Aluminium and aluminium alloys.* 1st ed. United States of America: ASM International, 1993.

39. LI, R. X., et.al. Age-Hardening Behavior of Cast Al-Si Base Alloy. *Materials Letters*, 2004, vol. 58. pp. 2096-2101.

40. GUPTA, A. K.; LLOYD, D. J. and COURT, S. A. Precipitation hardening processes in an Al-0.4%Mg-1.3%Si-0.25%Fe aluminium alloy. *Materials Science and Engineering A*, 2001, vol. 301. pp. 140-146.

41. MA, S. *A Methodology to Predict the Effects of Quench Rates on Mechanical Properties of Cast Aluminium Alloys.* Worcester Polytechnic Institute, 2006.

42. PEDERSEN, L. and ARNBERG, L. The Effect of Solution Heat Treatment and Quenching Rates on Mechanical Properties and Microstructures in AlSiMg Foundry Alloy. *Metallurgical and Materials Transactions A*, 2001, vol. 32. pp. 525-532.

43. ZHANG, D. L. and ZHENG, L. The Quench Sensitivity of Cast Al-7 Wt Pct Si-0.4 Wt Pct Mg Alloy. *Metallurgical and Materials Transactions A*, 1996, vol. 27. pp. 3983-3991.

44. EMADI, D., et al. Optimal heat treatment of A356.2 alloy. *Journal of Light Metals*, 2003 [cited 29 September 2009]. pp. 983-989. Available from <http://www.scopus.com/inward/record.url?eid=2-s2.0-1442356592&partnerID=40> SCOPUS.

45. DAVIDSON, C. J.; GRIFFITHS, J. R. and MACHIN, A. S. The effect of solution heat-treatment time on the fatigue properties of an Al-Si-Mg casting alloy. *Fatigue and Fracture of Engineering Materials and Structures*, 2002, vol. 25, no. 2 [cited 29 September 2009]. pp. 223-230. Available from <http://www.scopus.com/inward/record.url?eid=2-s2.0-0036466278&partnerID=40> SCOPUS.

46. TOTTEN, G. E. and MACKENZIE, D. S. Aluminum Quenching Technology: A Review. *Materials Science Forum*, 2000, vol. 331-337. pp. 589-594.

47. CROUCHER, T. and BUTLER, D. *Polymer Quenching of Aluminum Castings.* , 1981 [cited 1 October 2009]. Available from <http://www.scopus.com/inward/record.url?eid=2-s2.0-0019665044&partnerID=40> SCOPUS.

48. MA, S., et al. A Methodology to Predict the Effects of Quench Rates on Mechanical Properties of Cast Aluminum Alloys. *Metallurgical and Materials Transactions B*, 2007, vol. 38, no. 4. pp. 583-589. ISSN 1073-5615 (Print) 1543-1916 (Online).

49. STALEY, J. T. and TIRYAKIOĞLU, M. *Use of TTP Curves and Quench Factor Analysis for Property Prediction in Aluminum Alloys.* ASM International, 2001.

50. FINK, W. L. and WILLEY, L. A. Quenching of 75S aluminum alloy. *Transactions of the American Institute of Mining, Metallurgical and Petroleum Engineers (AIME)*, 1948, vol. 175. pp. 414-427.

51. EVANCHO, J. W. and STALEY, J. T. Kinetics of precipitation in aluminum alloys during continuous cooling. *Metallurgical Transactions*, 1974, vol. 5, no. 1. pp. 43-47.

52. STALEY, J. T.; DOHERTY, R. D. and JAWORSKI, A. P. Improved Model to Predict Properties of Aluminum Alloy Products after Continuous Cooling. *Metallurgical Transactions A*, 1993, vol. 24. pp. 2417-2427.

53. ROMETSCH, P. A. and SCHAFFER, G. B. Quench Modeling of Al-7Si-Mg Casting Alloys. *International Journal of Cast Metals Research*, 2000, vol. 12, no. 6. pp. 431-439.

54. ROMETSCH, P. A.; STARINK, M. J. and GREGSON, P. J. Improvements in Quench Factor Modeling. *Materials Science and Engineering A*, 2003, vol. 339. pp. 255-264.

55. BATES, C. E. and TOTTEN, G. E. *Application of Quench Factor Analysis to Predict Hardness under Laboratory Production Conditions.* , 1992.

56. TIRYAKIOĞLU, M. and SHUEY, R. T. Quench Sensitivity of an Al-7 Pct Si-0.6 Pct Mg Alloy: Characterization and Modeling. *Metallurgical and Materials Transactions B*, April 3, 2007, 2007, vol. 38B, no. August. pp. 575-582.

57. DORWARD, R. C. A Dynamic Quench Model for Strength Predictions in Heat-treatable Aluminum Alloy. *Journal of Materials Processing Technology*, 1997, vol. 66. pp. 25-29.

58. STALEY, J. T. Quench Factor Analysis of Aluminum Alloys. *Materials Science and Technology*, 1987, vol. 3, no. 11. pp. 923-935.

59. BERNARDIN, J. D. and MUDAWAR, I. Validation of the Quench Factor Technique in Predicting Hardness in Heat Treatable Aluminum Alloys. *International Journal of Heat and Mass Transfer*, 1995, vol. 38, no. 5. pp. 863-873.

60. TOTTEN, G. E., et al. *Industrial Use of Quench Factor Analysis: Application as a Specification Procedure for Quenchant Qualification.* ASM International, 2001.

61. BERNARDIN, J. D. and MUDAWAR, I. Validation of the Quench Factor Technique in Predicting Hardness in Heat Treatable Aluminum Alloys. *International Journal of Heat and Mass Transfer*, 1995, vol. 38, no. 5 [cited 2 October 2009]. pp. 863-873. Available from <http://www.scopus.com/inward/record.url?eid=2-s2.0-0029256880&partnerID=40> SCOPUS.

62. DOLAN, G. P. and ROBINSON, J. S. Residual stress reduction in 7175-T73, 6061-T6 and 2017A-T4 aluminium alloys using quench factor analysis. *Journal of Materials Processing Technology*, 2004, vol. 153-154, no. 1-3 [cited 2 October 2009]. pp. 346-351. Available from <http://www.scopus.com/inward/record.url?eid=2-s2.0-9444288108&partnerID=40> SCOPUS.

63. DAVYDOV, V. G.; BER, L. B. and KOMOV, V. I. *The TTT and TTP diagrams of commercial aluminum alloys used for quenching cooling and ageing regimes optimization.* , 2001 [cited 2 October 2009]. Available from <http://www.scopus.com/inward/record.url?eid=2-s2.0-0141649143&partnerID=40> SCOPUS.

64. DAVYDOV, V. G., et al. TTP and TTT diagrams for quench sensitivity and ageing of 1424 alloy. *Materials Science and Engineering A*, 2000, vol. 280, no. 1 [cited 2 October 2009]. pp. 76-82. Available from <http://www.scopus.com/inward/record.url?eid=2-s2.0-0033996736&partnerID=40> SCOPUS.

65. HABOUDOU, A., et al. Reduction of porosity content generated during Nd: YAG laser welding of A356 and AA5083 aluminium alloys. *Materials Science and Engineering A*, 2003, vol. 363, no.

1-2 [cited 4 August 2009]. pp. 40-52. Available from <http://www.scopus.com/inward/record.url?eid=2-s2.0-0242583788&partnerID=40> SCOPUS.

66. APELIAN, D. *Aluminum Cast Alloys: Enabling Tools for Improved Performance.* Wheeling, Illinois: North American Die Casting Association (NADCA). , 2009.

67. *ASTM Standard E155 - Standard Reference Radiographs for Inspection of Aluminum and Magnesium Castings.* West Conshohocken, PA: ASTM International, 2005.

68. Technical Committee CEN/TC 121 "Welding". *ISO 13919-2: Welding - Electron and laser beam welded joints - Guidance on quality levels for imperfections - Part 2: Aluminum and its weldable alloys.* 1st ed. , 2001.

69. ZLATEVA, G. and MARTINOVA, Z. *Microstructure of METALS AND ALLOYS - An Atlas of Transmission Electron Microscopy Images.* 1st ed. USA: CRC Press, 2008. ISBN 978-1-4200-7556-4.

70. SHARMA, R.; ANESH and DWIVEDI, D. K. Short communication: Solutionizing temperature and abrasive wear behaviour of cast Al-Si-Mg alloys. *Materials and Design*, 2007, no. 28. pp. 1975-1981.

71. ROSSO, M., et al. *Mechanical and microstructural characterization of semisolid Rheocast A356 and A357 aluminum alloys for automotive applications.* , 25 - 27 September, 2002.

72. STARON, P.; VAIDYA, W. V. and KOC¸AK, M. Precipitates in laser beam welded aluminium alloy AA6056 butt joints studied by small-angle neutron scattering. *Materials Science and Engineering A*, 2009, vol. 525. pp. 192-199.

73. KIM, J-S; HOFF, R. C. and GASKELL, D. R. *A Quench Factor Analysis of the Influence of Water Spray Quenching on the Age-Hardenability of Aluminum Alloys.* . VOLLER, R.; STACHOWICZ, M. S. and THOMAS, B. G. eds., The Minerals, Metals and Materials Society, 1991.

74. RAZAGHIAN, A., et.al. Sr effect on the microstructure and tensile properties of A357 aluminum alloy and Al_2O_3/SiC-A357 cast composites. *Mater Charact*, 2009, vol. xx. pp. xxx-xxx.

75. TOTTEN, G. E.; WEBSTER, G. M. and BATES, C. E. *Quench factor analysis: Step-by-step procedures for experimental determination.* ASM International, 1997.

APPENDIX A

Experimental Detail

Table 9: Matrix of experimental parameters changed during the first trial of laser welding bead-on-plate tests done at 3.8kW power at workpiece, 14 l/min He + 6 l/min Ar shielding gas (leading nozzle) and 5 l/min Ar purging gas. Focal plane is at top surface of plates.

Welding speed [m/min]	Power intensity distribution setting [mm]	Power intensity distribution [%]	Spot separation distance setting [mm]	Centre-to-centre spot separation distance [mm]	Porosity [Pores/mm]
3.75	12.3	52 / 48	17	0.48	0.52
4	12.3	52 / 48	16.825	0.38	0.57
4	12.3	52 / 48	16.85	0.4	0.48
4	12.3	52 / 48	16.9	0.42	0.78
4	12.3	52 / 48	17	0.48	1.00
4	12.3	52 / 48	17.1	0.53	1.22
3.5	***12.35***	***50/50***	***17***	0.48	***0.22***
3.5	***12.35***	***50/50***	***17***	0.48	***0.23***
3.5	12.35	50/50	17	0.48	0.48
3.5	12.35	50/50	17.1	0.53	0.44
3.5	12.35	50/50	17.1	0.53	0.67
3.75	***12.35***	***50/50***	***16.825***	0.38	***0.25***
3.75	12.35	50/50	16.825	0.38	0.37
3.75	12.35	50/50	16.9	0.42	0.39
3.75	12.35	50/50	17	0.48	0.33
3.75	12.35	50/50	17	0.48	0.55
3.75	12.35	50/50	17.1	0.53	0.73
4	***12.35***	***50/50***	***16.825***	0.38	***0.22***
4	12.35	50/50	16.825	0.38	0.41
4	12.35	50/50	16.825	0.38	0.64
4	***12.35***	***50/50***	***16.9***	0.42	***0.20***
4	12.45	47 / 53	16.825	0.38	0.43
4	12.45	47 / 53	16.825	0.38	0.73
3.5	12.5	47 / 53	17	0.48	0.48
4	***12.5***	***45 / 55***	***16.825***	0.38	***0.13***
4	***12.5***	***45 / 55***	***16.825***	0.38	***0.16***
4	***12.5***	***45 / 55***	***16.825***	0.38	***0.21***
4	12.5	45 / 55	16.825	0.38	0.53

Table 10: Tensile test results and fracture positions of (A) unmodified weld joint samples and (B) modified weld joint samples of 2nd material batch.

(A)

Heat Treatment	Mg %	HV10 BM	HV10 W	YS [MPa]	UTS [Mpa]	A [%]	Fracture Position
F	0.7	86	108	135	246	6.5	BM : Small cast defect
	"	"	"	134	241	8.0	BM
	"	"	"	132	244	9.5	BM : Micro-pores
T4+	0.68	127	141	363	371	4.7	BM : Micro-pores
	"	"	"	319	368	6.0/5.3	BM
	"	"	"	298	336	2.4	HAZ : Weld defect
T4	0.58	105	104	172	292	10.5	HAZ
	"	"	"	177	265	6.8	BM : Smlaa cast defect
	"	"	"	177	260	6.9	BM: Severe cast defect
T4+	0.63	125	126	305	356	6.3	BM / HAZ : Small cast defect
				312	355	5.2	BM : Small micro-pores
	0.63	128	133	344	367	4.2	BM : Small cast defect & micro-pores
	"	"	"	313	360	3.8	BM : Small cast defect
	"	"	"	314	359	3.2	BM : Small cast defect & micro-pores
T6 + Post-weld T6	0.68	125	137	312	356	6.3	BM
	0.67	132	134	322	364	7.5	BM : Small cast defect
T6				232	280	2.0	HAZ / WM : Micro-pores
				215	244	2.8	WM : Micro-pores

(B)

Heat Treatment	Mg %	HV10 BM	HV10 W	YS [MPa]	UTS [MPa]	A [%]	Fracture Position
F	0.7	86	108	136	231	7.4	BM : Small cast defect
	"	"	"	133	236	6.0	BM : Cast defect
	"	"	"	135	243	9.6	BM : Cast defect
T4+	0.68	127	141	278	284	5.3	BM : Severe casting defect
	"	"	"	311	360	7.6	BM : Cast defect
	"	"	"	312	346	2.4	BM : Cast defect
T4	0.58	105	104	179	285	11.6	BM : Cast defect
	"	"	"	173	288	13.8	BM
	"	"	"	172	288	15.2	BM
T4+	0.63	125	126	294	333	3.9	BM
	0.63	128	133	314	363	5.1	BM : Small cast defect
	"	"	"	317	365	6.3	BM
	"	"	"	321	363	5.5	BM : Small cast defect
T6 + Post-weld T6	0.68	125	137	321	361	5.9	BM : Cast defect
	0.67	138	134	303	306	3.8	BM : Cast defect
T6	0.68	140	110	245	322	2.5	HAZ
	"	"	"	242	315	4.0	HAZ / WM : Pores
	"	141	"	227	302	5.1	BM
	"	143	"	227	301	4.3	BM